UNIVERSITY OF CALIFORNIA
RIVERSIDE

Neuropathology Following Repeated Traumatic Brain Injury and the Influence of Inflammatory Status on Injury Outcome

A Dissertation submitted in partial satisfaction
of the requirements for the degree of

Doctor of Philosophy

in

Cell, Molecular, and Developmental Biology

by

Virginia Dorothy-Marie Donovan

August 2014

Dissertation Committee:
Dr. Andre Obenaus, Co-Chairperson
Dr. Monica J. Carson, Co-Chairperson
Dr. Iryna Ethell

The Dissertation of Virginia Dorothy-Marie Donovan is approved:

_____

_____

Committee Co-Chairperson

_____

Committee Co-Chairperson

University of California, Riverside

Acknowledgements

Chapter 2 of this dissertation, in part, is a reprint of the material as it appears in: Donovan, V., A. Bianchi, R. Hartman, B. Bhanu, M. J. Carson and A. Obenaus (2012). Computational analysis reveals increased blood deposition following repeated mild traumatic brain injury. Neuroimage Clin 1(1): 18-28. Dr. Andre Obenaus listed in that publication directed and supervised the research, which forms the basis for this dissertation. Anthony Bianchi and Dr. Bir Bhanu provided computational expertise and wrote the algorithm for analyzing blood and edema volumes from MRI images. Dr. Richard Hartman performed statistical analysis and Dr. Monica Carson provided intellectual input.

Additionally, Chapter 3 of this dissertation, in full, is a reprint of the material as it appears in: Donovan, V., C. Kim, A. K. Anugerah, J. S. Coats, U. Oyoyo, A. C. Pardo and A. Obenaus (2014). Repeated mild traumatic brain injury results in long-term white-matter disruption. J Cereb Blood Flow Metab 34(4): 715-723. Dr. Andre Obenaus listed in that publication directed and supervised the research, which forms the basis for this dissertation. Claudia Kim and Ariana Anugerah aided in analysis of EM, LFB and NF200. Jacqueline Coats helped performed the surgeries and provided intellectual input. Dr. Udo Oyoyo performed statistical analysis on the data and Dr. Andrea Pardo provided intellectual input.

I would like to thank the IGERT program in Video Bioinformatics for funding during my time as a fellow and the Graduate Division for awarding me a

dissertation year award. Additionally, I would like to thank my mentors Dr. Andre Obenaus and Dr. Monica Carson for their support and encouragement over the past five years and thank Dr. Iryna Ethell for her guidance. Lastly, I would like to thank my husband Zev Wisotsky and my family for their love and support.

ABSTRACT OF THE DISSERTATION

Neuropathology Following Repeated Traumatic Brain Injury and the Influence of Inflammatory Status on Injury Outcome

by

Virginia Dorothy-Marie Donovan

Doctor of Philosophy, Graduate Program in Cell, Molecular, and Developmental Biology Program
University of California, Riverside, August 2014
Dr. Andy Obenaus, Co-Chairperson
Dr. Monica J. Carson, Co-Chairperson

Traumatic brain injury (TBI) is an increasing public health concern, accounting for approximately 30% of injury related deaths. Clinical and experimental studies have demonstrated that the brain remains vulnerable following TBI and subsequent injuries may worsen tissue damage. Following injury, microglia, the brain macrophage, have demonstrated both cytotoxic and cytoprotective functions. However, the role of microglial activation in injury progression and resolution is not understood. This dissertation examines the progression of tissue damage following repeated mild TBI (rmTBI) and investigates whether inflammatory status at the time of a moderate-to-severe injury influences outcome.

Using a novel rmTBI model, we found acute 2-fold increases in tissue damage on T2-weighted magnetic resonance imaging (MRI) when injuries were

induced 7 (7D), but not 3 days (3D) apart. Furthermore, injuries 7D apart resulted in 2-fold more blood deposition, while those 3D apart showed more edema. Though sub-acute grey matter pathology was transient. We therefore assessed white matter, not directly underneath the impact, using diffusion tensor MRI and electron microscopy at sub-acute (14-day) and long-term (60-day) timepoints. At sub-acute times, we found that rmTBI 7D apart resulted in white matter changes localized to regions immediately adjacent to the impact sites. However, long-term assessment revealed that changes in white matter integrity within rmTBI animals became widespread.

The effect of inflammatory status on TBI induced hemispheric swelling and lesion pathology was tested 7D post injury. We compared MRI pathology with inflammatory molecule expression from naïve, wildtype (TBI; no pre-treatment), wildtype with LPS-challenge 24-hrs before TBI and TREM2KO animals. MRI showed an 80% reduction in hemispheric swelling within TREM2KO and LPS-challenged animals compared to wildtype. Reduced swelling coincided with a 2-fold increase in microglial expression of inflammatory genes compared to naïve animals. However, LPS-challenged and TREM2KO mice showed a reduced inflammatory response from wildtype. Furthermore, comparison of TREM2KO microglia with cortical tissue revealed an opposing number of expressed genes.

Overall, these studies demonstrate that (1) brain vulnerability is dependent on the time interval between and location of injuries, (2) rmTBI results in early

white matter disruption that progresses long-term and (3) reduced swelling occurs during limited microglial activation.

Table of Contents

List of Figures

List of Tables

Chapter 1

Introduction

Traumatic brain injury (TBI) is defined as any bump or jolt to the head that disrupts brain function (Faul 2010). Over 1.7 million civilian TBIs occur annually in the United States, costing an estimated 60 billion dollars every year (Faul 2010, Coronado 2011). Furthermore, head injuries, particularly mild TBI (mTBI) or concussions, have been identified as the signature injury in the Iraq and Afghanistan wars (Hoge 2008). Currently, an estimated 3.2-5.3 million Americans are living with chronic neurological and/or physical disabilities as a result of a TBI that decrease their quality of life and have prolonged economical impacts on society (Coronado 2011).

Traumatic Brain injury

TBI Severity

Clinically, brain injuries are grossly categorized as mild, moderate or severe. Diagnosis of brain injury severity depends on the duration of time in which consciousness is lost, altered or amnesia is experienced and on the extent of pathology seen on medical imaging (VA/DoD 2009). Moderate and severe TBIs can be difficult to distinguish, so these severity ranges are sometimes combined and collectively referred to as moderate-to-severe injuries. Moderate-to-severe injuries generally demonstrate obvious abnormalities on both magnetic resonance imaging (MRI) and X-ray computed tomography (CT). Typically,

individuals with a moderate-to-severe injury will demonstrate loss of consciousness for greater than 30min and altered consciousness and/or amnesia for greater than 24hrs following their injury (VA/DoD 2009). Furthermore surgical intervention, permanent disabilities and death are often associated with patient populations that sustain a moderate-to-severe TBI. In contrast, mTBI typically shows no obvious changes on medical imaging and may result in brief episodes of confusion (<1 day), disorientation (<1 day) and/or loss of consciousness (<30 min). Most individuals that acquire a mild head injury appear to recover normally following mTBI. However, clinical studies have reported that approximately 5-20% of concussed individuals experience a delayed onset of emotional and/or cognitive abnormalities in the weeks to months following an mTBI (Wood 2004, Malojcic 2008, Jotwani and Harmon 2010, Konrad 2011).

Repeated TBI

Mild injuries are the most common form of TBI, accounting for approximately 75% of all head trauma cases (Faul 2010). Acute mTBI symptoms are often subtle and can easily go unrecognized, leaving individuals susceptible to acquiring additional injuries. Both clinical and experimental studies have provided evidence of increased brain vulnerability following head injury to additional TBIs (Laurer 2001, Longhi 2005, Vagnozzi 2007, Vagnozzi 2008, Donovan 2012, Huang 2013). Athletes sustaining a second TBI, while still showing symptoms from a previous head injury, demonstrated significantly

worsened outcomes (Cantu and Gean 2010). Another clinical study performed by Vagnozzi et al. (2008) reported that patients sustaining concussions 10-13 days apart from each other demonstrated prolonged alterations in brain metabolites compared to those individuals only suffering a single injury. This study suggests that while patients appear to have recovered from a concussion, there are ongoing changes within the brain that may be exacerbated following a subsequent injury. Observations of increased brain vulnerability following TBI has sparked an ongoing debate as to when it is safe to "return-to-play" for athletes and resume military duty for soldiers.

Animal models have begun to focus on defining the window of time in which the brain remains vulnerable to subsequent injuries. Studies inducing two injuries to the same anatomical location have demonstrated a window of vulnerability of approximately 1-5 days following an mTBI, in which a second impact resulted in increased lesion volume, axonal injury and inflammation (Laurer 2001, Longhi 2005, Shitaka 2011). However two mTBIs to the same anatomical location 7 days apart did not result in exacerbation of injury (Longhi 2005). In contrast to previous literature, we have shown that repeated mTBI (rmTBI) induced to different anatomical locations did not exacerbate damage when injuries were spaced 3 days apart (Donovan 2012). However, brain vulnerability was observed when a second injury was induced 7 days following the initial insult (Donovan 2012, Donovan 2014). These data suggest that brain

susceptibility to subsequent injuries is dependent on both the time interval between and the anatomical locations of mTBIs.

Neuroimaging:

Neuroimaging facilitates diagnosis of TBI, injury severity and is also essential for surgical planning as it allows clinicians to determine operability and provides anatomical locations of lesions (Lee and Newberg 2005). One method for assessing a patient's need for neuroimaging following injury is the Glasgow Coma Scale (GCS), which rates an individual's consciousness and response to various stimuli from 3 (worst) to 15 (normal). Concussed patients typically score a GCS of 13-15, moderate TBI scores 9-12 and severe injuries result in a score of 3-8. Individuals scoring less than 13 typically receive CT imaging. However in addition to GCS, factors such as vomiting, headache and age, are also considered in determining whether concussed individuals require imaging (Lee and Newberg 2005). It is important to note that many of the neurological scales and tests, such as GCS, are problematic and their efficiency can be affected by the rater's experience level (Namiki 2011). Additionally, clinical studies have shown that patients with normal scores on neurological tests and lacking other obvious signs of head injury can have hemorrhages on medical imaging (Lee and Newberg 2005). These patients may potentially develop neurological deficits or require hospitalization later as studies have shown that hemorrhagic progression can occur in approximately 45% of TBI cases (Sifri 2004, Sifri 2006, Narayan

2008, Alahmadi 2010). These data suggest that both medical imaging and neurological testing are needed in determining patient care after TBI.

Standard Medical Imaging Techniques

Following TBI, CT is the preferred neuroimaging method as it has increased accessibility, acquisition speeds and is capable of detecting injuries, such as fractures and large hematomas, which require immediate surgical intervention (Edlow and Wu 2012). Comparison of clinical CT and conventional T1-weighted (T1WI) MRI, found that standard MRI techniques detected tissue abnormalities, including parenchymal lesions and diffuse axonal injury, at a higher rate than CT (Lee 2008). However when compared to more advanced MRI techniques, such as diffusion tensor (DTI) and susceptibility weighted (SWI) imaging, conventional MRI, including T1WI and T2-weighted (T2WI), demonstrates poor sensitivity and specificity for tissue abnormalities (Zivadinov 2008). This is likely due to the low contrast images produced by conventional MRI, which creates difficulty in injury evaluation and detection, as tissue changes are subtle. These limitations in standard MRI capabilities potentially explain why Lee et al. also found that neither CT nor standard MRI accounted for all observed cognitive deficits in their study, as several patients with neurological impairments had normal CT and MRI scans (Lee 2008).

Quantitating Standard MRI

Quantitative MRI values can be extracted from conventional MRI, such as T2WI, though this is not typically performed in the clinic due to time constraints and lack of computer algorithms that can readily analyze MRI scans. A few experimental studies using rodents have begun to develop quantitative semi-automatic MRI analysis protocols to investigate tissue pathology following moderate-to-severe TBI (Immonen 2009, Kharatishvili 2009, Irimia 2011). Using manually defined regions of interest, these studies reported positive correlations between T2-relaxation values and poor histological and behavioral outcomes at acute and sub-acute times following injury, suggesting that computational approaches could be used to predict long-term TBI outcome (Immonen 2009, Kharatishvili 2009). Similarly, we have developed a computational approach to semi-automatically categorize lesions into different types of pathology, including blood and edema, which have been shown to be detrimental to TBI outcome (Donovan 2012). More recently, an algorithm developed by Bianchi et al. utilized textural features from T2WIs of experimental mTBI and was able to identify lesion volumes with a 0.93 error rate when compared to manual segmentation (Bianchi 2013). Though, this algorithm limited lesion detection to the cortex, which was the region known to have had either an mTBI injury or sham surgery. While more work is required to develop automated programs for use in the clinic, these studies suggest that quantitative measures extracted from standard MRI can improve the diagnosis and prognosis of TBI.

Diffusion Tensor Imaging

Increasingly, DTI is being used in research to non-invasively detect white matter pathology following clinical and experimental TBI (Inglese 2005, Kraus 2007, Mac Donald 2007, Kumar 2009). DTI quantifies the directionality of water diffusion, which moves preferentially along white matter fibers with reduced movement perpendicular to axonal orientation due to cellular barriers, such as the myelin sheath and cytoskeletal structures (Niogi and Mukherjee 2010). A number of measures can be derived from DTI, including axial (AD) and radial (RD) diffusivities that represent axonal and myelin integrity, respectively. In addition, the mean diffusivity (MD), a reflection of total water diffusion in the tissues and fractional anisotropy (FA), an index of directional asymmetry, can also be measured using DTI. Experimental studies using shiverer mice have demonstrated that DTI measurements of AD and RD are good correlates of macroscopic axonal and myelin integrity, respectively (Song 2002). However, a study of multiple sclerosis using human spinal cord found that RD increased not only as a result of demyelination, but also as a result of axonal damage (Klawiter 2011). Thus while DTI correlates with particular types of white matter damage (myelin versus axonal), these measures are not absolute.

Clinically, DTI imaging of white matter in mild and moderate-to-severe TBI has revealed that all injury severities can result in altered water diffusion along fiber tracts (Inglese 2005, Kumar 2009, Kinnunen 2011). Few DTI studies however have been performed following experimental TBI, particularly in models

of mild injury. Interestingly, in a closed head injury model of rmTBI, induced 1 day apart to the same anatomical location, no DTI changes were detected immediately following the second injury, while reduced AD was observed 7 days later (Bennett 2012). Other experimental studies using moderate-to-severe TBI models have reported acute decreases in AD followed by delayed increases in RD 1-4 weeks post injury that correlated with histological measures (Mac Donald 2007, Mac Donald 2007, Li 2011, Li 2013). Using our model of bilateral repeated TBI, we have shown a widespread bilateral increase in RD within rmTBI animals at 14 and 60 days following injury, while only transient changes in AD at 14 and 21 days was observed. Our RD findings were consistent with electron microscopy (EM) findings, although EM analysis also revealed ongoing changes in axonal integrity not seen using MRI derived AD measures. Nevertheless, both experimental and clinical studies have demonstrated the importance of DTI, which can detect tissue abnormalities not visible using standard imaging.

Neuropathology

The extent of TBI pathology is dependent on the accumulation of damage caused by both the primary injury and the ensuing secondary cascades. Primary injury is unavoidable and occurs at the moment of TBI as a result of the impact force, causing skull fractures, brain contusions, diffuse axonal injury, and hemorrhage (Graham 1995). Following TBI, primary injuries immediately trigger secondary injury cascades that result in many of the observed TBI pathologies including edema formation, hemorrhage progression, white matter damage and

neuroinflammation (Povlishock and Katz 2005, Kurland 2012). Secondary damage greatly increases patient morbidity and mortality. Current TBI research focuses on identifying and better understanding secondary cascades, as it is thought that these pathways can be attenuated and/or prevented therapeutically.

Edema

Depending on TBI severity, edema formation peaks 24-48 hours following injury and resolves by approximately 7 days (Oehmichen 2003, Obenaus 2007). Brain edema is generally categorized as being vasogenic or cytotoxic. Where cytotoxic edema is defined as increased water movement into the cells from the extracellular space and vasogenic edema is characterized as increased water accumulation in the extracellular space from the vasculature. Vasogenic edema, resulting from blood brain barrier (BBB) disruption, has been reported within the first 60min following experimental TBI and resolves over the course of 7 days (Barzo 1997). In contrast, cytotoxic edema, believed to be the dominant form of edema following TBI, is observed within the first 24hrs of injury and continues to be seen 1-2wks following injury (Barzo 1997, Unterberg 2004). However, edema following TBI is believed to be a mix of the cytotoxic and vasogenic forms and contributes to brain swelling, which greatly increases the intracranial pressure (ICP) as the tissue begins to compress against the skull (Unterberg 2004). This then leads to compression of the vasculature, which reduces blood flow and oxygen delivery to the tissue, thus causing further hypoxic ischemic damage.

Clinical studies have reported that acute 5-10% increases in brain water content are associated with catastrophic outcomes, such as coma, following severe TBI (GCS<8) (Marmarou 2000, Ko 2012). Similarly an animal model of moderate TBI reported 2-3% increases in brain water content at 1 day following injury that continued to be observed at 1 week (Su 2014). Furthermore, animal models have shown that axonal injury and cell death occur for up to 2 weeks following TBI induced brain swelling, potentially leading to long-term white matter damage (Wang 2011, von Holst 2012). Clinically, brain swelling results in significantly increased patient morbidity and mortality, resulting in approximately 50% of all deaths following TBI (Balestreri 2006, Muehlschlegel 2013). Current treatments for brain swelling and increased ICP predominantly use osmotic therapy, such as hypertonic saline, hypothermia and decompressive craniotomies. However the effectiveness of these therapies are controversial and better methods for reducing brain swelling are needed. We have shown that manipulation of the inflammatory status at the time of experimental moderate-to-severe TBI reduces hemispheric swelling within 7 days of injury (unpublished data). Our data suggests that the immune system is a potential target for therapeutics designed to attenuate brain swelling following TBI.

Hemorrhage

Vessel damage at the time of TBI results in hemorrhage within the brain that can lead to further blood deposition in the hours and days following injury.

The expansion of an existing or the development of a new hemorrhagic lesion is referred to as hemorrhagic progression of a contusion (HPC) (Simard 2010). HPC has been observed clinically in both mild and moderate-to-severe TBI cases (Xue and Del Bigio 2000, Sifri 2004, Sifri 2006, Alahmadi 2010, Simard 2010, Kurland 2012). One clinical study quantified hematoma volume using CT, and reported that that 4% of hematomas shrank, 58% were unchanged and 38% increased in volume within 72 hours of TBI (mild to severe) (Chang 2006). Experimental moderate-to-severe TBI studies have shown that within 12 hours of injury, blood volume expanded (2-fold) from the cortical impact site to the hippocampus and thalamus (Simard 2009). Similarly, in our model of repeated mTBI, we found significantly increased blood deposition, particularly at the second injury site, at acute timepoints when injuries were spaced 7, but not 3, days apart (Donovan 2012).

Hemorrhage within the brain substantially increases tissue damage, as blood is particularly neurotoxic. Reactive oxygen intermediates, byproducts of aerobic respiration, react with iron to produce free radicals, which can damage DNA, lipids and proteins (Gaasch 2007). Experimental studies inducing intracerebral hemorrhage demonstrate increased TUNEL stained neurons and astrocytes within the lesion and peri-lesion at 24 and 48 hrs post injury (Matsushita 2000). Similarly, in vitro studies have shown that treatment of neuronal cultures exposed to hemoglobin with free radical scavengers attenuated apoptosis (Wang 2002). Edema formation and BBB disruption have also been

reported as a result of iron deposition within the tissue caused by intracerebral injection of lysed red blood cells (Xi 2001). Blocking of cellular cascades involved in vessel fragmentation attenuated HPC, decreased necrotic tissue and reduced behavioral deficits following experimental moderate-to-severe TBI (Simard 2009). However similar to edema induced brain swelling, current clinical management options primarily consist of invasive removal of blood clots that contribute to increased ICP and better therapeutics are needed to reduce hemorrhage induced tissue damage.

White Matter

White matter, comprised of axons (projections from neurons) and the myelin (from oligodendrocytes) that ensheathes them, is composed of fiber tracts that connects and allows communication between different brain matter regions. The long thin structure of white matter makes this tissue particularly vulnerable to the shearing forces of the TBI impact, which can stretch and twist these fibers. Additionally, neurons and oligodendrocytes can be damaged during secondary cascades initiated by blood deposition, edema formation and neuroinflammatory processes. Damage to fiber tracts is believed to play a significant role in the development of neurological and cognitive deficits (Kinnunen 2011). Several studies using DTI report increased axonal disruption, often involving several white matter structures, within the brains of patients exhibiting neurological deficits 2-7 years post injury (Kraus 2007, Kinnunen 2011). Histological studies

evaluating axonal pathology following human TBI have also reported acute (<120hrs) accumulation of amyloid precursor protein (APP) and long-term (27 days- 3yrs) axonal swelling and APP deposition (Blumbergs 1994, Chen 2009).

Animal studies have reported early axonal transport abnormalities within 14 days of injury that appeared to pseudo-normalize by 4 weeks in the absence of myelin changes (Spain 2010, Creed 2011, Shultz 2011). One long-term experimental study following a single moderate-to-severe TBI reported abnormalities in myelinated axon morphology at 3 months after injury and increased myelin debris and white matter thinning in the external capsule at 6 to 9 months following injury (Rodriguez-Paez 2005). Additionally, animal models of rmTBI have demonstrated white matter abnormalities at 7 days and lasting up to 7 weeks following injury (Laurer 2001, Shitaka 2011, Bennett 2012). Our data shows that repeated TBI induced to different anatomical locations results in both axonal and myelin damage at sub-acute times that continues to be observed chronically (Donovan 2014). Taken together these clinical and experimental studies demonstrate the evolving nature of white matter pathology, which has been shown to persist for years following clinical TBI, and potentially explains the chronic neurological deficits that are observed following head injury.

Neuroinflammation:

Inflammation occurs immediately following TBI and is believed to play a significant role in instigating secondary damage. Microglia, the resident CNS

macrophages, are highly motile in their “resting” state and are the first cells to respond to injury (Nimmerjahn 2005). Upon laser-induced lesion to the BBB, microglia immediately react by increasing directed contact with the damaged area (Nimmerjahn 2005). However, the benefit of microglial activation and response to injury is a topic of debate as animal studies have demonstrated that these cells can exert neuroprotective and neurotoxic functions.

In vitro studies of microglia exposed to necrotic neurons increased expression of pro-inflammatory cytokines, including IL-6 and TNF, and enzymes, such as iNOS (Pais 2008). Upon exposing healthy neurons to media collected from these activated microglia increased neuronal death was observed, suggesting that secreted molecules from microglia are neurotoxic (Pais 2008). In contrast a study exposing neurons to media from a mixed astrocyte/microglial culture activated by a toxicant demonstrated increased neuronal survival, suggesting that microglial activation in itself is not necessarily detrimental to neuron survival (Shinozaki 2014). Rather the type of activation and molecules secreted are important. Activated microglia are critical for the removal of apoptotic cells and cellular debris, which if not removed could cause further tissue damage. Our studies using a moderate-to-severe TBI have shown reductions in hemispheric swelling that coincide with increases in microglial activation compared to naïve animals. However this increased microglial inflammation demonstrates a different gene expression pattern from the whole tissue. Likely the beneficial and/or detrimental role of microglia following injury

depends on the pathologic conditions and timing from injury induction, as these cells are highly plastic.

While microglia predominantly mediate the brain response to injury, astrocytes and neurons can also contribute to ongoing inflammation through the expression of various cytokines, such as TNFα, which can activate microglia and play a role in the breakdown of the BBB (Liu 1994, Rosenberg 1995, Dong and Benveniste 2001). Additionally, peripheral leukocytes, including neutrophils, macrophages and T-cells, can infiltrate the brain parenchyma and contribute to inflammation (Czigner 2007, Hsieh 2013, Roth 2014). Similar to microglia, macrophages and neutrophils can carry out both cytotoxic and cytoprotective processes. However the roles of these cells are not well defined. Kenne et al. (2012) reported that depletion of neutrophils following mTBI attenuated tissue damage and acute reductions in brain water content, however, Roth et al. (2013) demonstrated that reducing neutrophil recruitment to the brain resulted in increased cell death following a mild compression TBI. Additionally, a study on the role of macrophages following moderate-to-severe TBI revealed that this cell population is heterogeneous with subsets being biased toward pro- or anti-inflammatory processes (Hsieh 2013). Though knockout of CCR2, a chemokine receptor expressed on pro-inflammatory monocytes, resulted in improved cognitive function following a moderate-to-severe TBI, suggesting that limiting macrophage infiltration into the brain is beneficial to injury outcome (Hsieh 2014). These studies demonstrate that the inflammatory response following brain injury

is highly complex, involving many different cell types and depending on injury severity. The interactions between these different cell types in addition to the pathways they activate need to be better explored in order to determine how to target the immune response for therapeutic intervention.

Dissertation Overview

Chapter 2 assesses the time window of brain vulnerability following rmTBI induced 3 or 7 days apart. Based on previous studies we hypothesized that injuries induced 3 days apart would result in exacerbated tissue damage, whereas a 7-day interval was not expected to show worsened outcomes. We found that rmTBI lesion volume and composition was dependent on location of and time between injuries. The results of this study have been published in Neuroimage Clinical (Donovan 2012). Exacerbated grey matter pathology was transient. We therefore assessed white matter pathology at times following resolution of obvious grey matter pathology in Chapter 3. We hypothesized that rmTBI induced 7 days apart would result in predominantly axonal disruption at sub-acute times, while myelin damage would be prevalent long-term. We found changes in both axonal and myelin integrity following rmTBI at both timepoints. However, at sub-acute times white matter damage was localized to regions immediately adjacent to the impact sites, while long-term changes in integrity appeared widespread. Long-term examination of white matter damage has been published in the Journal of Cerebral Blood Flow and Metabolism (Donovan

2014). In Chapter 4, we assessed the impact of inflammatory status at the time of injury on TBI pathology. Based on studies showing improvements following anti-inflammatory administration, we hypothesized that systemic inflammation (LPS 24hrs prior to TBI) or deficiency in a microglial anti-inflammatory molecule (TREM2) would exacerbate tissue damage following a moderate-to severe injury. Unexpectedly, this study revealed acute decreases in hemispheric swelling that coincided with limited microglial activation within TREM2KO and LPS-challenged animals. Taken together these studies lay a foundation for future experiments exploring the roles of inflammation in tissue damage and recovery following single and repeated TBI.

Chapter 2

Repeated Mild Traumatic Brain Injury Pathology is Dependent on the Time Between and Location of Injuries.

Abstract

Mild traumatic brain injury (mTBI) has become an increasing public health concern as subsequent injuries can exacerbate existing neuropathology and result in neurological deficits. Unlike previous studies, which induced mTBIs to the same anatomical location, this study investigated the temporal development of cortical lesions resulting from two mTBIs delivered to opposite hemispheres. We hypothesized that injuries induced 3 (rmTBI 3d), but not 7 (rmTBI 7d), days apart would result in worsened TBI damage assessed using MRI. Unexpectedly, quantification of lesion volumes 1d post last injury revealed increased tissue abnormalities within rmTBI 7d animals compared to other groups, particularly at the site of the second impact. Histogram analysis of MRI values from abnormal tissue suggested increased edematous tissue and blood deposition within rmTBI 3d and rmTBI 7d animals, respectively. Quantification of lesion composition supported our histogram findings, showing increased edema at the site of second impact in rmTBI 3d animals and elevated blood deposition in the rmTBI 7d group at the site of the first injury. Histological measurements revealed spatial overlap of regions containing blood deposition and microglial activation within the cortices

of all animals. In conclusion, our findings suggest TBI induced tissue damage is dependent on both the time interval between and the location of injuries.

Introduction

Traumatic brain injury (TBI) affects an estimated 1.7 million individuals and contributes to a third of injury-related deaths annually in the United States, with mild TBI (mTBI) accounting for approximately 75% of all TBI cases (Tagliaferri 2006, Corrigan 2010, Faul 2010). Comparison of clinical computed tomography (CT) and magnetic resonance imaging (MRI) scans found that MRI allows for increased detection of TBI related abnormalities (Lee 2008). However given the standardized definition of mTBI, which describes mild injuries as not having observable changes on standard MRI, new approaches are warranted to assess mTBI from neuroimaging data (VA/DoD 2009).

Mild Injuries produce low contrast subtle tissue changes on standard MRI, such as T2 weighted imaging (T2WI), creating difficulty in detecting an mTBI. As a result, enhanced MRI quantification methods are needed to identify and monitor the progression of mild injuries. Currently, many of the studies developing quantitative approaches for analyzing TBI damage have focused on moderate-to-severe injuries (Immonen 2009, Kharatishvili 2009, Irimia 2011). These studies have used semi-automatic approaches, where regions of interest are manually defined following experimental TBI, and reported positive correlations between T2 relaxation values and poor histological and behavioral outcomes (Immonen 2009, Kharatishvili 2009). However, little work has been

done using models of mTBI. One study in which an automated method of whole brain MRI analysis was developed, demonstrated increased abnormal gray matter within the first five hours following experimental mild and severe TBI (Colgan 2010). However, long-term (days, weeks) quantitative computational MRI analysis of the evolution of neuropathology following mild injuries, and in particular repeated injury, remains unexplored.

One of the many consequences of TBI is microvascular dysfunction, which can result in tissue ischemia, edema and hemorrhagic progression (Kurland 2012). Depending on the type and severity of brain injury, edema formation typically occurs 24-48 hours following injury and resolves by approximately 4-7 days, while hemorrhagic lesions can occur within 3-4 days and resolution can take months (Oehmichen 2003, Obenaus 2007, Kurland 2012). Hemorrhagic progression of a contusion (HPC) is the expansion of an existing or the development of a new hemorrhagic lesion (Simard 2010). HPC has been reported in observed mild to severe clinical cases and can substantially increase tissue damage, as blood is particularly neurotoxic (Xue and Del Bigio 2000, Sifri 2004, Sifri 2006, Alahmadi 2010, Simard 2010, Kurland 2012). A study using experimental moderate-to-severe TBI has demonstrated that vessel fragmentation plays a key role in HPC development and blocking these cellular cascades results in less necrotic tissue and improved behavioral outcomes (Simard 2009).

Most patients who sustain an mTBI appear to recover normally from the injury, though there is evidence that sustaining multiple mTBIs can result in cumulative detrimental effects (Belanger 2010). However little is known about the underlying pathology and long-term consequences of repeated mTBI (rmTBI). Animal models where two injuries were induced to the same location showed increased brain vulnerability if injuries were 1-5 days apart (Laurer 2001, Longhi 2005, Shitaka 2011). However two mTBIs 7 days apart did not result in exacerbation of injury (Longhi 2005). Additional models of rmTBI in which four or five injuries were induced to the same location 24 hrs apart, demonstrated persistent neurological deficits with no overt cell death or blood brain barrier disruption (DeFord 2002, Kane 2012, Shultz 2012). Surprisingly, all of the reported models of rmTBI had repeated injuries to the same anatomical location and what remains to be elucidated are the effects of multiple injuries to different brain locations.

The objective of our study was to evaluate whether the ongoing neuropathology from an initial mTBI was altered by a second contralateral injury induced 3 or 7 days later. We hypothesized that injuries induced 3d apart would result in larger lesion volumes at the site of the second injury, while little or no change in lesion volume was expected within groups receiving impacts 7d apart.

Methods

Mild Traumatic Brain Injury

Fifty adult male Sprague Dawley rats ages 2-4 months were randomly assigned to three experimental groups: Single mTBI and repeated mTBI induced either 3 (rmTBI 3d) or 7 (rmTBI 7d) days apart (Figure 2.1A). A mild controlled cortical impact (mCCI) was used to induce mTBI as previously described (Obenaus 2007), with minor modifications. Briefly, anesthetized rats (Isoflurane: 3% induction, 1-2% maintenance) were secured into a stereotactic frame and a midline incision exposed the skull surface. A craniectomy (5mm diameter) was performed over the right hemisphere 3mm posterior and 3mm lateral from Bregma (Figure 2.1B), where a mCCI (4mm diameter tip, 0.5mm depth, 6.0 m/s speed, 200 ms dwell) was delivered using an electromagnetically driven piston (Leica Biosystems Inc., Richmond, IL). Animals within the rmTBI groups received a second craniectomy and mCCI on the opposite (left) cortical surface (identical Bregma coordinates) 3 or 7 days after the first mCCI (Figure 2.1A, B). At the end of each surgery a sterile nylon flap (~1 cm^2) was placed over the craniectomy and the incision was closed.

MRI Data Collection:

Animals were anesthetized (isoflurane: 3% induction, 1% maintenance) for MRI at: 1d post first injury (D1), 1d post last injury (D1 Singles, D4 rmTBI 3d, D8 rmTBI 7d), 14d post injury (D14: 14d post first injury for all animals, D17: 14d post last injury for rmTBI 3dl D21: 14d post last injury for rmTBI 7d) and ≥60 (60-

68) days post first injury (Figure 2.1A). Due to imaging constraints, all MRI was performed within 24 hours of the targeted time point with the exception of the rmTBI 3d group, which received imaging at 17d rather than 21d post initial injury. *In vivo* T2 weighted images (T2WI; TR/TE/FA = 3453 ms/20 ms/20°, 25x1 mm slices) and susceptibility weighted images (SWI; TR/TE/FA = 39 ms/20 ms/20°, 48x0.8 mm slices) were acquired with a 256x256 matrix using a 4.7T Bruker Avance. SWI was used to identify extravascular blood within tissues and T2WIs were used to create T2 maps computed using in-house software (Obenaus 2007).

MRI Data Analysis:

Regions of interest (ROI), manually drawn on T2WIs using Cheshire image processing software (Hayden Image/Processing Group, Waltham, MA), included the right and left hemispheres and cortical areas containing observable abnormalities (hyper/hypo-intense signals). In a subset of animals (n=20) transient edema was observed within the corpus callosum following the initial impact that did not expand following a second impact and quickly resolved; in this group we only assessed cortical abnormalities.

T2 value ranges for blood, edema and normal appearing brain (NAB) containing voxels were determined by taking the average T2 value of manually segregated blood and edema lesion pixels. This was performed using a training-set composed of MRI scans (6 MRI scans evaluated) collected at 1d post last injury from animals in each group that contained lesion volumes representative of

the group average and contained both edema and blood. From this analysis, lesion voxels were classified as blood (<69 ms), edema (>90 ms), NAB (70-89 ms) or noise (>500 ms) (Figure 2.1C). T2 histograms of the entire lesion volume were created and kurtosis, skewness, mean and peak values were calculated for each injury histogram. Total (first+second) histograms were analyzed at 1d post last injury and 14d post first injury; first and second injury histograms were analyzed at 1d post last injury and 14d post injury (first: 14d post first, second: 14d post last injury).

Lesion, edema and blood volumes were divided by the whole brain volume to account for differences in brain size between animals. Total lesion volumes (first+second) were analyzed from animals at 1d post last injury, 14d post first injury and at the time of final MRI (Single, rmTBI 7d: 60-68d and rmTBI 3d: 21d post first injury). First and second lesion, blood and edema volumes were analyzed at 1d post last injury and 14d post injury (first: 14d post first, second: 14d post last injury). Calculations for total (first+second), first and second lesion volumes and blood and edema volumes were performed where: a) Total lesion volume was calculated by dividing the total lesion volume (first+second) by the total brain volume, b) first and second lesion volumes were calculated by dividing the first or second lesion volume by total brain volume and, c) blood and edema volumes were calculated by dividing the volume of blood or edema found in either the first or second lesion and dividing this by the respective first or second lesion volume.

Tissue Collection:

Following the final MRI session animals were sacrificed via transcardial perfusion. Extracted brains were prepared for staining as previously described (Obenaus 2007). Briefly, brains were post-fixed in 4% PFA overnight, undergoing two 30 min PBS washes following fixation. Prior to cryosectioning, brains were placed in 30% sucrose and embedded in optimal cutting temperature compound (O.T.C., Tissue Tek; Sakura Fine Tek, Torrance, CA). Coronal sections (30 μm) were collected using a Leica CM1850 cryostat (Leica Microsystems GmbH, Wetzlar Germany) and mounted directly on gelatin-chrome-alum-coated slides for histological staining (stored at –20°C) or were free floating (stored in cryoprotectant solution at 4°C) for immunohistochemistry.

Histochemistry:

All staining was performed on slices centered under the lesion site at 14d post first injury. Prussian blue staining was performed as previously described (Obenaus 2011) to detect extravascular blood within the tissue. Degenerating neurons were detected using Fluoro-Jade B (Millipore, Temecula, CA) staining on thawed tissue sections as previously described (Schmued and Hopkins 2000).

Immunohistochemistry was performed on free-floating sections as previously described (Obenaus 2007). Immunolabeling was performed for astrocytes, using glial fibrillary acidic protein (GFAP; Millipore, Temecula, CA, 1:1000), and microglia, using ionized calcium binding adaptor molecule 1 (IBA1;

Wako, Carpinteria, CA, 1:400). Secondary antibodies used included goat anti-mouse Alexafluor 488 (Invitrogen, Carlsbad, CA, 1:400) and goat anti-rabbit rhodamine (Millipore, Temecula, CA, 1:200). Negative controls omitted the primary antibody during the staining procedure.

The extent of blood deposition (Prussian blue) and activated microglia (IBA1) within the tissue was quantified using NIS Elements Software (Nikon Instruments Inc., Melville, NY, USA). A total of three animals (2 sections/animal), containing lesion volumes representative of the group average, were selected from each experimental group and were used to measure the medial-lateral and dorsal-ventral dispersal of blood deposition and activated microglia within the injured cortices. Activated microglia were identified based on visual signal intensity and cellular morphology as previously described (Obenaus 2008).

Statistics:

To correct for variability following the initial mTBI, data points were normalized to each animal's initial recorded value (current value/initial value), such that all animals received a score of 1 for the first impact. A non-parametric Kruskal-Wallis analysis of variance (ANOVA) was used for statistical analysis of the total (first+second) lesion volume as this data failed to meet the requirements of normality using a Shapiro-Wilk test. A one-tailed t-test was used to test the rmTBI 7d second lesion volume against the Single first lesion volume, as we hypothesized that the site of the second impact would have a greater injury volume than a Single injury alone. However, two-tailed t-tests were used to

compare the first and second lesion volumes of all groups at 14d post injury. Further, two-tailed t-tests were used to evaluate the first and second blood and edema volumes at 1d post last injury. A p value < 0.05 was considered significant (n=22 Single, 4 rmTBI 3d, and 15 rmTBI 7d); error bars represent the mean ± SEM.

Results

Lesion composition is dependent on the interval between rmTBI.

Analysis of the mTBI lesion was first evaluated using total lesion (first+second) T2 value histograms to ascertain temporal changes and identify rmTBI group differences at 1d post last injury. We hypothesized that histograms from rmTBI 7d animals would appear similar to those from the Single group. Compared to Singles, the rmTBI 3d animals exhibited a rightward shift in the T2 total lesion histograms suggesting increased edematous tissue that was not seen in the rmTBI 7d group (Figure 2.2, top panel). In contrast, a leftward shift was observed in the rmTBI 7d lesion compared to Single animals (Figure 2.2, top panel) consistent with increased blood deposition. We then further assessed each injury site independently and found that the T2 histogram at the site of the initial injury of both rmTBI groups had a leftward shift (increased blood) compared to animals receiving only a Single mTBI. However at the site of second injury, the rmTBI 3d group exhibited a dramatic shift rightward indicating increased edema, while the rmTBI 7d animals demonstrated a similar T2 profile to that observed in Single animals (Figure 2.2, top panel).

At 14d post first mTBI, total brain histograms revealed a strong leftward shift in all experimental groups, demonstrating that at this sub-acute time point the edema seen at 1d post last injury had resolved. Further, the strong leftward shift of the histogram (T2 peak values: Single =52.6ms, rmTBI 3d = 47.8ms, rmTBI 7d= 55.5ms; see Table 1.1) in all groups suggests that extravascular

blood deposition substantially contributed to the overall lesion composition at this later time point (Figure 2.2, bottom panel). A closer examination of the lesion created by the initial impact revealed that all groups exhibited a similar T2 profile at 14d post first injury (Figure 2.2). However at the second impact site, the rmTBI 3d animals demonstrated a leftward shift compared to its 1d post last injury data and the rmTBI 7d group at 14d post second injury, indicating the presence of blood and resolution of acute edema (Figure 2.2). The site of the second impact in rmTBI 7d animals shared a similar T2 distribution to that of Singles (Figure 2.2).

Quantitative evaluation of total lesion histogram features was undertaken (Table 1.1) with no significant differences in the T2 peak values between any group or time point. However, the mean histogram T2 values within the total lesion at 1d post last injury revealed a significant ($p=0.015$) increase in T2 values within the rmTBI 3d group compared to the rmTBI 7d group (Table 1.1). At 14d post first injury there were no significant differences between mTBI groups. Analysis of skewness (measure of distribution asymmetry) and kurtosis (peakedness of a distribution) revealed significant differences, with the rmTBI 3d group having increased skewness ($p=0.026$) and kurtosis ($p=0.034$) compared to the Single group but only at the 14d post injury time point (Table 1.1). In contrast, the rmTBI 7d group had significant increases in skewness ($p=0.042$) and kurtosis ($p=0.03$) compared to Singles only at the 1d post last injury time point (Table 1.1).

Injury volume is dramatically increased at acute time points in rmTBI animals.

We hypothesized that injuries induced 3, but not 7, days apart would result in increased abnormal tissue volume on MRI. The anterior-posterior extent of the mTBI injury volume was assessed computationally and included all tissue abnormalities, including blood (hypo-intense) and edema (hyper-intense) (Figure 2.3A). A Single mTBI resulted in an average total brain lesion volume of 1.4± 0.002% of total brain volume at 1d post first injury, which appeared to have a heterogeneous mixture of blood and edema (arrowheads; Figure 2.3A). Following a second mTBI (1d post last) the rmTBI 3d group exhibited increased edematous tissue (white arrowheads) at the site of the second impact, while a more heterogeneous lesion appeared at the site of the initial injury (Figure 2.3A). However in rmTBI 7d animals, injury was composed primarily of blood at the site of the initial impact, while a larger injury of similar composition to that of a Single mTBI was observed at the site of second impact (white arrowheads; Figure 2.3A). At the time of last MRI, little or no observable abnormalities were detected within the tissues (Figure 2.3A). Volumetric 3D reconstruction of mTBI volumes illustrates the location and extent of the mild injury of our model revealing an increase in total lesion volume within rmTBI 7d animals compared to other groups (Figure 2.3B).

Temporal mTBI injury volumes were further assessed to determine whether ongoing pathology from the first mTBI resulted in an exacerbation of lesion volume following a second mTBI (Figure 2.3C). The rmTBI 7d group

demonstrated a significantly increased lesion volume (p=0.018) compared to other groups at 1d post last injury (Figure 2.3C). The observed increases in the rmTBI 7d lesion volumes were transient with lesion volumes similar to those observed in other groups by 14d post first injury (Figure 2.3C). We then further dichotomized the mTBI injury volume by examining independently the first and second lesion volumes to test whether differences existed between the first and second injuries. This analysis revealed a significant increase (p=0.029) in lesion volume at the site of the second injury within rmTBI 7d animals 1d post last injury compared to Single animals, which was not observed in the rmTBI 3d group (Figure 2.3D). The rmTBI injuries seen at the site of initial impact appeared similar to that observed in Single animals at 1d post last injury (Figure 2.3D). By 14d post injury (first: 14d post first, second: 14d post last injury), significantly decreased lesion volumes were observed in all rmTBI animals compared to Singles (Figure 2.3D).

Interval between rmTBI dictates injury characteristics: edema versus blood

We next tested whether the formation of blood and edema differenced between the rmTBI groups. Based on visible MRI changes, we hypothesized that rmTBI 7d animals would demonstrate increased blood deposition, while rmTBI 3d rats would show more edema formation. To test this hypothesis, computational analyses of the first and second lesions was performed to determine the relative contribution of blood and edema (based on T2 values) at

each injury site (Figure 2.4). At 1d post last injury, computational analysis of the voxels containing blood (green), edema (red) and NAB (blue) at the injury sites clearly demonstrates that lesion within Single mTBI animals had a mixture of voxels containing blood, edema and NAB as was seen in the MR images (arrowheads; Figure 2.4A). In contrast rmTBI 3d animals exhibited predominately edema (red) at the site of the second rmTBI, as was observed in T2 MR images (hyper-intense signal; arrowheads). The site of first injury within rmTBI 7d animals exhibited almost entirely blood (green) containing voxels, which can also be seen in T2 and SWI MR images (arrowheads; Figure 2.4A).

Quantification of these voxel groups following a second impact in rmTBI 3d animals demonstrated a significant ($p=0.038$) increase in the number of edema voxels (increased volume) 1d post last injury, which dramatically resolved by 14d post injury (first: 14d post first, second: 14d post last injury) compared to Single animals (Figure 2.4B). Further the rmTBI 3d group had a significantly ($p=0.003$) greater edema volume than rmTBI 7d animals. The site of initial injury within the rmTBI 3d group also showed elevated edema volumes compared to other groups, though this was not significant (Figure 2.4B). In contrast, the second injury in rmTBI 7d animals exhibited similar edema volumes to that observed after a Single mTBI, while the first lesion had a significant ($p=0.001$) decrease in edematous tissue compared to the Single group at 1d post last injury (Figure 2.4B).

Both injury sites of rmTBI 7d animals demonstrated a significant increase (R: p=0.0001; L: p=0.025) in blood volume compared to a Single mTBI at 1d post last injury (Figure 2.4C). However, while there was an increase in the total amount of blood seen in the rmTBI 7d animals, the first and second blood volumes were not significantly different from each other. Further the rmTBI 7d group contained significantly more blood than the rmTBI 3d group (p=0.04). The first lesion within rmTBI 3d animals had a similar blood volume to that seen after a Single mTBI 1d post injury, while the site of second injury had a smaller blood volume compared to other injury groups (Figure 2.4C). Significant differences (p=0.047) in blood volume were still observed 14d following the initial injury, while blood deposition at the site of the second mTBI appeared similar between the rmTBI groups at 14d post second injury (Figure 2.4C).

Prussian blue staining for extravascular blood at the site of the lesions was performed 14d post first injury and supported our MRI analysis, demonstrating increased blood deposition within the rmTBI 7d animals compared to other groups (Figure 2.4D). Blood deposition also appeared concentrated underneath the impact site within the Single and rmTBI 3d groups, while the rmTBI 7d animals had a more diffuse deposition (see below, Figure 2.4D).

Activated microglia demonstrates spatial overlap with blood deposition.

We then asked whether increased microglial activation would be present within the cortex of rmTBI 7d animals. Based on our computational analysis of

lesion composition, we hypothesized that blood deposition would appear more diffuse and be associated with increased microglial activation at the site of the second injury within rmTBI 7d animals. We undertook an analysis of the distribution of Prussian blue staining (blood) at 14d post first injury (Figure 2.5), where we observed a modest increase in the blood containing area at the site of the first impact in rmTBI 7d animals (Figure 2.5A). In contrast, the site of the second injury in rmTBI 3d animals revealed blood deposition primarily underneath the impact site, while rmTBI 7d animals demonstrated a dramatic increase in width and depth of blood (Figure 2.5A), often down to the corpus callosum.

Measurements of activated microglia (IBA1) containing regions revealed a similar profile with locations encompassing blood deposition (Figure 2.5A). The site of initial injury demonstrated a smaller area of microglial activation compared to blood containing zones in both rmTBI 3d and Single groups, while regions were approximately the same size in rmTBI 7d animals (Figure 2.5A). In contrast, the site of second injury in both rmTBI groups had an increased dispersion of microglial activation beyond the regions containing blood, which was most prominent within the rmTBI 7d group (Figure 2.5A).

A modest number of Fluoro-Jade positive cell-bodies were observed at the site of the second impact in rmTBI 7d animals suggesting some ongoing neuronal degeneration, which was not seen in the first lesion or in other groups (Figure 2.6). However in all mTBI groups punctate staining was observed,

reminiscent of axonal or dendritic debris, at the site of the first injury but not in the left non-injured cortex of Single animals suggesting ongoing microstructural damage (Figure 2.6).

Discussion

We initially hypothesized that injuries induced 3 days apart would result in increased tissue damage, while those given 7 days apart not. Unexpectedly, we found that our starting hypothesis was incorrect. Rather, we found: 1) Increased lesion volume within rmTBI 7d animals, which was not observed in the rmTBI 3d animals; 2) Hemorrhagic progression of the lesion was detected, using a voxel-wise comparison, within the lesion of rmTBI 7d animals, while increased edematous tissue was observed in rmTBI 3d animals; 3) At the site of the second injury, an increased inflammatory response was detected in both rmTBI groups, while ongoing neuronal death was only observed in rmTBI 7d animals. Taken together, our study demonstrates that TBI pathology is dependent upon the interval between and location of mTBI events.

Lesion histograms predict temporal changes in rmTBI pathology.

Initially, we used voxel-wise T2 histograms to analyze rmTBI lesions to evaluate global temporal changes in tissue pathology. This is the first report using T2-histograms in an experimental model of mTBI, as there are no previous publications to our knowledge. In contrast, other clinical studies and animal models of central nervous system (CNS) injuries including tumors, spinal cord injury and ischemia, have used histogram analysis (Nevo 2001, Kopelman 2005, Veltkamp 2005, Emblem 2008).

Clinically, histograms have also been employed to quickly assess whole brain and tissue-specific (white and grey matter) MRI changes in mild to severe TBI (Shanmuganathan 2004, Lipton 2008, Marquez de la Plata 2011). While histogram analysis has demonstrated some ambiguity in sensitivity from clinical data others have reported its effectiveness to discriminate TBI. Whole-brain histograms in mTBI patients undergoing diffusion tensor imaging (DTI) found no differences in the mean diffusivity (MD) and fractional anisotropy (FA) measurements between injured and control patients (Inglese 2005). However when the histogram analysis was focused to ROIs drawn within white matter tracts susceptible to mTBI, increased MD and decreased FA were observed in injured patients (Inglese 2005). In contrast, application of global histograms (whole white matter) from DTI images was able to discriminate between mTBI, reporting decreased FA without the need for ROIs (Benson 2007). These clinical studies suggest that histograms have the potential to detect subtle tissue changes associated with mild injuries when analysis is focused on specific brain regions rather than performing whole-brain histogram analysis. In our study we observed temporal histogram skewness and kurtosis changes within defined mTBI lesions, suggesting tissue heterogeneity associated with edema resolution and ongoing blood deposition. These findings confirm that histogram analysis has the potential to discriminate between the mTBI groups as the lesions progress and resolve over time. Our results set a foundation for future comparisons of whole brain and regional histogram analysis so that additional

methods can be developed for efficient and accurate comparisons of clinically defined mTBI.

Exacerbation of rmTBI lesion volume is dependent on the time interval between injuries.

We found that tissue damage was exacerbated following a second mTBI, particularly when the injuries were 7d apart. The increased lesion volume was predominantly due to exacerbated tissue damage at the site of the second injury. This suggests that a Single mTBI can affect distant brain regions in such a way that they remain vulnerable to a subsequent injury.

The neuropathology and long-term consequences of rmTBI are not well understood. Rodent models of experimental rmTBI have demonstrated that there exists a window of vulnerability in which two injuries can result in exacerbated tissue damage (Longhi 2005, Vagnozzi 2007). Animals sustaining mTBIs 3 or 5 days apart on the same hemisphere exhibited increased cognitive deficits for up to a week following injury and cell death and axonal disruption 72 hours following the last injury (Longhi 2005). Similarly, an examination of changes in energy metabolism using MR spectroscopy, demonstrated the greatest changes following mTBIs sustained 3d apart and which persisted for up to a week (Vagnozzi 2007). However, the changes observed by Longhi et al (2005) were not observed in animals receiving two impacts 7 days apart, while alterations in metabolism described by Vagnozzi et al. (2007) were not observed

in animals sustaining injuries 5 days apart. Collectively, these studies suggest that by >5 days the tissue has had enough time to heal and so a second impact was similar to sustaining a Single mTBI when delivered to the same hemisphere. Additional rmTBI studies inducing two impacts 24 hours apart have further supported these findings, where in the absence of gross histological abnormalities, increased neurological deficits were persistent for several weeks with an acute increase in axonal injury and increased inflammation (Laurer 2001, Shitaka 2011).

However these models induced rmTBI to the same anatomical location, while our model induces mTBI injuries distant from each other. This suggests that brain vulnerability is dependent not only on the interval between injuries but also the location where the injuries are sustained. Patients sustaining an mTBI demonstrated metabolic tissue deficits for approximately 1 month following injury while those sustaining a second mTBI within 10-13 days of the first demonstrated a prolonged alteration (Vagnozzi 2008). While perhaps brain regions close to each other may have a shorter window of vulnerability, locations farther apart appear to have a delayed or lengthened period of vulnerability.

HPC primarily contributes to the lesion volume of rmTBI 7d animals.

Computational analysis of blood and edema contribution to the abnormal tissue volume revealed that rmTBI 3d animals had increased edema volumes, while the rmTBI 7d group exhibited increased blood deposition. By 14d post

injury (14d post first and 14d post last injury) the lesions of both rmTBI groups appeared to have a persistent increase in blood deposition, while edema resolved. It is important to note that extravascular blood can demonstrate a temporal change in MRI signature, as observed in an animal model of intracranial hemorrhage (IHC) (Belayev 2007). However due to the mild nature of our TBI model and the ongoing blood deposition, as a result of hemorrhagic progression, we would expect a different temporal course of extravascular blood deposition than that observed following IHC.

Our findings of increased blood deposition with time concur with the concept of hemorrhagic progression of the contusion (HPC), which has been modeled experimentally in moderate to severe traumatic brain and spinal cord injury (Gerzanich 2009, Simard 2009). Within 12 hours of a moderate to severe TBI, HPC was observed where the blood volume expanded (2 fold) into the hippocampus and thalamus (Simard 2009). Similarly, in our rmTBI 7d model, at 1d post last injury we observed a 2.5 fold increase in blood volume at the site of the initial injury in the rmTBI 7d group. Several studies have demonstrated concordance between Prussian blue staining of tissue iron deposition and T2 weighted MRI (Thulborn 1990, Belayev 2007, Gupta 2012). Our histological staining for extravascular blood further supported the expansion of bleeding in the rmTBI 7d animals, which was not observed in other mTBI groups nor has been reported in other models of rmTBI.

Models of CNS injury have identified the sulfonylurea receptor1-regulated $NC_{Ca\text{-}ATP}$ channel (SUR1/TRPM4) as a key mediator in the development of HPC (Gerzanich 2009, Simard 2009). These molecules are upregulated following trauma and upon depletion of ATP, a deregulation of this channel occurs leading to capillary fragmentation and hemorrhage (Simard 2010). HPC in our model was identified using temporal MRI at acute time points and Prussian blue staining at sub-acute times following injury. Our tissue was collected at late time points, thus we could not identify the cellular cascades, which occur within hours to days following trauma (Simard 2009).

Clinically, HPC has been identified using CT, where approximately 45-50% of patients develop this pathology following a mild to severe TBI (Sifri 2004, Sifri 2006, Narayan 2008, Alahmadi 2010). In a clinical study quantifying changes in hematoma size, using CT following a TBI (mild to severe), found that 4% shrank, 58% were unchanged and 38% increased in volume within 72 hours (Chang 2006). Clinical evidence of HPC suggests that medical imaging can be used to identify this pathology, though future experimental studies of the underlying cascades need to be performed to validate and better understand the underlying HPC mechanisms.

Another potential mechanism for our observed increase in blood volume could be due to extracellular matrix remodeling and subsequent revascularization of the tissue. In models of ischemic stroke, hemorrhagic transformation has been observed and associated with breakdown of the extracellular matrix (ECM),

which contributes to microvascular integrity (Hamann 1995, Fukuda 2004). Metalloproteinases (MMP) have been shown to be associated with microvessel ECM degradation and blood brain barrier permeability following experimental models of stroke (Fukuda 2004, Gidday 2005). In models of moderate to severe TBI, MMPs are upregulated with maximal levels being reached at 24 hours and can remain high for up to 7 days following injury (Wang 2000, Hayashi 2009). In cell culture models of ischemia, microglia increased secretion of the inactive form of MMP-9, which in non-human primate models of stroke demonstrated a linear relationship with blood deposition (Del Zoppo 2012). Treatment of moderate TBI with Minocycline, a drug shown to suppress microglial activation, inhibited MMPs and resulted in increased synaptic preservation (Ding 2009). Additionally, knockout of MMP-9 demonstrated decreased lesion volumes and improved neurological outcomes following moderate TBI compared to control mice (Wang 2000). Future examination could include tissue collected at these early time points for changes in the ECM as a result of MMPs. Collectively these studies demonstrate that MMPs play a role in tissue exacerbation following trauma though their role in HPC is not clear.

Increased neuroinflammation at the site of the second injury in rmTBI animals.

Extravascular blood within brain tissues can result in apoptosis and initiate a neuroinflammatory response, including peripheral leukocyte infiltration and microglial activation (Gong 2000, Xue and Del Bigio 2000). We found that there

was a distinct overlap of brain regions containing activated microglia and extravascular blood, although microglial responses encompassed a slightly larger area at the site of the second impact, particularly in the rmTBI 7d group. Microglia have been identified as potential aggravators of CNS tissue damage. During CNS infection or injury classically activated microglia release reactive oxygen species causing further tissue damage, but suppression of microglia demonstrates decreased TBI related tissue loss (Boje and Arora 1992, Homsi 2009). A study of the inflammatory response to microhemorrhages within brain tissue found that microglia within 200□m of blood can remain responsive for up to 7 days (Rosidi 2011). Our observed increase in microglial response and its detrimental effects is consistent with increased lesion volumes observed at the site of second injury within rmTBI 7d animals.

Conclusions

Our new model of rmTBI, in which injuries were induced to opposite hemispheres, demonstrated that there exists a window of tissue vulnerability following an initial mTBI. We previously hypothesized that animals receiving impacts 7d apart would not exhibit increased tissue damage, while injuries sustained 3d apart would result in larger lesion volumes specifically at the site of the second injury. However, our data supports that this temporal window occurs at a later time point than previously described (7d vs. 3d) and is likely the result of the second injury location being distant from the first. Analysis of cortical

abnormalities using our rapid computational approach revealed increased blood deposition within rmTBI 7d animals consistent with HPC, which was not observed in the rmTBI 3d group. This increased blood deposition was also observed to co-localize with regions of activated microglia, which may further cause tissue damage at regions distant from the impact site leading to the increased lesion volumes observed in rmTBI 7d animals. The vulnerability to a second impact resulted in both a greater volume of tissue damage and increased blood deposition following a second temporally and spatially distant mTBI. The differences in observed blood and edema volumes between the rmTBI groups are most likely the result of temporal cellular cascades, such as HPC, initiated by an initial injury. However additional investigations are needed to uncover the mechanisms leading to increased brain vulnerability and blood deposition within rmTBI 7d animals and determine the long-term effects of this observed tissue exacerbation. Further computational analysis methods need to be developed for experimental models of TBI so that they can be optimized for future clinical use.

Figures and Legends

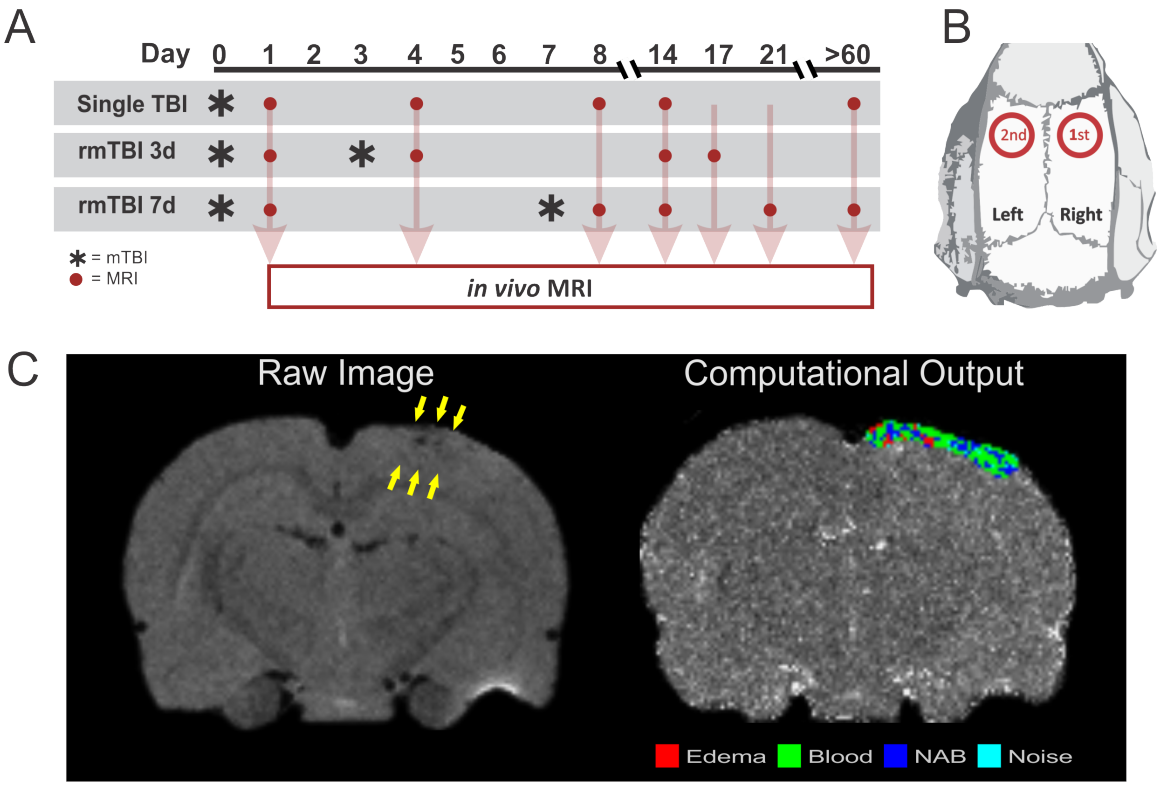

Figure 2.1: Experimental design.

A. Experimental mTBI and neuroimaging timeline. An mTBI was induced to the right cortex on D0 (denoted as an *) in all animals. A second mTBI was induced to the left cortex at either 3 or 7 days later (*). MR imaging was performed 1d post first injury (D1), 1d post last injury (D1 Singles, D4 rmTBI 3d, D8 rmTBI 7d) and 14d post injury (D14: first injury for all animals, D17: second injury rmTBI 3d, D21: second injury rmTBI 7d) (red circles). **B.** Illustration of the mTBI locations for the first (right) and second (left) injuries. **C.** Raw T2WIs revealed abnormal signal intensities after a Single mTBI (yellow arrows) that were classified as being blood (<69 ms; green), edema (>90ms; red), normal appearing brain (NAB; 70-89 ms; blue), or noise (>500ms; cyan) containing voxels.

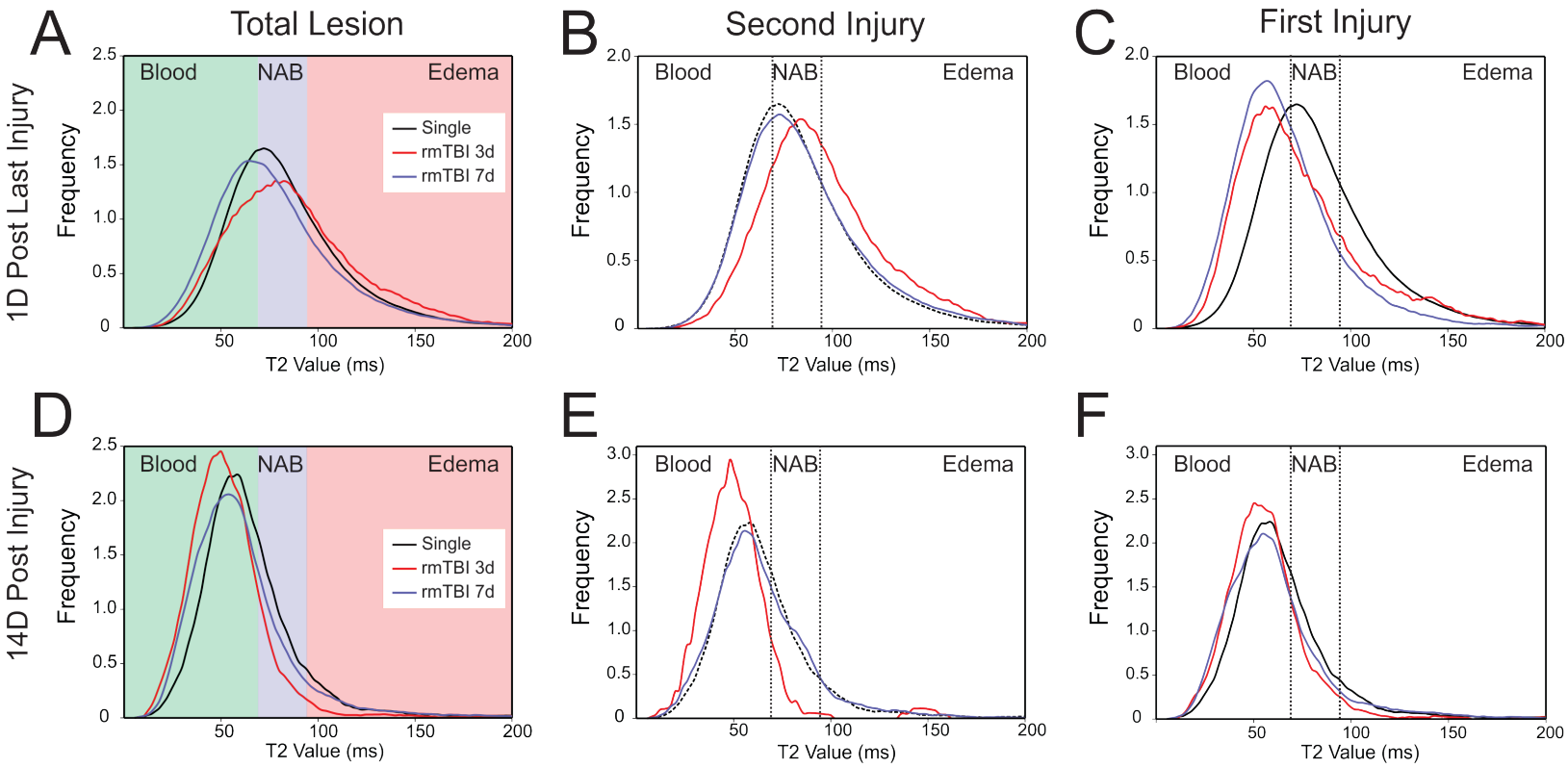
A
Total Lesion
B
Second Injury
C
First Injury
D
E
F
1D Post Last Injury
14D Post Injury
Frequency
T2 Value (ms)
Blood
NAB
Edema
Single
rmTBI 3d
rmTBI 7d

Figure 2.2: Temporal shifts in T2 value distribution following rmTBI. **A and D.** Histograms of the total lesion (first + second) at 1d post last **(A)** and 14d post injury (14d post first injury) **(D)** demonstrate global changes in T2 value distribution between Single (black), rmTBI 3d (red) and rmTBI 7d (blue) groups. Background color-coding in the total lesion histograms illustrates the range of T2 values for tissue classification: blood (green), edema (red), or normal appearing brain (NAB; blue). **B, C, E, F.** Show the total lesion separated into first and second lesion at 1d post last injury **(B-C)** and 14d post injury (first: D14, second: D17 rmTBI 3d, D21 rmTBI 7d) **(E-F)** to illustrate the differences in T2 distribution between the two injury sites of Single (black) rmTBI 3d (red) and rmTBI 7d (blue) groups. Single mTBI histograms in the second lesion graphs (black dotted line) are those taken from the injured cortex (first injury) for comparison.

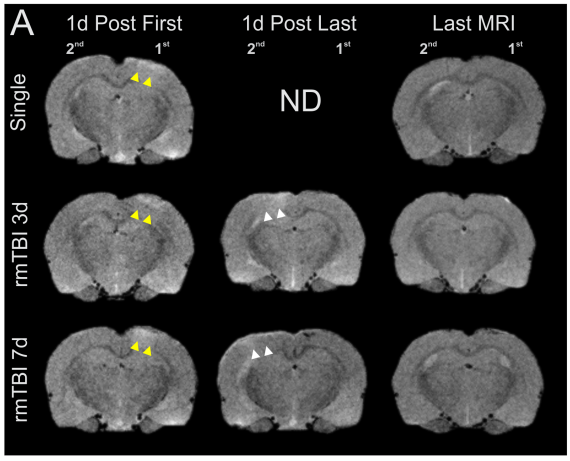
A
1d Post First
1d Post Last
Last MRI
2nd
1st
ND
Single
rmTBI 3d
rmTBI 7d

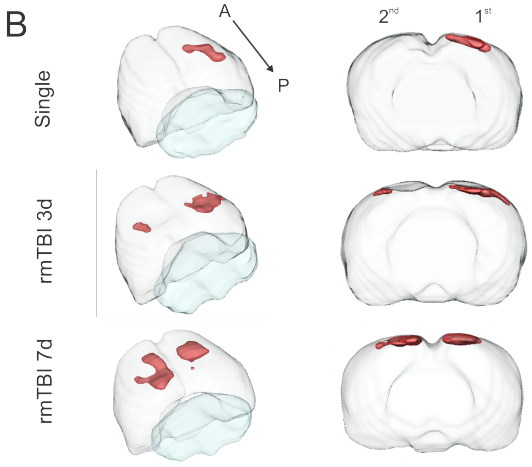
B
A
P
2nd
1st
Single
rmTBI 3d
rmTBI 7d

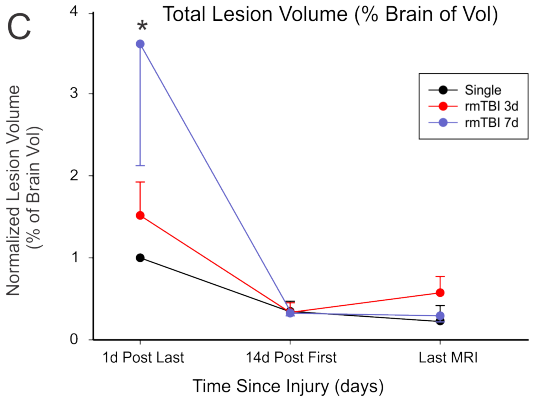
C
Total Lesion Volume (% Brain of Vol)
Normalized Lesion Volume (% of Brain Vol)
Time Since Injury (days)
1d Post Last
14d Post First
Last MRI
Single
rmTBI 3d
rmTBI 7d
*

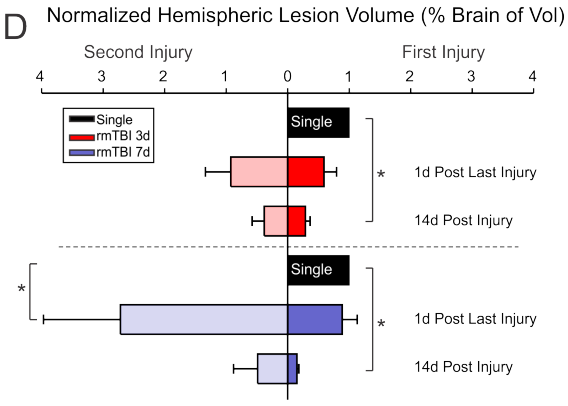
D
Normalized Hemispheric Lesion Volume (% Brain of Vol)
Second Injury
First Injury
Single
rmTBI 3d
rmTBI 7d
1d Post Last Injury
14d Post Injury
*

Figure 2.3: rmTBI 7d animals have increased lesion volumes.

A. T2WIs illustrate the presence of abnormal tissue after the initial (1d post first: D1; yellow arrows) and second (1d post last: D4 rmTBI 3d, D8 rmTBI 7d; white arrows) mTBI. **B.** 3-D reconstructions of injury volumes illustrate the mild nature of the injury, where average total lesion volumes from Single (1.4%), rmTBI 3d (0.9%) and rmTBI 7d (2.0%) animals were collected 1d post last injury. **C.** The temporal evolution of total (first + second) mTBI lesion volumes over the experimental period, demonstrates a significantly increased lesion volume in rmTBI 7d animals (blue) 1d post last injury compared to rmTBI 3d (red) and a Single mTBI (black). **D.** Evaluation of the first and second injuries revealed a transient increase ($p=0.029$) in the second lesion volume of rmTBI 7d animals (blue) compared to a single injury (black) 1d post last injury. Normalized data presented as means ± SEM, where $*p<0.05$.

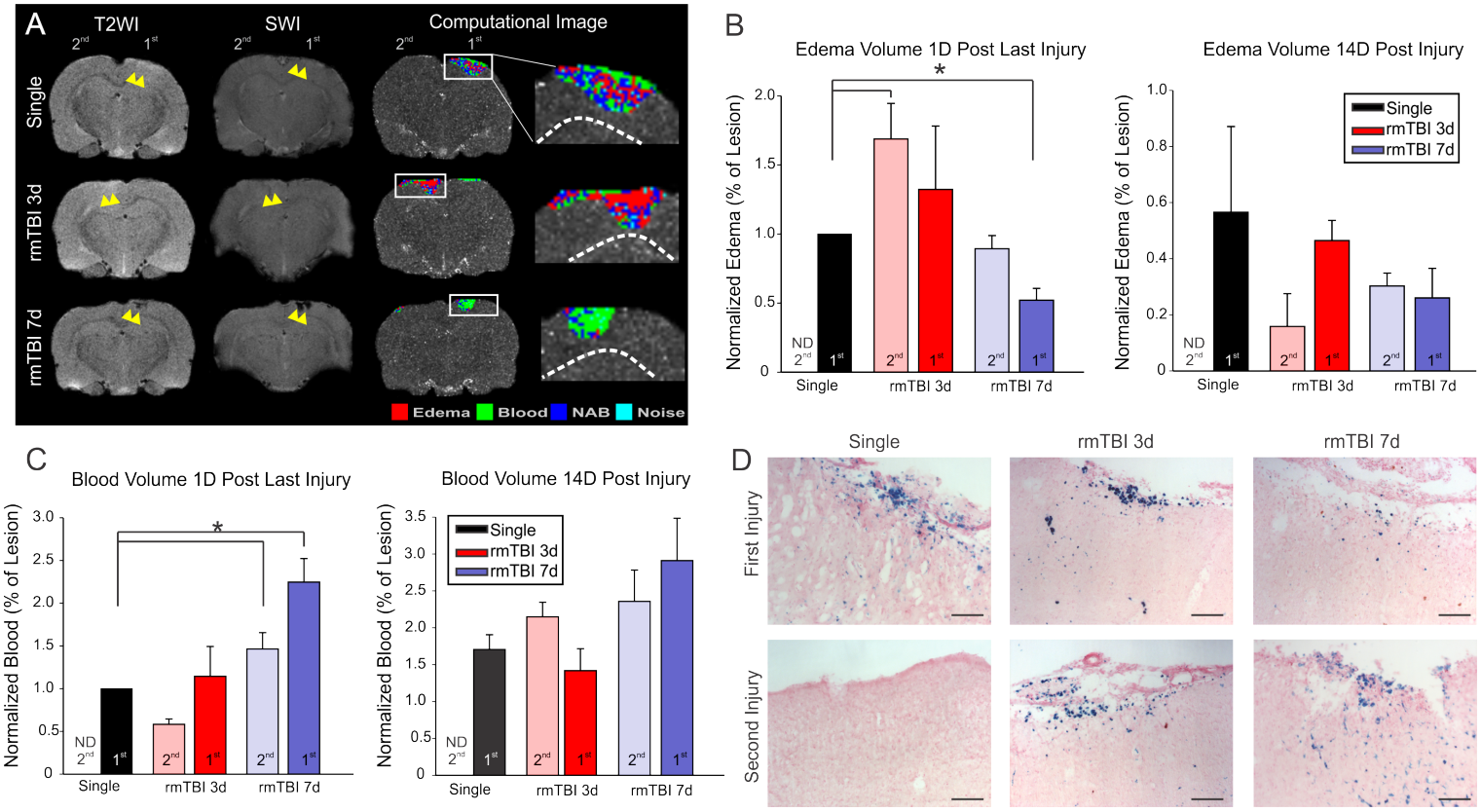
A
T2WI
SWI
Computational Image
Single
rmTBI 3d
rmTBI 7d
Edema
Blood
NAB
Noise
B
Edema Volume 1D Post Last Injury
Edema Volume 14D Post Injury
Normalized Edema (% of Lesion)
ND
Single
rmTBI 3d
rmTBI 7d
C
Blood Volume 1D Post Last Injury
Blood Volume 14D Post Injury
Normalized Blood (% of Lesion)
D
First Injury
Second Injury

Figure 2.4: Increased blood volume occurred in rmTBI 7d animals.

A. MR images taken 1d post last injury reveals abnormal tissue on T2 (yellow arrows) and blood deposition on SWI (yellow arrows) following mTBI. Computationally color-coded images illustrate voxel characterization (green=blood, red=edema, blue=normal appearing brain) in these animals. **B.** Edema volume analysis within the first and second lesions revealed changes in edematous tissue at 1d post last injury (D1: Single, D4 rmTBI 3d, D8 rmTBI 7d), while no differences were observed between groups at 14d post injury (first: D14, second: D17 rmTBI 3d, D21 rmTBI 7d). **C.** Analysis of blood volume within the first and second lesions demonstrated significantly increased blood deposition within rmTBI 7d animals at 1d post last injury and between the first lesions at 14d post injury (first: 14d post first, second: 14d post last injury). **D.** Prussian blue staining in the first and second lesions of animals 14d post first injury at the site of maximal lesion shows increased blood deposition in the tissues from rmTBI 7d animals. Normalized graphs presented as means ± SEM where *$p<0.05$; cal bar = 100µm.

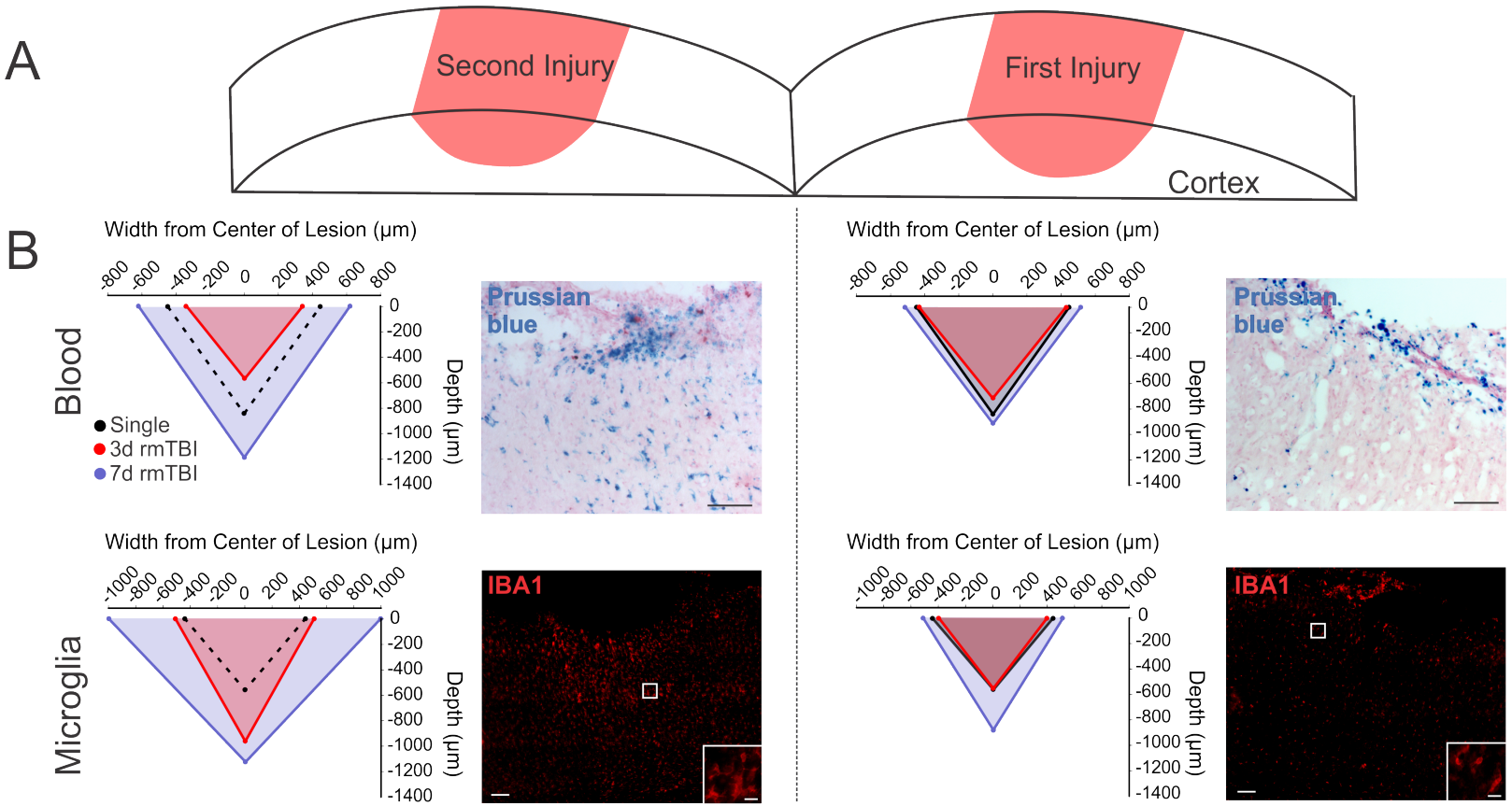
A
Second Injury
First Injury
Cortex
B
Blood
Microglia
Width from Center of Lesion (μm)
Depth (μm)
Single
3d rmTBI
7d rmTBI
Prussian blue
IBA1

Figure 2.5: Microglial activation and blood deposition demonstrates spatial overlap within the lesion sites.

A. A depiction of the rat cortex illustrates the locations of observable tissue damage where blood and microglial measurements were taken. **B.** Depth and width graphs demonstrate a spatial overlap in blood and activated microglial localization at 14d post first injury within Single mTBI (black), rmTBI 3d (red) and rmTBI 7d (blue). Single data in the second lesion (dotted line) is from the injured cortex (first lesion) for comparison. Confocal micrographs were taken of Prussian blue (blue) and IBA1 (red) staining from the cortex of rmTBI 7d animals (second lesion) and Single mTBI (first lesion) animals. cal bar = 100μm; inset cal bar = 20 μm.

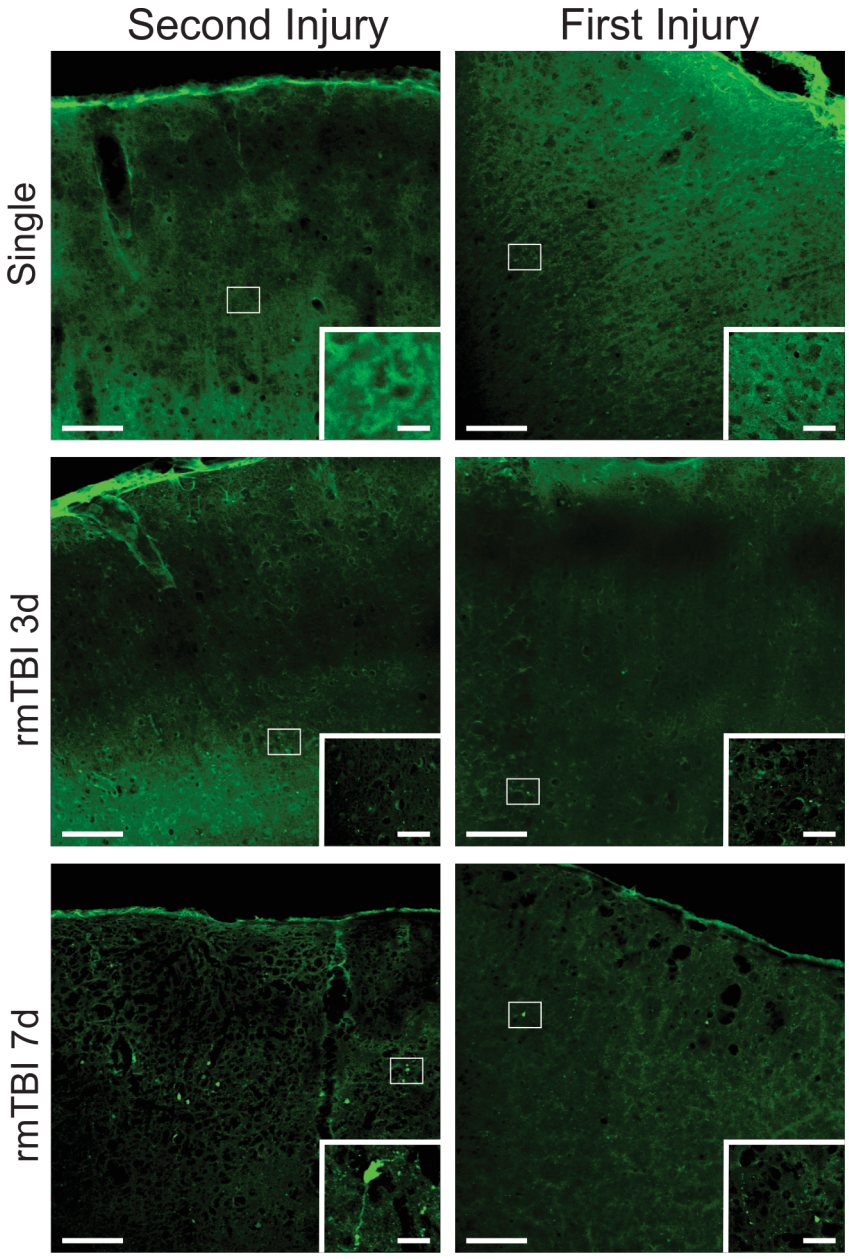
Second Injury
First Injury
Single
rmTBI 3d
rmTBI 7d

Figure 2.6: The rmTBI 7d animals reveal Fluoro-Jade positive cell bodies at the second injury site.

The first and second injury sites of Single, rmTBI 3d and rmTBI 7d animals showed punctate Fluoro-Jade staining. However, rmTBI 7d animals also revealed Flouro-Jade positive neurons at the site of the second injury, which was not seen in other groups. cal bar=100 μm; inset cal bar=20μm

Table 2.1: Total lesion histogram peak T2 values, mean T2 values, skewness and kurtosis measurements.

	Time Point	Single	rmTBI 3d	rmTBI 7d	p Value
T2 (ms) Peak	1D post last injury	70.5 ± 1.5	74.2 ± 6.1	68.3 ± 2.5	p= 0.505
	14d post injury	52.6 ± 3.0	47.8 ± 5.4	55.5 ± 2.8	p= 0.342
Mean T2 Value (ms)	1D post last injury	85.0 ± 1.4	92.6 ± 5.3*	78.8 ± 2.6*	p = 0.015
	14d post injury	63.9 ± 2.9	55.8 ± 2.9	62.6 ± 3.0	p = 0.263
Skewness	1D post last injury	2.3 ± 0.12*	2.3 ± 0.27	2.9 ± 0.2*	P = 0.042
	14d post injury	2.4 ± 0.22*	5.3 ± 0.62*	3.8 ± 0.65	p = 0.026
Kurtosis	1D post last injury	14.8 ± 1.2*	13.7 ± 2.2	21.3 ± 2.6*	p = 0.030
	14d post injury	14.7 ± 1.8*	47.8 ± 10.4*	29.6 ± 7.6	p = 0.034

*Groups that are statistically different from each other. Measurements ± SEM.

Chapter 3

White Matter Damage Following Repeated Mild Traumatic Brain Injury is Progressive and Ongoing Long-Term.

Abstract

White matter damage following mild traumatic brain injury (mTBI) contributes to the delayed neurological and behavioral deficits observed following injury. Results from previous experimental TBI studies suggest that axonal damage occurs early (<7-14 days) and appears to resolve over time, while changes in myelin integrity are delayed and observed later (>14-30 days). However the progression of white matter damage following mTBI is not well understood and even less is known about changes in myelin and axon integrity following repeated injuries. We assessed white matter damage in anterior corpus callosum (CC), distant from the impact sites, using a model of rmTBI in which two mild controlled cortical impacts were induced to opposite hemispheres 7 days apart. Animals were sacrificed at sub-acute 14- or 21-day (14D, 21D) and long-term 60-day (60D) timepoints for diffusion tensor imaging (DTI) and transmission electron microscopy (TEM) analysis. Based on previous findings, we hypothesized that axonal damage would predominate at earlier sub-acute times, followed by changes in myelin integrity later at our long-term timepoint.

At sub-acute times, DTI showed a bilateral increase in axial diffusivity (axonal) within rmTBI 14D and 21D animals compared to Shams. Regional analysis of the CC revealed that increased axial diffusivity was localized to white

matter anterior to the second impact site of rmTBI 14D rats, but by 21D axial measures returned to Sham levels. In contrast, radial diffusivity (myelin) demonstrated bilateral increases in rmTBI 14D animals compared to other groups that appeared to pseudo-normalize by 21D. However long-term analysis of DTI measures revealed a widespread bilateral increase in radial diffusivity following rmTBI, which was not seen in Single or Sham animals, while little change in axial diffusivity measurements were seen between groups. Examination of myelinated axons using TEM revealed that white matter adjacent to the second injury within rmTBI 21D animals had decreased axonal caliber and myelin thickness compared to the surgery site of Sham controls. By 60D, the rmTBI group continued to demonstrate decreased myelin thickness compared to Shams, however, axonal caliber at this later time was significantly increased from other groups.

We assessed oligodendrocytes using Olig2 (progenitor and mature) and APC (mature) at sub-acute times to see whether these populations might be affected by rmTBI. We found that rmTBI 21D animals had decreased Olig2, but increased APC positive cells in white matter adjacent to the second injury compared to the surgery side of Single and Shams. Additionally, neurofilaments (NF200) were evaluated, as changes in the axonal cytoskeleton have been correlated with altered axonal caliber. NF200 staining showed decreased signal intensity within the rmTBI 21D group at sub-acute times and appeared to resolve long-term. Taken together these data demonstrate that bilateral rmTBI, induced

7 days apart, leads to myelin and axon damage that progresses over time and provides a morphological basis for neurological abnormalities that are seen following repeated injuries in the clinic.

Introduction

Mild traumatic brain injury (mTBI) is a growing public health concern accounting for approximately 75% of all reported head injury cases (Faul 2010). Following a concussive event a series of pathophysiological processes ensue, including changes in metabolism, cerebral blood flow and neurotransmission (Barkhoudarian 2011). Despite these alterations most individuals appear to recover normally from mTBI, however several clinical studies have reported the presence of long-term emotional and cognitive sequelae following a single mild injury (Malojcic 2008, Konrad 2011). In addition, several clinical and experimental studies provide evidence of increased brain vulnerability following a mild head injury in which a second mTBI may result in exacerbated tissue damage and neurological deficits (Longhi 2005, Vagnozzi 2007, Vagnozzi 2008, Donovan 2012).

Little is understood about the underlying pathophysiology that leads to long-term deficits following repeated mTBI (rmTBI). Clinically, patients sustaining a second mild injury 10-13 days following an initial concussion demonstrate alterations in brain metabolites (N-acetylaspartate-to-creatine ratio) compared to those individuals only suffering a single injury (Vagnozzi 2008). Experimentally animal models in which injuries were induced to the same anatomical location revealed a time window of vulnerability, in which a second injury within 3 days of the first exacerbated ongoing metabolic, behavioral and tissue changes (Laurer 2001, Longhi 2005, Tavazzi 2007, Vagnozzi 2007, Shitaka 2011). These

outcomes were not observed if a second injury was induced 5-7 days following the first injury, suggesting that the ongoing pathologies appeared to resolve (Longhi 2005, Vagnozzi 2007). However, we have previously reported that rmTBI induced to different anatomical locations did not result in exacerbated damage when injuries were spaced 3 days apart, but brain vulnerability was increased when a second injury was induced 7 days following the initial insult (Donovan 2012). These data suggest that brain vulnerability to subsequent injuries may be dependent on both the time interval between and the anatomical locations of mTBIs.

White matter is particularly vulnerable to mTBI. Damage to white matter fibers can develop over time and has been reported years following human concussion (Kinnunen 2011). Difficulties in clinical evaluation of white matter integrity have led to the development of diffusion tensor imaging (DTI) to non-invasively detect myelin and axon pathology (Inglese 2005, Kraus 2007, Mac Donald 2007, Mac Donald 2007, Kumar 2009). In white matter structures, water preferentially diffuses along fiber tracts with less movement in the perpendicular direction as a result of cytoskeletal structures and the myelin sheath (Niogi and Mukherjee 2010). This asymmetric diffusion of water can be quantified using DTI and used to derive axial (AD) and radial (RD) diffusivities, which correlate with axonal and myelin integrity, respectively. Clinically, white matter DTI following TBI has revealed that mild and moderate-to-severe injuries exhibit altered water diffusion along fiber tracts and that this imaging modality can be used to detect

damage that may not be visible using standard imaging methods (Inglese 2005, Kumar 2009, Kinnunen 2011). Experimental studies investigating the timecourse of white matter damage following moderate TBI have reported early decrements in AD followed by delayed increases in RD in the weeks following injury (Mac Donald 2007, Mac Donald 2007, Li 2011, Li 2013). Similarly, animal models of mTBI have reported changes in RD at 7 and 30 days following blast injury (Rubovitch 2011). Imaging of closed head rmTBI, induced 1 day apart to the same anatomical location, demonstrated no immediate changes in DTI measures, but by 7 days reduced AD was seen (Bennett 2012). These studies demonstrate the progressive nature of white matter damage following head injury. However, the development of white matter damage following single and repeated mTBI is not well understood and further investigations are needed.

Histological studies evaluating axonal pathology following human TBI have reported acute (<120hrs) accumulation of amyloid precursor protein (APP) and long-term (27 days- 3yrs) axonal swelling and APP deposition (Blumbergs 1994, Chen 2009). Similarly, a long-term experimental study of mTBI using both single and repeated injuries reported that both injury types result in corpus callosum thinning accompanied by neurological deficits 1 year following injury (Mouzon 2014). In contrast, sub-acute experimental mTBI studies have reported axonal swelling and transport dysfunction, in the absence of myelin disruption, within 14 days of injury that pseudo-normalized by 4 weeks (Spain 2010, Creed 2011, Shultz 2011). However, a few studies have shown acute and sub-acute

changes in oligodendrocyte integrity following TBI (Flygt 2013, Sullivan 2013). Flygt et al (2013) have reported that within 21 days following TBI, elevated numbers of apoptotic oligodendrocytes are present within the white matter. TBI studies have also reported an early (by 7 days) and sub-acute (21 days) increase in oligodendrocyte progenitors within the corpus callosum and increased myelin gene transcription 2-7 days following a single TBI, consistent with remyelination (Flygt 2013, Sullivan 2013). Although at this 7-day time point increases in redundant myelin sheaths were also observed using electron microscopy, indicating that some myelination was abnormal at this time (Sullivan 2013). Animal models of rmTBI have also demonstrated exacerbation of axonal and myelin abnormalities at 7 days and 7 weeks following injury (Laurer 2001, Shitaka 2011, Bennett 2012). These experimental studies, however, focused primarily on white matter changes at sites underneath the impact, despite the widespread damage that is often seen following human concussion (Kinnunen 2011). Other models of trauma investigating secondary degeneration using optic nerve transection have observed chronic axonal swelling and defects in myelin compaction within regions spatially distant from the injury site (Payne 2011). Due to the vulnerability of white matter to mTBI and the observed evolution of pathology following injury, analysis of regions distant from the impact site can be useful in assessing the spatial and temporal effects of single and repeated mTBIs.

Experimental studies of rmTBI, especially those in which injuries are induced to different anatomical locations, are critical to understand the clinical consequences of repeated injuries on white matter integrity. Furthermore, due to the evolving nature of mTBI, both early and long-term studies evaluating tissue distant from the injury site are warranted to better understand how white matter damage evolves over time. The purpose of our study was to evaluate sub-acute and long-term axonal and myelin damage within the anterior corpus callosum, a region which was not directly under the impact site, following rmTBI in which injuries were induced to contralateral locations 7 days apart. We hypothesized that rmTBI would result in predominantly axonal disruption at sub-acute times and changes in myelin integrity at long-term timepoints following injury.

Materials and Methods

Animals

All animal experiments and care were in compliance with federal regulations and approved by the Loma Linda University Animal Health and Safety Committee. Male Sprague Dawley rats weighing 250-500g (2-5 months old) were housed in a temperature controlled animal facility on a 12-hour light-dark cycle. Animals were randomly assigned to Sham control, Single mTBI or rmTBI groups (Figure 3.1A). Sham and Single animals were sacrificed at 14- (14D; sub-acute) and 60- (60D; long-term) day timepoints following surgery. rmTBI animals were sacrificed at 14D (14 days post first injury), 21 days (21D; 14 days post second injury) and 60D (60 days post first injury) (Figure 3.1A). Following sacrifice, animals underwent either magnetic resonance imaging (MRI) followed by histology or transmission electron microscopy (TEM) analysis.

Controlled Cortical Impact

The controlled cortical impact (CCI) method was used to induce mild injuries as previously described (Donovan 2012). Briefly, a midline incision exposed the skull surface of anesthetized rats and a 5 mm craniectomy was performed over the right hemisphere 3mm posterior and 3mm lateral from Bregma (Figure 3.1B). A mild CCI (4mm diameter tip, 0.5 mm depth, 6.0 m/s speed, 200 ms dwell) was then delivered to the cortical surface using an electromagnetically driven piston. The rmTBI group received a second craniectomy and mild CCI to the left cortical surface using identical parameters and coordinates as the first injury (Figure

3.1A, B). Sham controls underwent a single craniectomy and did not receive a CCI.

Ex Vivo Magnetic Resonance Imaging and Analysis

Animals were sacrificed via transcardial perfusion using 4% PFA and extracted brains were then post-fixed in 4% PFA overnight followed by two 30 minute washes in 1x PBS (Obenaus 2007). DTI and T2 weighted imaging (T2WI) data were collected at room temperature with a 256x256 matrix, 2 cm field of view and 1mm slice thickness from ex vivo brains using an 11.7T Bruker Avance instrument (Bruker Biospin, Billerica, MA). T2WIs were acquired with a TR/TE= 1769.9/10.2 ms and DTI was acquired from a total of seven directions using a spin echo diffusion sequence (TR/TE = 552.5 ms/15.1ms) with a single b_o value (b_o=43.3 s/mm^2) and six weighted DTI images (b=2013.3 s/mm^2).

The anterior (bregma, -1.0 to +0.5 mm) corpus callosum (CC) was chosen for evaluation because it was not directly under the impact site (Figure 3.1C). The anterior CC was manually outlined on three consecutive T2WI slices using Cheshire image processing software (Hayden Image/Processing Group, Waltham, MA) by investigators blinded to group allocation. The midline and third ventricles were used to identify and facilitate segmentation of the right and left CC regions of interest (ROI) (Figure 3.1C, left). To examine regionally distinct CC changes, the center slice was used to separate the CC into 12 ROIs (6 each bilaterally) along the medial-lateral axis. These regional ROIs were drawn on T2WIs using boundaries defined by the orientation of white matter fibers

observed within RA color maps of Sham animals (Figure 3.1C, right). To account for size and shape differences after injury, the RA color maps of injured animals were also used to facilitate manual segmentation. Since all T2 and DTI images were acquired using the same geometry, ROIs drawn on T2WIs were copied directly to the exact DTIs and data means were extracted for AD and RD ($\mu m^2/ms$). The AD, RD and RA were derived using software written in Matlab (MathWorks, Natick, MA) as previously described (Sun 2006).

Tissue Preparation for Histology

Following MRI, brains from each group were randomly selected and prepared for cryosectioning as previously described (Obenaus 2007). Briefly, brains were placed in 30% sucrose and embedded in optimal cutting temperature compound (O.T.C., Tissue Tek; Sakura Fine Tek, Torrance, CA). Coronal sections (30 □m) were then either mounted directly on gelatin-chrome-alum-coated slides for Luxol fast blue staining (LFB; stored at –20°C) or were free floating (stored in a cryoprotectant solution at 4°C) for immunohistochemistry.

Luxol Fast Blue Staining and Quantification

LFB was performed on a minimum of 3 adjacent sections centered within the anterior CC to evaluate changes in structural integrity. Staining was performed as previously described with modifications (Kluver and Barrera 1953). Briefly, mounted slices were thawed to room temperature for 30 minutes and placed into a 0.1% LFB staining solution (Solvent Blue 38 in 95% alcohol and 0.5% acetic acid) overnight at 56ºC. Excess stain was removed by 95% alcohol

and distilled water rinses for 1 minute each. Stained slices then underwent alternating 1-minute immersions in 0.05% lithium carbonate and 70% alcohol solutions for approximately 10 minutes. Subsequently, distilled water and 95% alcohol washes were performed for 1 minute each. Slices were then cleared using Histoclear (National Diagnostics Inc., Charlotte, NC) and cover-slipped with permount mounting medium (Fisher Scientific, Fairlawn, NJ).

Slices stained with LFB were imaged on an Olympus BX-51 microscope using the same imaging parameters (1.25x objective, 1 sec exposure) and illumination. Quantification of myelin integrity was performed by investigators blinded to group allocation using Cheshire image processing software. Measures taken included the right and left staining intensity, area (mm^2) and width (mm) of the whole CC, cingulum (cingulum + CC) and CC adjacent to the midline (Figure 3.1D). The right and left area and width measurements were normalized to the respective right or left brain hemisphere area (mm^2), in order to account for any differences in hemispheric size between animals. All sections were stained simultaneously, but staining intensities for each right and left CC were normalized to that in the piriform cortex.

Immunohistochemistry and Analysis

Tissue sections centered in the anterior CC underwent immunohistochemistry as previously described (Obenaus 2007). Briefly, free-floating sections were labeled with primary antibody at 4ºC overnight. Primary antibodies included: anti-rabbit NF200 (Sigma-Aldrich, St. Louis, MO; 1:1000) for

axonal integrity, anti-mouse APC (Millipore, Temecula, CA; 1:500) for mature oligodendrocytes, anti-mouse Olig2 (Millipore, Temecula, CA; 1:2000) for oligodendrocyte precursors and anti-rabbit Ki67 (Abcam, Cambridge, MA; 1:1000) as a marker for cellular proliferation. Sections were then stained with goat anti-rabbit rhodamine (Millipore, Temecula, CA; 1:1000) or goat anti-mouse Alexafluor 488 (Invitrogen, Carlsbad, CA; 1:400) secondary antibody for 1.5 hours at room temperature. Following the staining procedure, slices were mounted onto gelatin-chrome-alum-coated slides using Vectashield hardset mounting medium (Vector Laboratories Inc., Burlingame, CA). Negative controls omitted the primary antibody during the staining procedure.

Micrographs of NF200 immunolabeled tissue sections were taken with identical imaging parameters (20x, 1000ms exposure). ImageJ/Fiji (Schindelin 2012) was used by investigators blinded to group allocation to detect the mean staining intensity of the right and left CC underneath the cingulum, CC adjacent to the midline, cingulum and cortex (above the cingulum). NF200 intensity measurements resulted in no significant differences between the groups within any of the right and left regions. As a result, signal intensity measurements from the right and left regions were averaged together separately for every animal. Olig2, Ki67 and APC staining was imaged using a Zeiss LSM 710 NLO laser scanning confocal microscope. Two images (20x magnification) from both the right and left CC above the lateral ventricle were collected from each slice. Images underwent deconvolution (fast-iterative) and were filtered for noise (fine

filter) using the default settings in Volocity Software (PerkinElmer, Waltham, MA). Image-Pro Premier software (Media Cybernetics Inc., Rockville, MD) was used to count DAPI, Olig2, APC and Ki67 positive cells within the CC, which was manually outlined by a blinded investigator. Olig2 and APC counts were visually inspected to colocalize with DAPI nuclei. Only those cells that were a minimum of 10 pixels were counted and cell splitting was performed using the software default settings to separate cells that were in close proximity. The percent of Olig2 and APC was determined by dividing the Olig2 or APC cell counts by the total pixel count of the CC ROI.

Transmission Electron Microscopy and Quantification

Animals were perfused transcardially with 1x PBS followed by a 2% gluteraldehyde (Electron Microscopy Sciences, Hatfield, PA) and 2% paraformaldehyde in 1x PBS fixative solution. Animals were decapitated and brains were initially post-fixed in situ at 4ºC overnight in the perfusion fixative, followed by further fixation of the extracted brains in 1% gluteraldehyde for approximately 3 days. The anterior brain region was cut coronally (approximately 1mm thick) allowing the CC (right CC of Single and Sham animals; left CC of rmTBI 7d animals) to be identified under a dissecting scope. The CC was carefully dissected as a 1x2 mm^2 block 0.5 mm lateral from the midline to the end of the cingulum (Figure 3.1D). Following extraction the tissue blocks were then stored in 1x PBS at 4ºC for plastic embedding.

Tissue blocks were embedded in epon as previously described (Mnatsakanyan 2011). Briefly, blocks were fixed in 2% osmium tetroxide for 1-2 hours then rinsed in 0.1M cacodylate buffer followed by distilled water. Following washes, blocks were stained overnight with 1% uranyl acetate at room temperature. Increasing concentrations of ethanol followed by propylene oxide were then used to dehydrate the tissue. Dehydrated tissue blocks were incubated in a 50/50 mixture of epon/propylene oxide for 3-4 hours, followed by an 80/20 epon/propylene mixture and then 100% epon overnight. Following epon infiltration, the tissue blocks were placed in an embedding mold using 100% epon, which was polymerized through incubation at 60°C in an oven for 2 days.

Ultra-thin sections were cut from the sample using a diamond knife on an ultramicrotome and mounted onto copper grids for TEM (JEOL, Peabody, MA). Four random fields per grid from a total of two grids were analyzed per animal. Five random images within each field were collected at 5000X and analyzed using ImagePro Plus (MediaCybernetics, Rockville, MD) by an investigator blinded to group allocation. The axon and total fiber (axon+myelin) diameters were determined by taking the average of two separate measurements for every myelinated axon, from a minimum of 800 axons for each experimental group, where the entire axon had to be visible to be analyzed. The g-ratio was calculated for each myelinated axon by dividing the average axon diameter by the average total fiber diameter. The myelin thickness measurements were

calculated by subtracting the total fiber and axon diameter measurements. TEM analysis of the Single mTBI and rmTBI groups sacrificed at 60 days post initial injury were compared to Sham controls 14 days following a craniectomy only.

Statistics

Statistical analysis was performed using SAS v9.1.3 (SAS, Cary, NC) and Sigma Plot Software (Systat Software Inc, San Jose, CA). Data normality was assessed with the Kolmogorov-Smirnov or Shapiro-Wilk tests for each outcome variable and experimental group in each experiment. Whole CC DTI and histological (LFB and NF200) data were compared among the control and experimental groups using the Generalized Linear Model procedure specifying an identity link function with a normal distribution. Using a one-way analysis of variance (ANOVA) with Bonferroni post-hoc testing animal body weights were found to be significantly ($p<0.001$) different between groups at the time of the initial injury, however at the time of perfusion no differences ($p=0.250$) in weights were found between groups. As a result, body weights at the time of the initial surgery in addition to the number of histological sections (LFB 3-6 slices, NF200 1-2 slices) were included as covariates in statistical testing of the whole CC DTI and histological data. Additionally, the DTI, LFB and NF200 slices were treated independently as they spanned a large brain region. Analysis of the segmented CC DTI was performed using a two-way ANOVA with Bonferroni post-hoc tests. Electron microscopy data (g-ratio, axon caliber and myelin thickness) were tested

using a Bonferroni repeated measures one-way ANOVA. Data are presented as the Mean ± SEM. A $p < 0.05$ was considered significant.

Results

rmTBI results in early white matter damage that progress long-term within the corpus callosum

We hypothesized that predominantly axonal disruption would be observed at sub-acute times, while changes in myelin integrity would be altered long-term. We tested this hypothesis using DTI to quantify axial (axonal; AD) and radial (myelin; RD) measures within the anterior corpus callosum (Figure 3.2 and 3.3). At sub-acute times we found significant ($p<0.009$) AD increases within the left (second injury) CC of rmTBI 14D animals, which remained elevated at 21D compared to the right (first injury) CC of the Single and Sham groups (Figure 3.2B). However at this sub-acute time, the right CC of all injured animals exhibited similar AD measures that were also significantly ($p<0.001$) increased from Sham controls (Figure 3.2B). In contrast to AD, RD analysis revealed a significant ($p<0.035$) bilateral increase in measurements from the CC of rmTBI 14D animals compared to those at 21D, which appeared to pseudo-normalize to values seen in the Single group (Figure 3.2C).

Long-term AD measures found no significant differences between any of the groups within the right or left CC (Figure 3.3B). However, a >16% bilateral increase ($p<0.001$) in RD was observed in the rmTBI group compared to Sham and Single animals (Figure 3.3C). Importantly, at 60D these elevations in RD were found to be equally bilateral with no differences between the left and right

CC within rmTBI animals. Furthermore, no differences in RD were observed between the Sham control and Single mTBI groups (Figure 3.3C).

White matter damage is initially located in regions adjacent to injury sites, but becomes widespread throughout the corpus callosum long-term.

We then asked whether particular regions within the CC were more susceptible to damage than others. We hypothesized that segments immediately adjacent to white matter underneath the impact site would demonstrate increased white matter damage at both the sub-acute and long-term timepoints. We therefore segmented the left and right CC ROIs into smaller regions that spanned the medial-lateral axis to test this hypothesis, where segments R2-4 and L2-4 were immediately adjacent to white matter underneath the first and second impact sites, respectively (Figures 3.1).

Regional examination of the right CC revealed increased AD in segments R1 and R3 within rmTBI 14D animals compared to Sham, though these changes were no longer observed at 21D (Figure 3.4A). One segment in Single animals, R4, showed significantly ($p<0.03$) increased AD in the right CC relative to Shams at the sub-acute timepoint. Though no significant AD changes were observed between the rmTBI 14D and Single groups within the right CC (Figure 3.4A). Similarly in the left CC, increases in AD were seen in rmTBI 14D animals within segments L1-L3 compared to Shams; region L3 in rmTBI 14D animals also exhibited significantly ($p<0.05$) increased AD compared to the Single group

(Figure 3.4A). However by 21D, none of the CC segments showed any significant differences in AD measures compared to Shams (Figure 3.4A). Unlike AD measures, RD was not significantly altered between any of the groups in the left CC (Figure 3.4B). However, RD in the right CC demonstrated significant ($p<0.05$) differences in regions R2 and R3 between rmTBI 14D and Sham animals, and in region R1 between Single and Sham controls (Figure 3.4B). Though these differences were no longer observed at the 21D timepoint.

By 60D, no significant differences were found in any of the medial-lateral CC segments for AD or RD measurements (Figure 3.5). Interestingly each of the rmTBI CC segmented regions, demonstrated an elevated RD compared to other groups suggesting that myelin disruption is widespread and that not any single region of the CC predominantly contributes to the overall increase in RD observed within the whole CC analysis (Figure 3.3C and 3.5B).

CC thickness is increased after rmTBI, while LFB staining intensity increases over time.

We hypothesized that myelin loss would be observed at the long-term timepoint, but not sub-acutely. We tested this hypothesis using LFB staining to assess CC thickness and palor at both the sub-acute and long-term timepoints. Quantification of CC measures revealed a significant ($p<0.007$) increase in the left CC area and thickness of rmTBI 21D animals compared to the Sham and Single groups (Table 3.1). Similarly, the right CC of both rmTBI 14D and 21D

animals demonstrated a significant ($p<0.039$) increase in CC area and thickness compared to Shams (Table 3.1). LFB staining density within the left CC and width ROIs demonstrated no differences between rmTBI animals and Sham or Single groups (Table 3.2). However, the right CC of rmTBI 21D animals showed significantly ($p<0.001$) decreased LFB staining intensity compared to all experimental other groups (Table 3.2).

Analysis at 60D showed significant bilateral increases ($p<0.018$ Left, $p<0.001$ Right) in the CC area and midline width ROIs between the Single and rmTBI groups, however no differences were found between injured animals and Sham controls (Table 3.3). Furthermore, the left cingulum of rmTBI animals demonstrated increased ($p<0.001$) widths compared to other groups, while the right cingulum of rmTBI groups showed significant ($p=0.009$) increases compared to Single animals only (Table 3.3). LFB staining intensity was also significantly increased in all ROIs within the right CC of rmTBI animals compared to Shams (Table 3.4). However, only the left cingulum within rmTBI showed a significant ($p=0.032$) increase from Sham controls long-term (Table 3.4).

White matter ultrastructure is compromised following rmTBI

We then tested whether changes in myelinated axon morphology contributed to the observed DTI pathology following rmTBI. Similar to our DTI experiments, we hypothesized that changes in axonal morphology would be observed at sub-acute times, while changes in myelin integrity would be seen

long-term. We quantified axonal and myelin morphology within the CC using TEM at the site of the second injury in rmTBI animals and at the site of the first injury in the Single and Sham groups. We observed normal myelinated axons as a compact sheath closely encompassing an axon predominantly within Shams (Figure 3.6B1), while injured animals frequently demonstrated various abnormalities including separation of myelin from the axon (Figure 3.6B2), decompaction (Figure 3.6B3) and fragmentation of the myelin sheath (Figure 3.6B4-5). No significant differences in g-ratio were found between any of the groups at the sub-acute timepoint (data not shown). However, axon caliber was significantly ($p<0.001$) decreased sub-acutely in both Single and rmTBI 21D animals compared to Shams (Figure 3.6C). Furthermore, rmTBI 21D animals also demonstrated significantly ($p<0.001$) decreased myelin thickness compared to other groups at this sub-acute time (Figure 3.6C).

Similarly by 60D, the rmTBI group continued to demonstrate changes in myelinated axon morphology (Figure 3.7A). In contrast to sub-acute times, a significantly increased g-ratio was observed in rmTBI animals compared to the Sham ($p=0.017$) and Single ($p=0.007$) groups (Figure 3.7B). No g-ratio differences were observed between the Sham and Single animals. Axonal caliber was significantly increased ($p<0.001$) in rmTBI animals, but significantly decreased ($p<0.001$) in the Single group compared to Sham controls at 60D (Figure 3.7B). Additionally, myelin thickness measurements revealed that both

the Single and rmTBI groups were significantly ($p<0.001$) decreased from Shams (Figure 3.7B).

We also assessed whether axonal integrity was altered using NF200 staining, as Jafari et al. (1997) have shown correlations between cytoskeletal abnormalities and altered axonal caliber. NF200 staining in the right CC of rmTBI 21D animals demonstrated similar values to those observed in Shams (Figure 3.6D). While significant ($p<0.048$) increases in NF200 intensity were seen in the Single group at the sub-acute timepoint (Figure 3.6D). However, the left CC revealed sub-acute decreases in signal intensity within rmTBI animals. Though by 60D, no differences between the groups were observed in either the right or left CC (data not shown).

rmTBI alters the oligodendrocyte cell population in the corpus callosum adjacent to the second injury site at sub-acute times.

We hypothesized that the mature oligodendrocyte population would be decreased in the CC, while progenitors would be increased at sub-acute times. To test this hypothesis we used both Olig2 staining, to detect progenitor and mature oligodendrocyte populations, and APC staining, to identify mature oligodendrocytes (Figure 3.8). In the left CC (second injury) we found that the percent of Olig2 positive cells were significantly ($p<0.033$) decreased in rmTBI 21D animals compared to other groups (Figure 3.8B). While increased numbers of APC positive cells were observed in the left CC of rmTBI 21D animals

compared to the Sham and Single groups (Figure 3.8C). The right CC (first injury) demonstrated no differences in either the number of Olig2 or APC positive cells between any of the experimental groups at this sub-acute time. Furthermore sporadic Ki67 positive oligodendrocytes were detected within the CC of animals, and no differences between groups were found, indicating low levels of cell proliferation within the CC at this sub-acute time (data not shown).

Discussion

Initially we hypothesized that in the anterior CC, not directly underneath the impact site, rmTBI induced 7 days apart would result in predominantly axonal changes at sub-acute times, while altered myelin integrity would be observed long-term. However our TEM data demonstrates that both axonal and myelin integrity are altered sub-acutely and persist long-term. DTI analysis revealed a localized increase in AD within the left CC of rmTBI 14D animals that was also seen at 21D, though increases in AD were no longer focal (Figure 3.9A). RD showed transient sub-acute increases in rmTBI animals, however, by 60D bilateral increases in RD were apparent in rmTBI animals compared to other groups (Figure 3.9B). Ultrastructural analysis revealed that myelin within rmTBI animals was thinner at both the sub-acute and chronic timepoints compared to Shams (Figure 3.9C). Additionally, while axonal caliber decreased at sub-acute times within rmTBI 21D animals, by 60D it was significantly increased compared to other groups (Figure 3.9C). Taken together, our findings demonstrate that rmTBI results in early white matter changes that progress long-term in regions distant from the injury site.

Diffusion tensor imaging of rmTBI identifies focal increases in axial diffusivity that are followed by widespread elevation of radial diffusivity long-term.

Surprisingly, few DTI studies have been performed in animal models of mTBI. In the anterior CC, 1-2 mm distant from the injury site, a bilateral increase

in AD was observed in rmTBI animals compared to Shams at sub-acute times. While RD was also increased bilaterally in rmTBI 14D animals, diffusivity appeared to pseudo-normalize by 21D. This data suggests that sub-acute white matter damage in our model is primarily axonal. Our TEM data however, demonstrated that myelin is thinner at this sub-acute time compared to Shams. Thus transient sub-acute increases in RD suggest that disruption to myelin is short-lived, but TEM data reveals ongoing myelin thinning. Increased pathology, such as inflammation, edema and tissue loss, has been reported to affect the sensitivity and specificity of DTI derived measures (Wang 2011). Therefore, ongoing edema and inflammatory processes likely contribute to the absence of RD changes in rmTBI 21D animals. An experimental model of rmTBI, inducing two closed head injuries 1 day apart, reported decreases in AD within the CC, while no changes in RD were detected 7 days following the initial injury (Bennett 2012). Though we did find differences in RD at 14D post rmTBI, experimental differences between this study and our own, such as location of injury, time interval between mTBI events and timepoints assessed, likely contribute to differences.

However by 60D we found a bilateral increase in RD within rmTBI animals, while little change in AD was seen between groups. While our TEM data were consistent with DTI data, showing thinner myelin at this later time, it also revealed changes in axonal caliber. Additionally, our DTI analysis did not detect changes in axonal integrity, but a recent human study of multiple sclerosis in the

spinal cord found that RD increased not only as a result of demyelination, but also as a result of axonal damage (Klawiter 2011). Thus increases in long-term RD may reflect both axonal and myelin disruption. A model of mild blast TBI also observed changes in sub-acute (7 days) and long-term (30 days) RD within the hypothalamus and thalamus, however, unlike our study this model resulted in decreased RD (Rubovitch 2011). Though the pathology that ensues following a diffuse blast injury is likely to be different than that following a focal mild TBI, resulting in different DTI outcomes. Also, the decreased RD reported by Rubovitch et al. (2011) may reflect continued tissue swelling or inflammation not observed at our later 60 day time point.

White matter tracts are particularly susceptible to TBI induced damage due to their long thin structure, which can be stretched and twisted as a result of head injury. Axonal injury caused by TBI typically progresses from a focal injury in white-matter regions into a more diffuse pathology (Buki and Povlishock 2006). This is consistent with our sub-acute DTI data, where we observed that white matter segments immediately adjacent to regions directly underneath the impact site showed the greatest increases in AD within rmTBI 14D animals, but pseudo-normalized by 21D. Further, by 60D we found that rmTBI animals showed widespread, along the medial-lateral axis, increases in white matter damage. Thus, our data suggests that following rmTBI, white damage is initially focal and becomes more diffuse over time, potentially explaining the delayed long-term cognitive deficits observed following human concussion.

White matter structure is damaged following repeated injuries.

We found a bilateral increase in CC thickness in rmTBI 21D animals at sub-acute timepoints that resolved in all regions by 60D, except the left cingulum, compared to Shams. Taken together with our DTI, which showed transient elevation in RD at 14D, increases in rmTBI D21 CC thickness and decreases in palor at sub-acute times may be due to ongoing edema at this timepoint. Depending on injury severity, edema can be seen for up to 2 weeks following TBI (Barzo 1997, Unterberg 2004). Thus pseudo-normalization of CC thickness observed at 60D may then result from resolution of edema at this later timepoint. Additionally, the increased thickness seen within the rmTBI cingulum at 60D may be the result of the increased axonal caliber we found using TEM.

LFB staining intensity was decreased within the rmTBI 21D group, but increased in rmTBI 60D animals within the right CC ROIs, while the left cingulum at 60D also showed increased palor, compared to Sham controls. Thinned myelin as seen on TEM may contribute to the decreased palor observed at sub-acute times. Additionally, increased CC size due to swelling, may also decrease LFB signal intensity (dilution effect) at sub-acute times. In contrast, the increased palor observed within rmTBI 60D animals may be due to myelin fragmentation as we also see thinned myelin using TEM long-term and CC size pseudo-normalized at this time. Similarly, a study using moderate TBI reported abnormalities in myelinated axon morphology at 3 months after injury with increased myelin debris and white matter thinning in the external capsule at 6 to

9 months following injury (Rodriguez-Paez 2005). Though our LFB data are consistent with increased myelin debris seen in this study, we did not observe white matter thinning. However, several reasons exist for the discrepancies between this study and our own: (a) our study was only carried out to 60 days post injury, (2) we utilized a mild injury and (3) rmTBI could influence the temporal evolution of axonal and myelin damage.

Healthy white matter has a g-ratio of 0.7 to 0.8, where a value of 1.0 may suggest overt demyelination or increased axonal caliber (Crawford 2009). Quantification of myelinated axon morphology revealed no significant changes in g-ratio at 21D, so we examined the axon caliber and myelin thickness (fiber-axon) as subtle change in morphology could be present in the absence of an altered g-ratio. Comparison of axon caliber and myelin thickness revealed that rmTBI animals exhibited significantly decreased axonal caliber and myelin thickness at 21D, thus explaining the absence of changes in g-ratio. Sub-acute reductions in axonal caliber were seen in the presence of altered neurofilament (NF200) staining. Stretch injury models have demonstrated that reductions in axon caliber correlate with neurofilament compaction, while disorganized cytoskeleton (neurofilaments and microtubules) was observed in axons with increased caliber (Jafari 1997). These data suggest that sub-acute reductions in axonal caliber within our model are likely due to cytoskeletal disruption, such as neurofilament compaction.

At 60D, rmTBI animals continued to show reduced myelin thickness on TEM compared to Shams. Furthermore the axonal caliber within rmTBI 60D animals was also increased compared to other groups. However at this late timepoint, neurofilament disruption appeared to normalize as we found no changes in staining intensity between experimental groups. Causes of increased caliber at this long-term timepoint are not clear and further investigations are needed. However one potential cause of increased caliber is altered microtubule integrity, as these cytoskeletal components also play an integral role in maintenance of axon integrity. Both microtubule and neurofilament disruption have been shown to result in acute axonal swelling (Tang-Schomer 2012). Furthermore, previous studies using axonal stretch and TBI models have demonstrated that microtubule density is lost acutely (<6hrs) following injury (Maxwell 1996, Pettus and Povlishock 1996). Another potential reason for increased caliber is disruption to the axon-myelin relationship. Previous studies have shown that myelin, and specifically its expression of myelin-associated glycoprotein, plays a critical role in regulating axonal cytoskeleton and overall caliber (Schnaar and Lopez 2009). Additionally, a model of multiple sclerosis has shown that axons are damaged by long-periods of demyelination (Crawford 2009). Thus it is likely that the relationship and/or communication between axons and the myelin that ensheathes is critical for maintenance of integrity. Our findings of decreased myelin integrity at sub-acute and long-term times suggests

that disruption to the axon-myelin relationship is occurring and potentially contributes to changes in axonal caliber.

rmTBI results in altered oligodendrocyte populations within the corpus callosum at sub-acute timepoints.

Using APC, for mature oligodendrocytes, and Olig2, for mature and progenitor oligodendrocytes, we found that white matter adjacent to the second injury in rmTBI 21D animals had decreased numbers of Olig2 positive cells, but increased APC positive cells, compared to other groups. An experimental moderate-to-severe TBI study demonstrated increased apoptosis of mature oligodendrocytes for up to 21 days following injury (Flygt 2013). Furthermore, studies using moderate-to-severe models have also shown that Olig2 positive progenitors proliferate within 21 days of injury (Flygt 2013, Sullivan 2013). However we found no evidence of increased Ki67 positive staining within the CC of any of the animals at sub-acute times. The absence of sub-acute proliferation in our model suggests that proliferation may occur sooner after injury than reported by other studies. Future studies however, should include earlier timepoints to assess whether proliferation of oligodendrocyte progenitors is affected by rmTBI. Several other possibilities may also contribute to the decreased Olig2 positive cell population within rmTBI 21D animals, including progenitor apoptosis, reduced migration and accelerated differentiation into mature myelinating cells. However additional studies need to be performed in

order to determine the cause of reduced Olig2 positive cells following rmTBI at sub-acute timepoints.

We hypothesize that reduced Olig2 cells are a result of accelerated differentiation as increased numbers of APC positive cells were also found in white matter near the second injury site. Our TEM data shows that myelin in this region is thinned and demonstrates various abnormities, such as decompaction. Similarly using TEM, Sullivan et al (2013) assessed myelination 7 days following a moderate-to-severe TBI and found increased abnormalities within myelin at times in which oligodendrocyte progenitors were increasing expression of mature oligodendrocyte genes. This may suggest that remyelination early following TBI does not occur normally, perhaps resulting from ongoing axonal damage or inflammatory processes. Aberrant remyelination following TBI may persist long-term and is consistent with our TEM findings of altered myelin integrity at 60D in rmTBI animals.

Conclusion

Repeated mTBI, compared to a single injury, results in progressive white matter damage within the corpus callosum at regions distant from the impact site. We hypothesized that rmTBI would result in sub-acute changes in axonal integrity, followed by long-term myelin disruption. However while our DTI data supports our hypothesis, unexpectedly we also found evidence of thinned myelin at sub-acute times and increased axonal caliber long-term using TEM. These

findings clearly demonstrate that repeated mTBI results in sub-acute changes in axonal and myelin integrity that persists long-term following repeated injuries. Our sub-acute data also suggests that reduced axonal caliber is affected by altered neurofilament organization, while axon remyelination may be affected by a reduced Olig2 positive oligodendrocyte population. Our experimental results provide a potential morphological basis for many of the evolving abnormalities reported in clinical studies of mTBI. However, further investigation of the relationship between myelin and axon integrity and the effects of rmTBI on oligodendrocyte populations are warranted to delineate the evolution of white matter damage following repeated injuries.

Figures and Legends

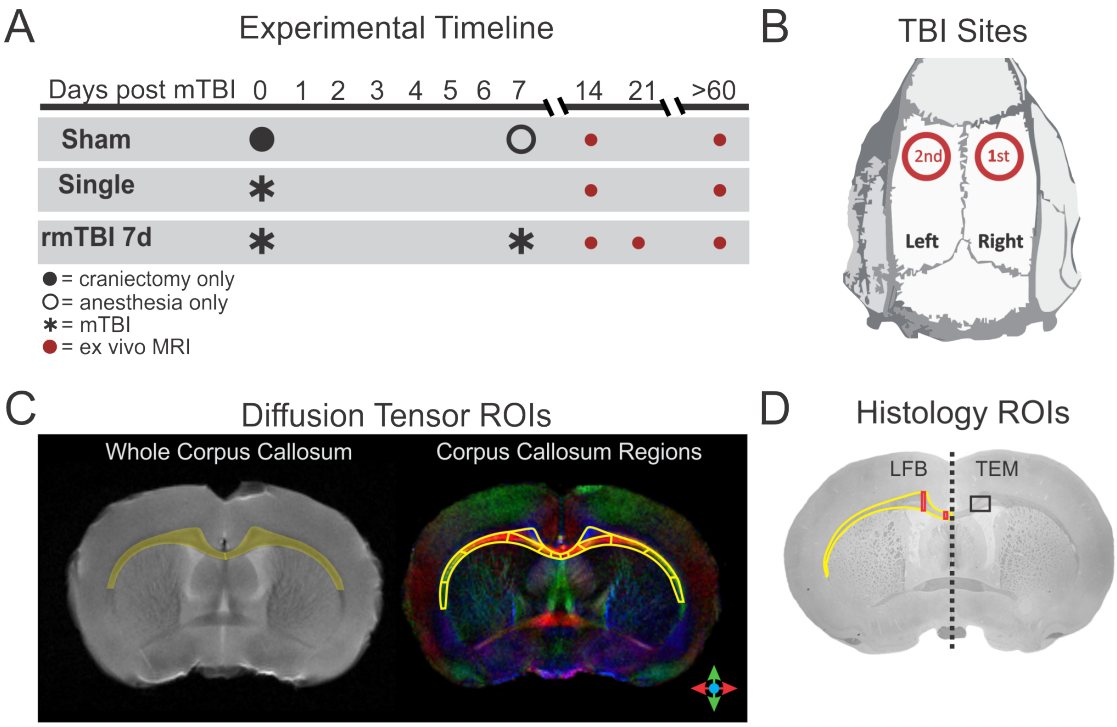

Figure 3.1: Experimental Design and Region of Interest Analysis.

A. mTBI (denoted as *) was induced to the right cortex of all injured animals, while Sham controls only received a craniectomy. A second mTBI was then induced to the left cortex of rmTBI animals 7 days later (*). Sham and single groups were sacrificed at 14 and 60D, while rmTBI animals were sacrificed at 14D (14D post first injury), 21D (14D post second injury) and 60D for ex vivo DTI. **B.** Schematic of the first (right) and second (left) mTBI locations. **C.** DTI images were analyzed using the whole right and left corpus callosum (CC; left, yellow ROIs). The CC was then examined using a total of 12 ROIs (6 each bilaterally) as shown on the relative anisotropy color maps, which depict the directionality of water diffusion along the CC (red: medial-lateral; green: dorsal-ventral; blue: anterior-posterior). **D.** Changes in CC integrity were further examined using Luxol fast blue staining and transmission electron microscopy. The area of the whole right and left CC (yellow ROI), cingulum (cingulum + CC) width and midline CC width (red boxes) were measured in addition to LFB staining intensity. TEM analysis was performed on the right CC of Single and Sham animals and the left CC of rmTBI animals (black box denotes CC region).

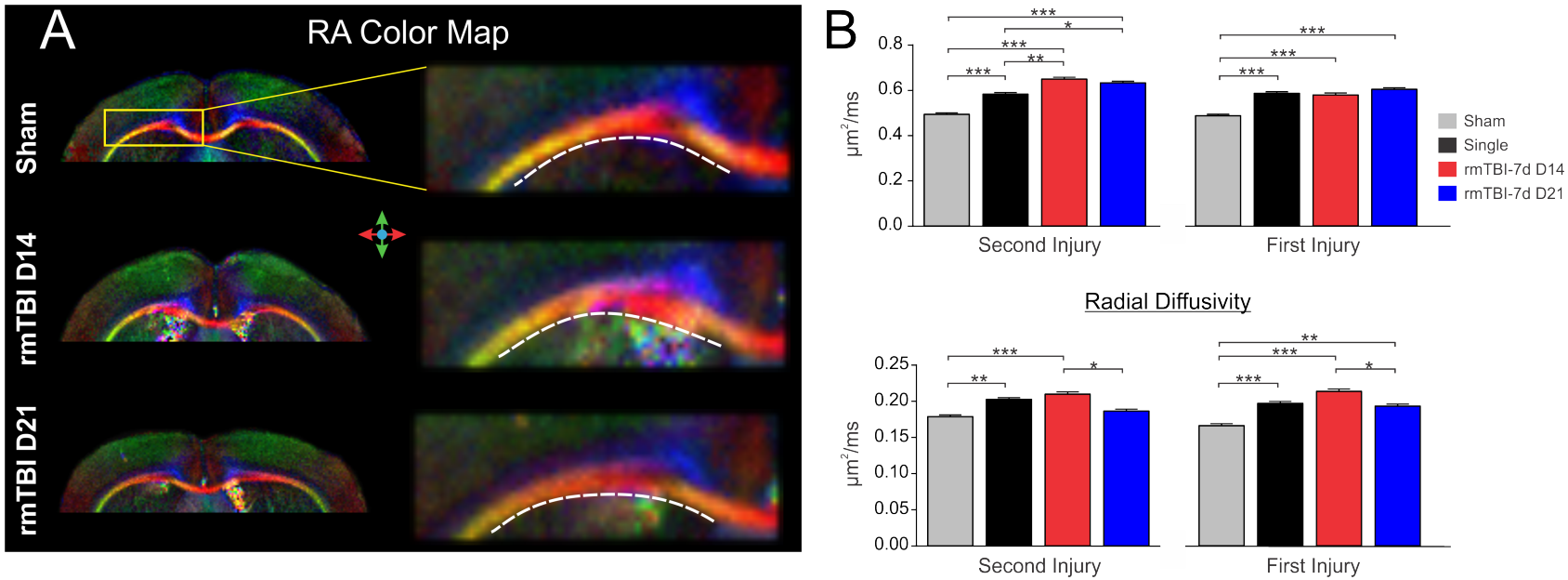
A
RA Color Map
Sham
rmTBI D14
rmTBI D21
B
Axial Diffusivity
μm²/ms
0.8
0.6
0.4
0.2
0.0
Second Injury
First Injury
Sham
Single
rmTBI-7d D14
rmTBI-7d D21
Radial Diffusivity
μm²/ms
0.25
0.20
0.15
0.10
0.05
0.00
Second Injury
First Injury

Figure 3.2: Axial diffusivity is increased in white matter adjacent to the second injury following rmTBI.

A. Relative anisotropy (RA) color maps illustrate differences in water diffusion along the anterior corpus callosum (red: medial-lateral; green: dorsal-ventral; blue: anterior-posterior). **B.** Examination of axial diffusivity (AD) revealed significantly increased measurements within the left (second injury) CC of both rmTBI 14D and 21D animals compared to Singles, while increased diffusivity was observed in the right (first injury) CC of all TBI animals compared to Shams. **C.** Radial diffusivity (RD) analysis showed a bilateral increase in measurements taken from rmTBI 14D animals compared to those from the rmTBI 21D group. *p<0.05; **p<0.01; ***p<0.001

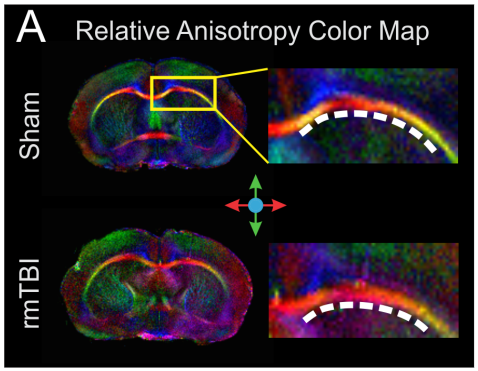
A
Relative Anisotropy Color Map
Sham
rmTBI

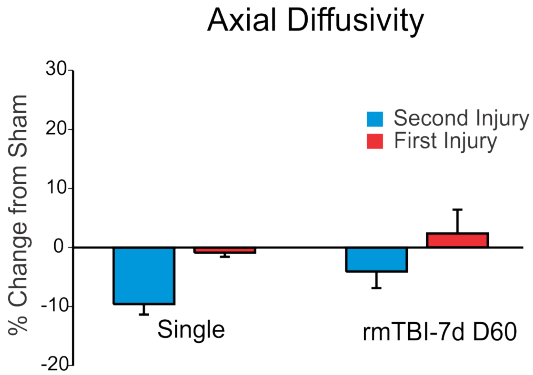
B
Axial Diffusivity
% Change from Sham
30
20
10
0
-10
-20
Second Injury
First Injury
Single
rmTBI-7d D60

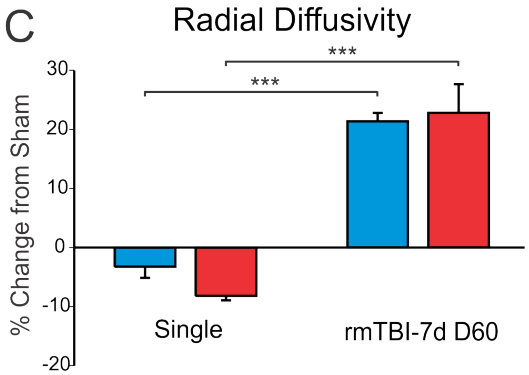
C
Radial Diffusivity
% Change from Sham
30
20
10
0
-10
-20
***
***
Single
rmTBI-7d D60

Figure 3.3: Radial diffusivity is increased in rmTBI animals 60D post rmTBI. **A.** Representative DTI images illustrate changes in axial (AD) and radial (RD) diffusivities between Sham and rmTBI animals. The relative anisotropy (RA) color map reflects overall differences in water diffusion between the groups (red: medial-lateral; green: dorsal-ventral; blue: anterior-posterior). **B.** Evaluation of AD revealed no significant differences between the injured groups within the right and left corpus callosum (CC). **C.** A significant increase in RD was observed bilaterally within the rmTBI animals compared to the Single and Sham groups. *p<0.05; **p<0.01; ***p<0.001

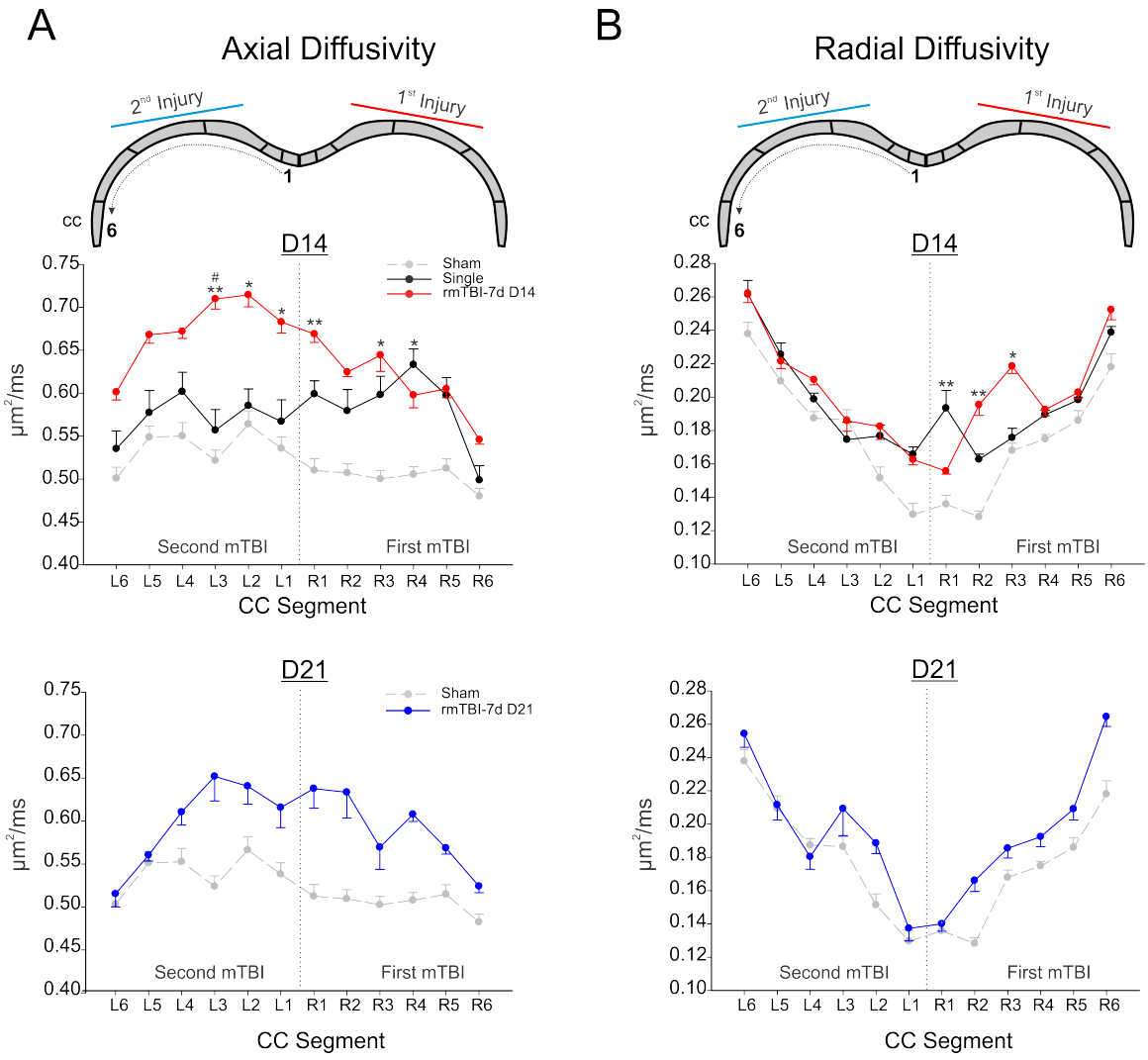
A
Axial Diffusivity
2nd Injury
1st Injury
1
cc
6
D14
Sham
Single
rmTBI-7d D14
μm²/ms
Second mTBI
First mTBI
L6 L5 L4 L3 L2 L1 R1 R2 R3 R4 R5 R6
CC Segment
D21
Sham
rmTBI-7d D21
B
Radial Diffusivity

Figure 3.4: Axial diffusivity is elevated in white matter regions adjacent to the injury site in rmTBI animals at sub-acute times.

A. Regional CC analysis demonstrated increased AD within segments found immediately adjacent to the first and second impacts in rmTBI 14D animals compared to Sham controls that pseudo-normalized by 21D. **B.** RD analysis of the segments revealed changes at the site of the first injury within the rmTBI D14 group that pseudo-normalized by 21D. *p<0.05; **p<0.01; ***p<0.001 vs. Sham; $^{\#}$p<0.05 vs. Single

A

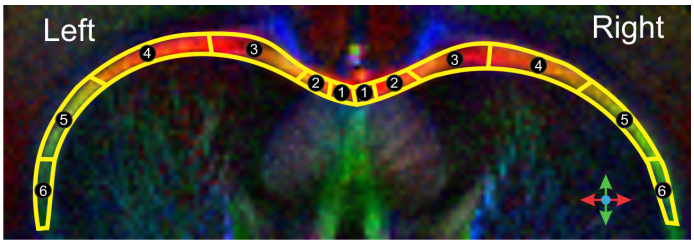
Left
Right
1
2
3
4
5
6

B

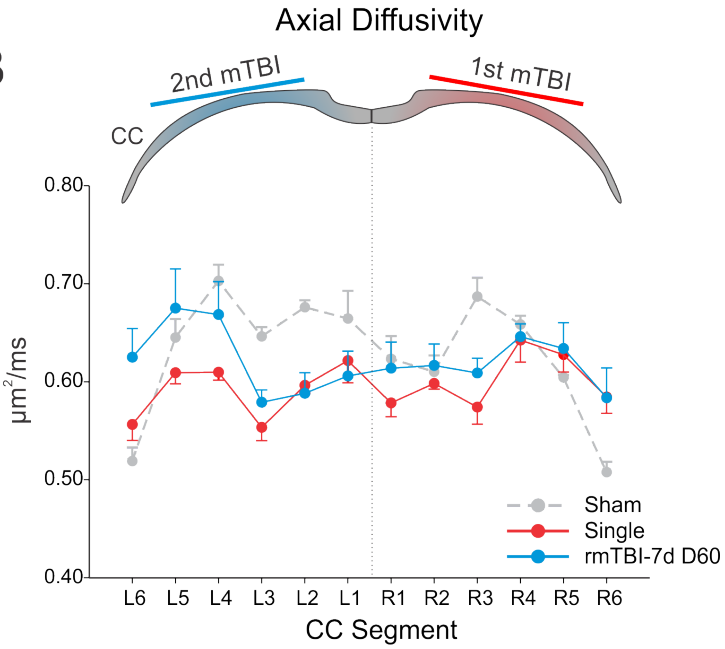
Axial Diffusivity
2nd mTBI
1st mTBI
CC
0.80
0.70
0.60
0.50
0.40
µm²/ms
Sham
Single
rmTBI-7d D60
L6 L5 L4 L3 L2 L1 R1 R2 R3 R4 R5 R6
CC Segment

C

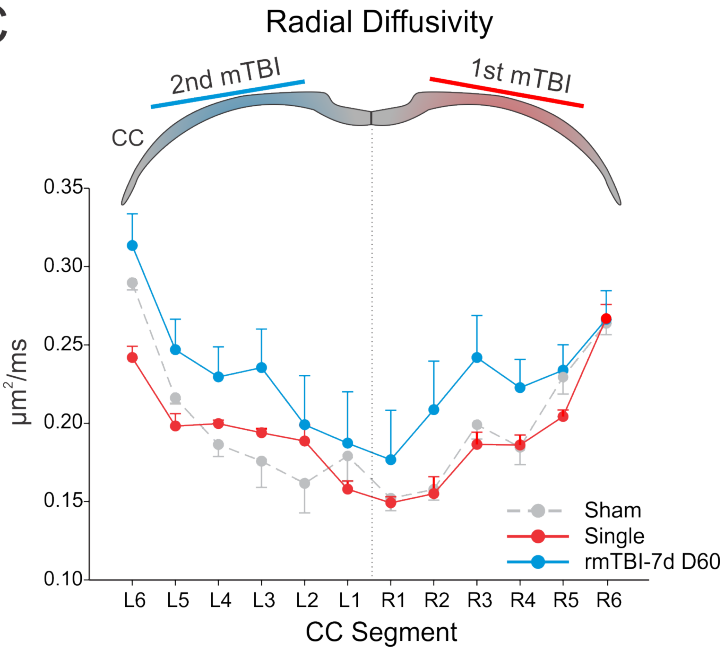
Radial Diffusivity
2nd mTBI
1st mTBI
CC
0.35
0.30
0.25
0.20
0.15
0.10
µm²/ms
Sham
Single
rmTBI-7d D60
L6 L5 L4 L3 L2 L1 R1 R2 R3 R4 R5 R6
CC Segment

Figure 3.5: Radial Diffusivity is Elevated Throughout the Entire Corpus Callosum in rmTBI Animals at 60D post rmTBI.

A. Schematic depicting the right and left ROIs used to further examine regional DTI changes within the CC (red: medial-lateral; green: dorsal-ventral; blue: anterior-posterior). **B.** Axial diffusivity (AD) measurements revealed no significant changes between the groups within the right (first mTBI) or left (second mTBI) corpus callosum (CC). **C.** Radial diffusivity (RD) measurements taken from the segmented regions showed no significant differences between the experimental groups. However, the rmTBI animals demonstrated elevated RD in every segment compared to the Sham and Single groups.

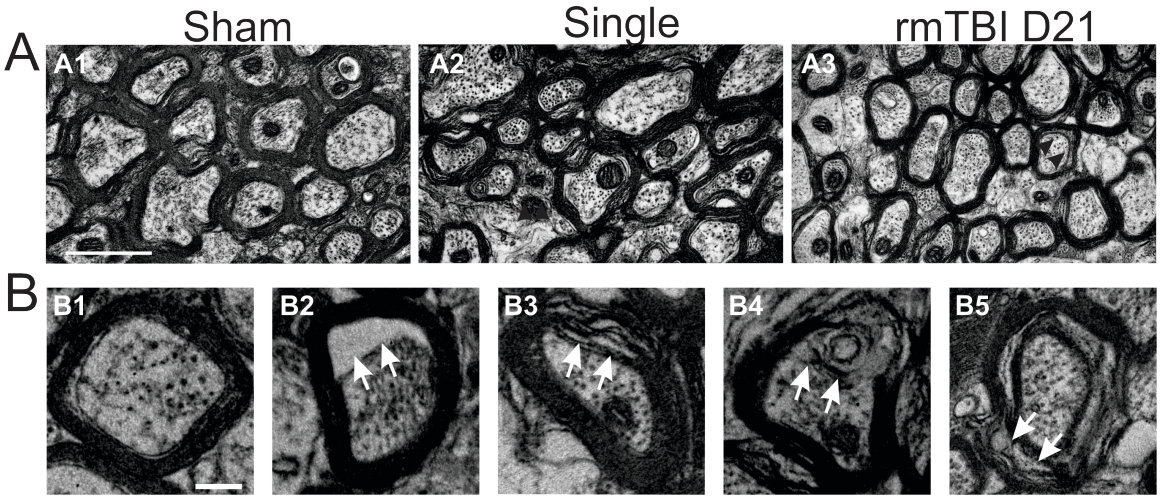
A
Sham
Single
rmTBI D21
A1
A2
A3
B
B1
B2
B3
B4
B5

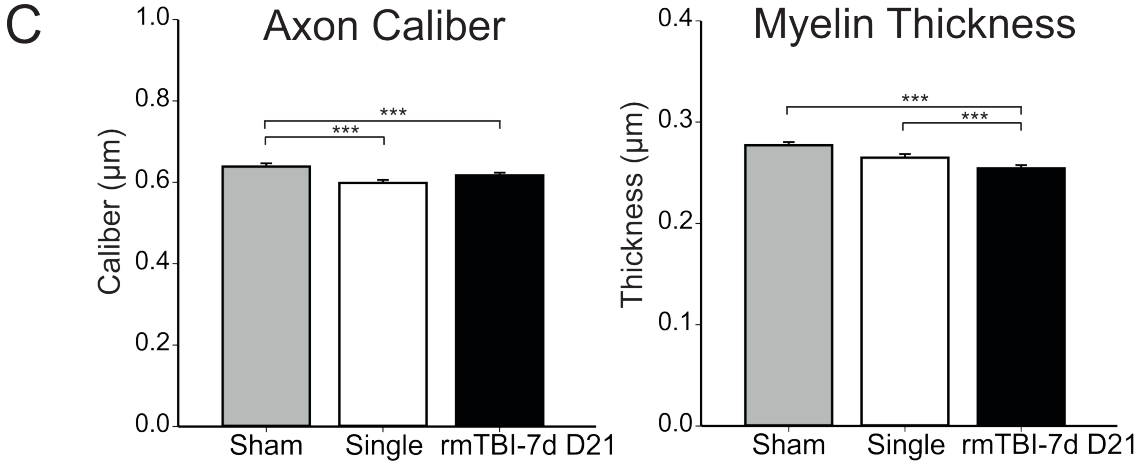
C
Axon Caliber
Caliber (µm)
1.0
0.8
0.6
0.4
0.2
0.0
***
***
Sham
Single
rmTBI-7d D21
Myelin Thickness
Thickness (µm)
0.4
0.3
0.2
0.1
0.0
***
***
Sham
Single
rmTBI-7d D21

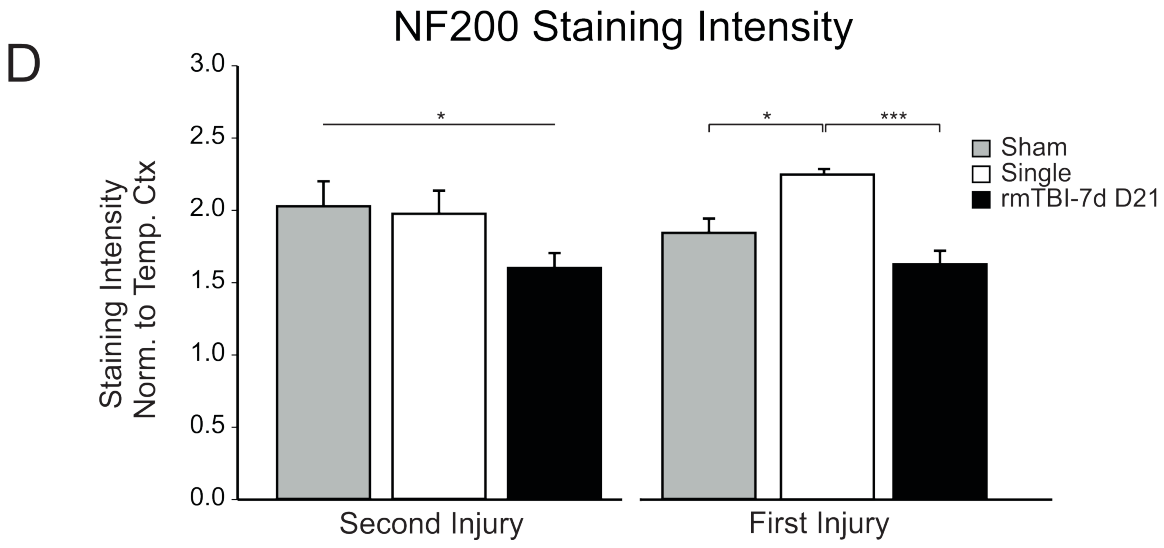
D
NF200 Staining Intensity
Staining Intensity
Norm. to Temp. Ctx
3.0
2.5
2.0
1.5
1.0
0.5
0.0
*
*
***
Sham
Single
rmTBI-7d D21
Second Injury
First Injury

Figure 3.6: rmTBI reveals increased white matter abnormalities 21D post TBI on the side of second injury.

A. Representative transmission electron microscopy (TEM) micrographs from the site of the first injury (right) of Sham and Single controls and second injury (left) of rmTBI 21D animals demonstrate increased abnormalities within injured animals (black arrows); cal bar= 1μm. **B.** Normal myelinated axons appeared with a tightly wrapped sheath located near the axon (B1). Typical abnormalities (arrows) within the corpus callosum (CC) included large separations of the myelin sheath from the axon (B2), breaking of the sheath layers (B3) and deterioration of the myelin (B4, B5); cal bar= 0.2μm. **C.** The rmTBI 21D and Single groups exhibited significantly decreased axonal caliber compared to Shams. Examination of myelin revealed significantly decreased thickness within rmTBI 21D animals compared to other groups. **D.** NF200 staining revealed significant differences within white matter adjacent to the second injury (left). While the side of the first injury (right) revealed increased NF200 staining intensity within Single animals compared to other groups. *p<0.05; **p<0.01; ***p<0.001

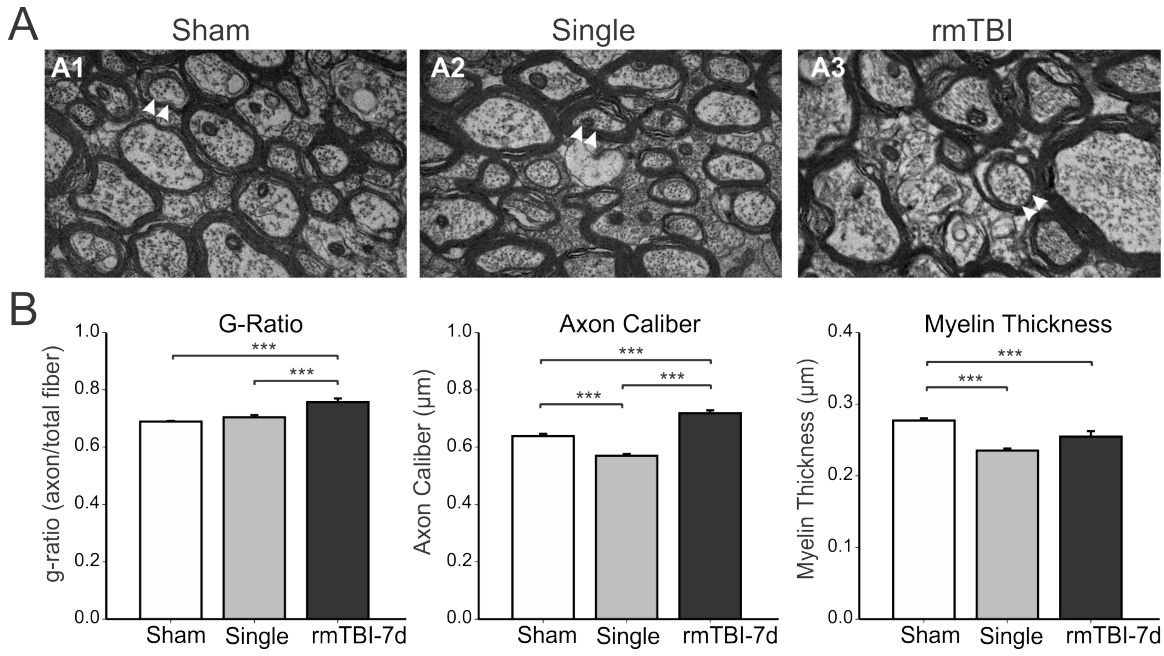
A
Sham
Single
rmTBI
A1
A2
A3
B
G-Ratio
g-ratio (axon/total fiber)
1.0
0.8
0.6
0.4
0.2
0.0
***
***
Sham
Single
rmTBI-7d
Axon Caliber
Axon Caliber (μm)
1.0
0.8
0.6
0.4
0.2
0.0
***
***
Sham
Single
rmTBI-7d
Myelin Thickness
Myelin Thickness (μm)
0.4
0.3
0.2
0.1
0.0
***
***
Sham
Single
rmTBI-7d

Figure 3.7: Ongoing White Matter Damage is Evident in the Corpus Callosum at 60D post rmTBI.

A. Representative transmission electron microscopy (TEM) images illustrate increased white matter abnormalities (arrows) within rmTBI animals (A3) at the site of the second injury (left) compared to the site of first injury (right) within the Sham (A1) and Single (A2) groups; cal bar= 1μm. **B.** The rmTBI group revealed a significant increase in g-ratio (axon/fiber diameter) compared to other groups. Similarly, the axon caliber of rmTBI animals was also increased compared to Sham and Single groups. The Single group also exhibited a significant decrease in axon caliber compared to Shams. Both the Single and rmTBI groups demonstrated a significant decrease in myelin thickness compared to Sham animals. *$p<0.05$; **$p<0.01$; ***$p<0.001$

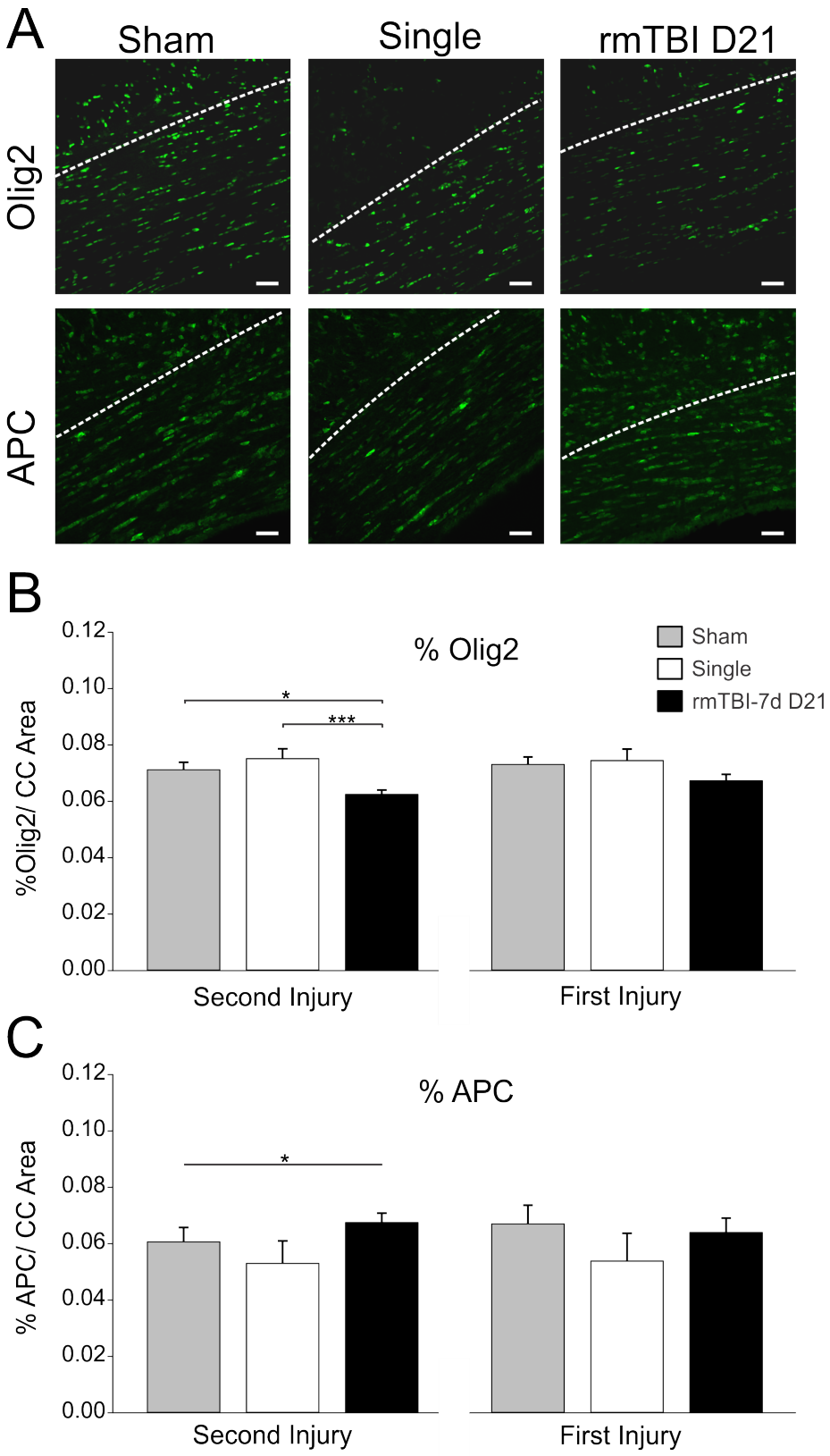
A
Sham
Single
rmTBI D21
Olig2
APC
B
% Olig2
Sham
Single
rmTBI-7d D21
%Olig2/ CC Area
0.12
0.10
0.08
0.06
0.04
0.02
0.00
*
***
Second Injury
First Injury
C
% APC
% APC/ CC Area
0.12
0.10
0.08
0.06
0.04
0.02
0.00
*
Second Injury
First Injury

Figure 3.8: Corpus Callosum adjacent to the second injury site revels decreased Olig2, but increased APC cell populations 21D following rmTBI. **A.** Representative Olig2 and APC staining within the left corpus callosum (CC; dotted line) of Sham, Single and rmTBI D21 groups. **B.** Olig2 staining within the CC revealed significant decreases in the left (second injury) CC of rmTBI animals compared to other groups, while no significant differences were observed in the right (first injury) CC. **C.** APC staining showed significant increases in counts on the side of the second injury within rmTBI animals, while no differences were seen on the first injury side. Cal bar= 40μm; *p<0.05; **p<0.01; ***p<0.001

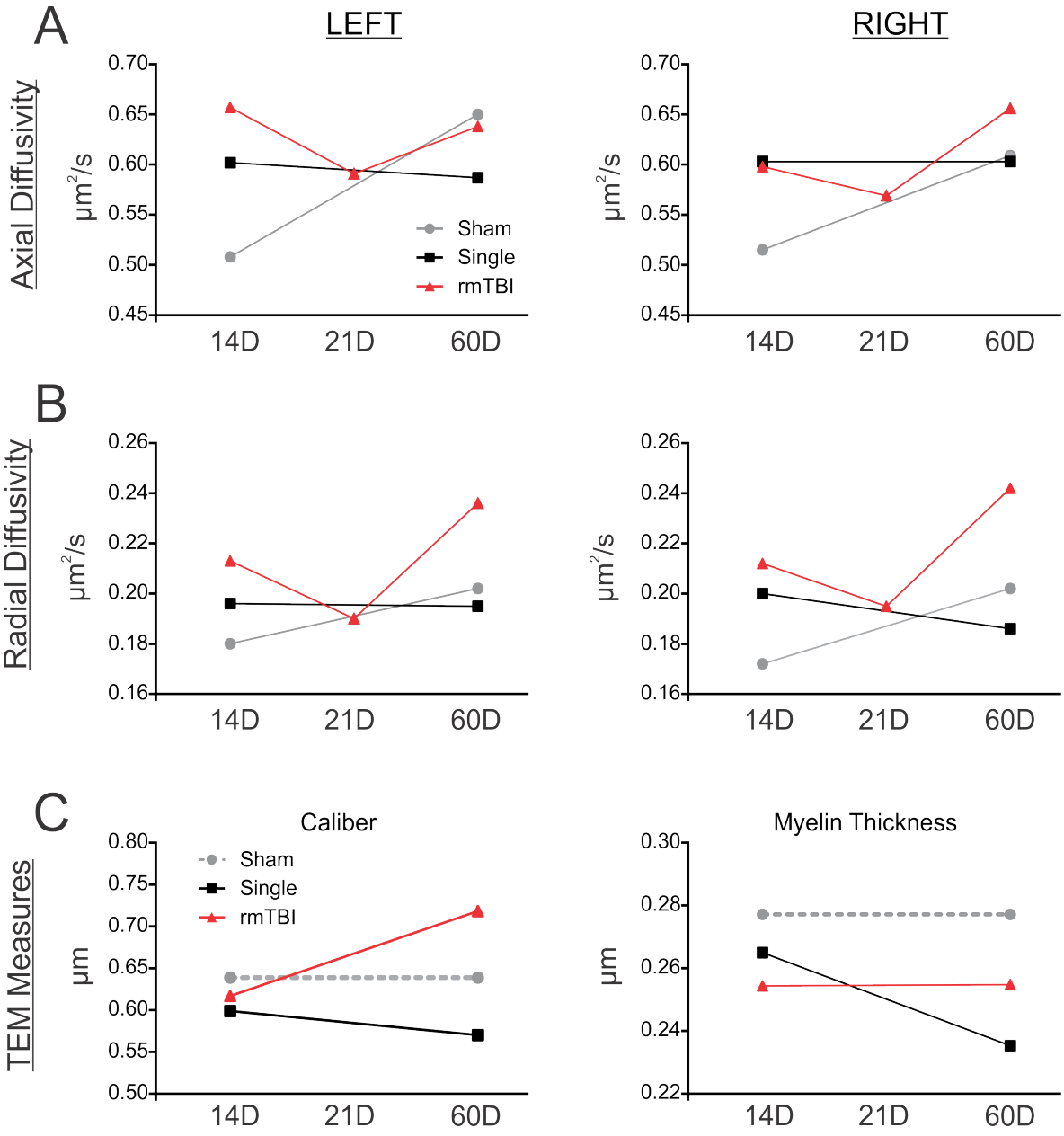
A
LEFT
RIGHT
Axial Diffusivity
μm²/s
0.70
0.65
0.60
0.55
0.50
0.45
Sham
Single
rmTBI
14D
21D
60D
B
Radial Diffusivity
μm²/s
0.26
0.24
0.22
0.20
0.18
0.16
C
TEM Measures
Caliber
μm
0.80
0.75
0.70
0.65
0.60
0.55
0.50
Myelin Thickness
0.30
0.28
0.26
0.24
0.22

Figure 3.9: Temporal summary of diffusion tensor and electron microscopy data

Shows the left and right axial **(A)** and radial **(B)** diffusivity between experimental groups at 14D, 21D and 60D post injury. **C.** Depicts the axonal caliber and myelin thickness measures from transmission electron micrographs (TEM) for each experimental group. Shams (grey dotted line) were only assessed at 14D post injury.

Table 3.1: Sub-acute Luxol fast blue fast blue area and width measurements from corpus callosum regions.

	Whole CC Area (mm^2)		Midline CC Width (mm)		Cingulum Width (mm)	
	Left	Right	Left	Right	Left	Right
Sham	4.84 ± 0.51	4.93 ± 0.64	2.19 ± 0.24	2.14 ± 0.16	4.55 ± 0.58	4.28 ± 0.85
Single	4.84 ± 0.39	5.19 ± 0.42	2.24 ± 0.22	2.24 ± 0.17	4.55 ± 0.41	4.60 ± 0.54
rmTBI D14	4.53 ± 0.46	5.09 ± 0.35	2.11 ± 0.38	2.05 ± 0.24	4.20 ± 0.55	5.05 ± 0.38
rmTBI D21	5.08 ± 0.83	5.01 ± 1.0	2.25 ± 0.53	2.15 ± 0.48	4.98 ± 0.48	4.73 ± 0.76
P Value Sham vs. Single	p=1.000	p=1.000	p=1.000	p=1.000	p=1.000	p=0.381
P Value Sham vs. rmTBI D14	p=0.741	p=0.011	p<0.001	p=0.036	p=1.000	p<0.001
P Value Sham vs. rmTBI D21	p<0.001	p=0.039	p<0.001	p<0.001	p<0.001	p=0.006
P Value Single vs. rmTBI D14	p=0.425	p=0.184	p=0.001	p=0.405	p=1.000	p=0.153
P Value Single vs. rmTBI D21	p<0.001	p=0.525	p<0.001	p=0.024	p<0.001	p=1.000
P Value rmTBI D14 vs. rmTBI D21	p=0.007	p=1.000	p=1.000	p=1.000	p<0.001	p=1.000

Area= $10^{-2} \pm 10^{-2}$; Width= $10^{-4} \pm 10^{-4}$

Table 3.2: Sub-acute Luxol fast blue fast blue signal intensity (SI) measurements from corpus callosum regions.

	Whole CC Area (AU)		Midline CC Width (AU)		Cingulum Width (AU)	
	Left	Right	Left	Right	Left	Right
Sham	0.96 ± 0.1	1.03 ± 0.0	1.10 ± 0.1	1.16 ± 0.1	1.01 ± 0.1	1.05 ± 0.0
Single	1.04 ± 0.1	1.03 ± 0.1	1.17 ± 0.1	1.16 ± 0.1	1.06 ± 0.1	1.06 ± 0.1
rmTBI D14	0.99 ± 0.1	1.07 ± 0.1	1.11 ± 0.1	1.18 ± 0.1	1.02 ± 0.1	1.10 ± 0.1
rmTBI D21	0.96 ± 0.1	0.94 ± 0.1	1.05 ± 0.1	1.04 ± 0.1	0.98 ± 0.1	0.96 ± 0.1
P Value Sham vs. Single	p=0.071	p=1.000	p=0.338	p=1.000	p=0.690	p=1.000
P Value Sham vs. rmTBI D14	p=0.607	p=1.000	p=1.000	p=1.000	p=1.000	p=1.000
P Value Sham vs. rmTBI D21	p=1.000	P<0.001	p=1.000	p=<0.001	p=1.000	p=<0.001
P Value Single vs. rmTBI D14	p=1.000	p=1.000	p=1.000	p=1.000	p=1.000	p=1.000
P Value Single vs. rmTBI D21	p=0.311	p<0.001	p=0.077	p<0.001	p=0.702	p<0.001
P Value rmTBI D14 vs. rmTBI D21	p=0.790	p<0.001	p=0.082	p<0.001	p=0.701	p<0.001

Table 3.3: Long-term Luxol fast blue signal intensity (SI) and thickness measurements from left corpus callosum regions.

		Sham	Single	rmTBI	Sham vs. Single	Sham vs. rmTBI	Single vs. rmTBI
Whole CC	Area[1]	5.45 ± 3.6	5.22 ± 6.5	5.91 ± 11	p=1.000	p=0.532	p= 0.018
	SI (AU)	0.91 ± 0.1	0.97 ± 0.1	0.98 ± 0.1	p=0.558	p=0.125	p=1.000
Midline CC	Width[2]	2.48 ± 2.1	2.34 ± 2.3	2.74 ± 4.3	p=1.000	p=0.208	p< 0.001
	SI (AU)	1.02 ± 0.1	1.12 ± 0.1	1.10 ± 0.1	p=0.011	p=0.084	p=1.000
Cingulum	Width[2]	5.22 ± 4.8	4.69 ± 8.3	6.11 ± 5.4	p<0.001	p<0.001	p< 0.001
	SI (AU)	0.93 ± 0.1	1.00 ± 0.1	1.01 ± 0.1	p=0.186	p=0.032	p=1.000

[1]Area= $10^{-2} \pm 10^{-3}$ (mm^2); [2]Width= $10^{-4} \pm 10^{-5}$ (mm)

Table 3.4: Long-term Luxol fast blue signal intensity (SI) and thickness measurements from right corpus callosum regions.

		Sham	Single	rmTBI	Sham vs. Single	Sham vs. rmTBI	Single vs. rmTBI
Whole CC	Area[1]	5.53 ± 4.3	5.23 ± 5.5	6.08 ± 11	p=1.000	p=0.164	p=0.001
	SI (AU)	0.95 ± 0.1	1.01 ± 0.1	1.03 ± 0.1	p=0.150	p=0.005	p=1.000
Midline CC	Width[2]	2.58 ± 2.6	2.33 ± 1.4	2.71 ± 4.3	p=0.069	p=1.000	p<0.001
	SI (AU)	1.08 ± 0.1	1.16 ± 0.1	1.15 ± 0.1	p=0.006	p=0.032	p=1.000
Cingulum	Width[2]	5.33 ± 6.2	5.01 ± 12	6.19 ± 11	p=1.000	p=0.144	p= 0.009
	SI (AU)	0.97 ± 0.1	1.03 ± 0.1	1.05 ± 0.1	p=0.212	p= 0.005	p=1.000

[1]Area= $10^{-2} \pm 10^{-3}$ (mm^2); [2]Width= $10^{-4} \pm 10^{-5}$(mm)

Chapter 4

Reduced Hemispheric Swelling Occurs in the Presence of Limited Microglial Activation

Abstract

Traumatic brain injury (TBI) can result in long-term neurological deficits and increased risk of neurodegenerative diseases. The cellular mechanisms that exacerbate tissue damage and lead to chronic disability following TBI are not well known. Inflammation and specifically microglia, the CNS resident tissue macrophages, can acquire alternative and classical activation states associated with cytoprotective and cytotoxic processes, respectively. A subset of microglia exclusively express triggering receptor on myeloid cells-2 (TREM2), which is upregulated following CNS injury or systemic inflammation. Experimental studies indicate that TREM2 is a critical anti-inflammatory molecule, where loss of this receptor results in early onset dementia and mutation in the receptor's ligand binding pocket correlates with a 3-fold increased risk of Alzheimer's disease. Thus, immune cells are clearly linked to neurodegenerative diseases and their ability to participate in cytotoxic and cytoprotective roles have identified them as potential aggravators of TBI pathology with the potential for being manipulated therapeutically.

We hypothesized that systemic inflammation or TREM2 knockout (TREM2KO) at the time of a moderate-to-severe controlled cortical impact (CCI) would exacerbate TBI pathology. We compared lesion size, hemispheric volume

and microglial activation within the impacted cortex 7 days following TBI in wildtype, wildtype with systemic LPS challenge and TREM2KO animals and activation in naïve wildtype mice. Unexpectedly, MRI analysis revealed virtually no swelling in TREM2KO animals and reduced hemispheric volume in LPS challenged mice compared to wildtype at 7 days post TBI. These changes in hemispheric volume occurred in the absence of altered lesion volume or composition. Nanostring analysis of microglial activation showed that while all TBI groups demonstrated 2-fold or more expression in inflammatory molecules from naïve mice, the LPS challenged and TREM2KOs revealed lower levels of activation than wildtype following TBI. Furthermore, we found that microglia showed lower inflammatory molecule expression levels compared to the impacted tissue within TREM2KOs. Taken together these data suggest that limited microglial inflammation following TBI is beneficial to hemispheric swelling outcome.

Introduction

Traumatic brain injuries (TBI) contribute to a third of all injury related deaths and affect an estimated 1.7 million Americans each year (Tagliaferri 2006, Corrigan 2010, Faul 2010). Brain injury severity is grossly categorized as mild, moderate or severe, where individuals typically appear to recover normally from mild injuries, but can show long-lasting or permanent deficits following a moderate-to-severe head trauma. Currently, no effective therapeutics to reverse TBI tissue damage exists. As a result an estimated 3.2-5.3 million Americans currently live with a chronic neurological and/or physical disability caused by TBI, greatly decreasing their quality of life and having prolonged economical impacts on society (Coronado 2011).

Following TBI, primary injuries immediately trigger secondary injury cascades that result in further tissue damage including edema formation, hemorrhage progression and white matter damage (Povlishock and Katz 2005, Kurland 2012). Brain swelling, which can result from increased edema formation and blood deposition, significantly increases patient morbidity and mortality, resulting in approximately 50% of all TBI related deaths (Balestreri 2006, Muehlschlegel 2013). Hemorrhage is also particularly harmful as it can take months to be cleared from the brain and iron within the blood can facilitate the production of free radicals that damage DNA, lipids and proteins (Gaasch 2007). Moderate and severe TBIs as well as repeated injuries have been associated with increased susceptibility to developing neurodegenerative diseases (Smith

2013). However the secondary mechanisms that leads to exacerbated and chronic TBI pathology remains poorly understood. Current TBI research focuses on identifying the cellular mechanisms responsible for initiating secondary cascades as these pathways may be targeted therapeutically to attenuate and prevent further tissue damage.

Inflammatory responses occur immediately after injury and can persist years following TBI (Davalos 2005, Ramlackhansingh 2011). Microglia, the resident CNS macrophages, are the first cells to respond to tissue damage and can acquire activation phenotypes associated with cytotoxic and cytoprotective processes. Thus, they have been identified as having the potential to aggravate and instigate secondary damage cascades. Classically (M1) activated microglia and macrophages are functionally associated with neurotoxic processes and are characterized by high expression of pro-inflammatory molecules such as iNOS, TNFα and IL-1β (Block and Hong 2005). Studies exposing microglia to necrotic neurons or myelin debris in culture, revealed increased microglial activation and expression of the classical molecules IL-6, TNF and iNOS (Pais 2008, Pinteaux-Jones 2008). Subsequent exposure of healthy neurons to media collected from activated microglial cultures increased neuronal death indicating that secreted molecules produced by classically activated microglia are neurotoxic (Pais 2008, Pinteaux-Jones 2008). In contrast, alternative (M2) activation states are functionally associated with repair processes and characterized by YM1, Arginase1 and CD206 expression (Mosser and Edwards 2008). Upon blocking

the microglial response to injury via purinergic receptor antagonists or preventing microglial process outgrowth resulted in increased lesion size and apoptosis following brain injury (Hines 2009, Roth 2014). Microglia also play critical roles in the removal of debris following injury, which is critical for rapid recovery following injury (Kotter 2006). While acute treatment using anti-inflammatory compounds have shown improved outcomes following TBI, many of these compounds failed in clinical trials or have demonstrated adverse effects when used chronically (Browne 2006, Kumar and Loane 2012). Thus a better understanding of the roles that classical and alternative microglial activation plays following TBI is needed.

In the CNS, microglia exclusively express triggering receptor expressed on myeloid cells-2 (TREM2), which has been shown by several studies to play a critical anti-inflammatory role following injury. TREM2 activity blocks the expression of pro-inflammatory cytokine expression and is necessary for the phagocytosis of cellular debris (Takahashi 2007, Hsieh 2009). Antibody mediated blocking of TREM2 following EAE resulted in increased inflammation and aggravated pathology (Piccio 2007). However, intravenous injection of TREM2 expressing precursor cells alleviated experimental autoimmune encephalomyelitis pathology (Takahashi 2007). Unexpectedly, a recent study of experimental stroke in TREM2 knockout animals revealed that while pro-inflammatory cytokine (TNFα, IL-6, IL-1β) expression was reduced, no change in lesion volume was observed at 7 or 28 days following injury (Sieber 2013).

Clinically, TREM2 loss-of-function results in Nasu-Hakola disease, which is associated with early onset cognitive dementia in the 20's followed by death in the 40-50's (Paloneva 1993). Recently, a TREM2 mutation in the ligand-binding pocket has also been associated with a 3-fold risk in developing Alzheimer's disease (Guerreiro 2013, Abduljaleel 2014). Since only microglia, and not neurons, express TREM2 the occurrence of Nasu-Hakola disease and increased susceptibility of Alzheimer's Diseases provides direct evidence for the role of inflammation in neurodegenerative diseases.

In addition to CNS injury, microglia can be activated by and increase their expression of TREM2 in response to systemic inflammation, such as the cold or flu (Piccio 2007, Takahashi 2007, Davis 2011). Intraperitoneal (IP) lipopolysaccharide (LPS) injections (0.1-2.5mg/kg) have revealed acute (<24hrs) changes in microglial morphology and increased expression of both pro-inflammatory (IL-1β, TNFα) and anti-inflammatory (TGFβ, IL-10, TREM2) expression within the rodent brain (Turrin 2001, Davis 2011, Longhi 2011, Biesmans 2013). Peripheral cytokines produced by IP injection of LPS can induce neuroinflammation via activating BBB endothelial cells or vagal nerve projections that in turn activate cells within the brain (Dantzer 2001, Quan 2008). A single low dose (0.1-0.2 mg/kg) injection of IP LPS given within 5 days before induction of a moderate-to-severe TBI or experimental stroke resulted in decreased lesion volume and altered the inflammatory response (Rosenzweig 2004, Longhi 2011). However a higher IP LPS dose (4 mg/kg) given immediately

following a severe TBI revealed increased cytokine (TNFα, IL-6) expression and apoptotic cells 1-7 days following injury (Hang 2004). These studies suggest that the cytoprotective or cytotoxic processes initiated by LPS treatment is both dose and time dependent.

Overall neuroinflammation clearly plays an important role in the progression and resolution of TBI. However the beneficial and/or detrimental role of microglial inflammation following TBI is not clear. We hypothesized that deficiency in TREM2 would result in worsened TBI outcome, as it has been previously shown to inhibit pro-inflammatory cytokine production and is critical for debris clearance. We also predicted that a high (5 mg/kg) IP LPS dose 24hrs prior to TBI would result in worsened tissue damage, as systemic challenge increases neuroinflammation.

Materials and Methods

All animal care and protocols were performed in compliance with federal regulations and the institutional review boards at Loma Linda University and the University of California, Riverside.

Animals

A total of 42 adult 6-9 week old male C57Bl/6 (15.6-26.6g; The Jackson Laboratory, Bar Harbor, ME) and TREM2KO mice (19.0-23.7g; bred in the Carson Lab, UC Riverside) were single-housed in a temperature controlled animal facility on a 12-hour light/dark cycle and had access to food and water *ad libitum*. C57Bl/6 mice were randomly assigned to either naïve, wildtype (TBI, no pretreatment) or IP-LPS, 5mg/kg (78-133 µl) 24hrs prior to TBI induction. TREM2KOs received no treatment prior to TBI.

Traumatic Brain Injury

A controlled cortical impact (CCI) was used to induce a moderate TBI as previously described (Donovan 2012), with minor modifications. Briefly, mice were anesthetized and secured into a stereotactic frame equipped with a heating pad. A midline incision exposed the skull surface and a craniectomy (5 mm diameter) was performed immediately adjacent to the coronal and sagittal sutures over the right hemisphere using an ice cold trephine. Subsequently, a moderate CCI (3mm diameter tip, 1mm depth, 5.0 m/s speed, 200 ms dwell) was delivered to the right cortical surface using an electromagnetically driven piston (Leica Biosystems Inc., Richmond, IL). Following injury, animals were sutured

closed and placed in a warmed recovery chamber until consciousness and grooming resumed at which point the animals were returned to their cages.

Magnetic resonance imaging and analysis

Wildtype (n=4), IP-LPS (n=3) and TREM2KO (n=5) mice underwent *in vivo* T2 weighted imaging (T2WI) 3 and 7 days post TBI as previously described with minor modifications (Donovan 2012). During imaging animals were anesthetized (isoflurane: 3% induction, 1% maintenance) and body temperature was maintained using a heated water pad. T2WIs (TR/TE=2972.1ms/10.2ms, 25x0.5mm slices) were collected with a 128x128 matrix and a 2cm field of view on an 11.7T Bruker Avance instrument (Bruker Biospin, Billerica, MA).

T2WIs were analyzed as previously described (Donovan 2012). Briefly, the right hemisphere, left hemisphere and lesioned area were manually segmented (Bregma, 1.10 to -3.52) using Cheshire image processing software (Hayden Image/Processing Group, Waltham, MA) by a user blinded to the groups. Lesion and hemispheric volumes (mm^3) were extracted and the percent change in hemispheric volume was calculated by dividing the right hemispheric volume by the left hemispheric volume for each animal. Similarly the percent lesion volume was calculated for each animal by dividing the lesion volume by the whole brain (sum of the right and left hemispheres) volume. Lesioned tissue was then analyzed for blood, edema and normal appearing brain (NAB) using our previously published method (Donovan 2012), with modifications. The lesioned area from n=3 animals (1 per group) was manually segmented into blood and

edema containing pixels to determine the appropriate T2 value ranges for blood, edema and NAB in this TBI model using mice. Voxels containing blood (<41ms), edema (>55ms) and NAB (42-54ms) were then extracted as volumes and divided by the lesion volume so as to determine the composition of lesions following TBI.

Nanostring gene expression assay and analysis

Extracted RNA from purified microglia (n=8-12) and cortical tissue (n=2) underwent analysis using Nanostring (Nanostring Technologies, Seattle, WA). The Nanostring nCounter GX Mouse immunology kit was used to profile 561 mouse inflammatory genes. The assay was performed by Nanostring personnel according to the manufacturer's protocol. Briefly, 100ng of RNA was incubated with bar-coded reporter and capture probes for 16hrs at 65°C. Following incubation un-hybridized probes were removed and RNA molecules hybridized to probes were quantified using the nCounter Prep Station and GEN2 Digital Analyzer. Raw counts of RNA transcript numbers were normalized via the nCounter software using internal positive control counts and reference housekeeping genes.

Genes of interest were identified as those with 2-fold changes between comparisons. This 2-fold threshold was selected based on the 95% confidence intervals and correlation plot slopes of fold change differences between groups. Comparing fold changes between molecules isolated from the microglia of TBI groups (wildtype, IP-LPS, TREM2KO) and wildtype naïve animals revealed that the 95% confidence intervals fell between 5 and 18 whereas the correlation plot

slopes were between 1.2-1.7. However fold change comparisons of molecules isolated from the microglia of IP-LPS or TREM2KO TBI groups and wildtype TBI animals showed 95% confidence intervals of -1.6 to 3.3 and correlation plot slopes of -0.00001to -0.00002. Based on these results we determined that fold changes of 2 were appropriate for analysis of our data sets, where fold changes of -1.9 to 1.9 were considered no change. Genes of interest were then entered into PANTHER Classification System and analyzed using the functional classification function (Mi 2013).

Statistics

Statistical analysis was performed using Sigma Plot Software (Systat Software Inc, San Jose, CA). Hemispheric volume was analyzed using a repeated measures one-way analysis of variance (ANOVA), while the lesion volume and composition data were analyzed with a one-way ANOVA. Tukey post-hoc tests were used for all statistical tests. Data are presented as the Mean ± SEM. A $p < 0.05$ was considered significant.

Results:

Reduced hemispheric swelling occurred in the absence of lesion volume or composition changes in animals having systemic inflammation or TREM2 deficiency at the time of TBI.

We hypothesized that animals having systemic inflammation or TREM2 deficiency at the time of TBI would demonstrate worsened tissue damage when compared to controls. To test this hypothesis, we used T2WI to assess lesion and hemispheric volumes in addition to lesion composition. T2WIs illustrated lesions of similar size and composition, but differences in hemispheric volume between the wildtype, IP-LPS and TREM2KO groups at 3 and 7 days post injury (Figure 4.1A). Quantification of hemispheric volume revealed virtually no swelling within the TREM2KO group at both timepoints and an 80% reduction in swelling within the impacted cortex of IP-LPS animals compared to wildtypes at 7 days post TBI (Figure 4.1B). Additionally, wildtype animals demonstrated a 37% decrease in swelling over the course of 7 days (Figure 4.1B). Unexpectedly, the decreased hemispheric volume within the TREM2KO and IP-LPS animals occurred in the absence of significant lesion volume differences from wildtype mice (Figure 4.1C). Blood, edema, and NAB volumes within the lesion were also not significantly altered between the groups at any time (Figure 4.1D-F).

TBI results in increased microglial inflammation within the impacted hemisphere by 7 days, independent of inflammatory status at the time of injury.

We hypothesized that microglial inflammatory transcript levels, independent of inflammatory status at the time of TBI, would be increased in the impacted hemisphere of injured animals compared to those found in wildtype naïve mice. To test this hypothesis we used Nanostring technology to analyze and compare the fold changes in microglial transcript numbers between the TBI groups (wildtype, IP-LPS and TREM2KO) and naïve wildtype animals for each inflammatory molecule (Figure 4.2). TBI animals demonstrated more genes that increased (wildtype=391; IP-LPS=362; TREM2KO=359) than decreased (wildtype=29; IP-LPS=35; TREM2KO=34) 2-fold from wildtype naïve (Figure 4.2A). Also, approximately 75% of the increased genes and 37% of the decreased genes were shared between the TBI groups. Classification of increased genes revealed that similar pathways in approximately the same proportions were seen within the TBI groups when compared to naïve controls (Figure 4.2B). Additionally, genes that decreased within the TBI groups also appeared to have similar pathway representation between the groups (Figure 4.2B). We also found that the interleukin (13.8-15%), chemokine (12.4-13.2%) and TNF (4.1-5.9%) gene families were predominantly increased from naïve, as fewer molecules from these families were seen in the decreased gene list. In contrast, the toll receptor, IGF and oxidative stress families showed higher

representation within the decreased gene lists as compared to those that were increased.

Microglial inflammation is decreased in IP-LPS and TREM2KO groups compared to wildtype 7 days following TBI.

We asked whether inflammatory status at the time of TBI altered the microglial inflammatory response to injury and hypothesized that the level of gene expression would be similar between the TBI groups. To test this hypothesis we compared the fold changes in microglial inflammatory gene transcript numbers of IP-LPS or TREM2KO groups with wildtype animals 7 days following TBI (Figure 4.3). Fold change analysis revealed that IP-LPS and TREM2KO mice had more genes with 2-fold decreases (IP-LPS=17; TREM2KO=19) than increases (IP-LPS=242; TREM2KO=229) from wildtype TBI animals (Figure 4.3A). Approximately 73% of the decreased and 44% of the increased genes were shared between the IP-LPS and TREM2KO groups (Figure 4.3A). The same pathways in similar proportions were observed within the decreased gene lists of both IP-LPS and TREM2KOs compared to wildtype (Figure 4.3B). Signaling pathways with the most gene representation included cytokines (12.3% - 14.3%), interleukins (13.5% - 15.3%) and TNF (5.2% - 6.1%). In contrast, the pathways seen in the increased gene lists varied in representation between the IP-LPS and TREM2KO groups, though this is likely due to the low gene numbers in these lists.

Microglia demonstrate less gene transcripts for inflammatory molecules compared to impacted cortical tissue in TREM2KO mice 7 days following injury.

TREM2KO microglia were hypothesized to show increased inflammation when compared to the impacted cortical tissue 7 days post TBI. To test this hypothesis inflammatory molecules were compared between TREM2KO microglia and cortical tissue as fold changes from wildtype microglia and tissue 7 days following TBI (Figure 4.4). We found that the TREM2KO impacted hemisphere had larger numbers of genes with 2-fold increases, from wildtype tissue, than the microglia (cortex=317; microglia=19), which had more genes that were decreased 2-fold or more from wildtype microglia (cortex=1; microglia=242) (Figure 4.4A). The increased gene list within the hemispheric tissue showed that the interleukin (13.8%), chemokine (14.7%) and TNF (6.0%) signaling pathways had the highest representation (Figure 4.4B). The increases in pathways observed within the tissue were similar to those observed in the decreased gene list of TREM2KO microglia (seen in Figure 4.3B), thus the tissue and microglia demonstrated opposing gene expression patterns. In contrast, the only gene found to be decreased in the TREM2KO tissue compared to wildtype was TREM2, as would be expected as these animals lacked TREM2, at 7 days following TBI (Figure 4.4B).

Inflammatory status at the time of TBI alters microglial expression patterns of signaling molecules 7 days following TBI

We predicted that when considering all genes tested using Nanostring, including those categorized as no-change, microglial and tissue patterns would still be observed. To test this hypothesis, all genes within the TNF, JAK/STAT, interleukin and chemokine families, which showed large representation within the increased and/or decreased gene lists, were used to generate an expression heatmap (Figure 4.5). We found that heatmaps generated from these gene families confirmed the microglial and tissue patterns observed within the gene lists. All TBI groups (wildtype, IP-LPS, TREM2KO) demonstrated large numbers of microglial genes with at least 2-fold increases from naïve mice in all four gene families. Comparison of the IP-LPS and TREM2KO groups with wildtype following TBI, demonstrated that the majority of the genes, though not all, within the gene families were decreased. Furthermore, comparison of the TREM2KO microglia with impacted hemispheric gene expression, revealed that the tissue had increased numbers of genes with 2-fold or more expression levels in inflammatory molecule transcript numbers compared to the microglia (Figure 4.5).

Discussion

Based on previous findings, we hypothesized that TBI pathology would be exacerbated by increased inflammation or TREM2 deficiency at the time of injury. Unexpectedly our data did not support this hypothesis. Rather we found that TREM2 deficiency at the time of TBI resulted in little swelling, while systemic inflammation led to reduced swelling by 7 days following injury compared to wildtype. Additionally, gene expression analysis of inflammatory molecules revealed increased microglial expression within the TBI groups compared to Naïve mice. However the levels of expression for many of these molecules showed 2-fold less expression in the IP-LPS and TREM2KOs compared to wildtype following TBI. Furthermore the impacted cortical tissue and microglia isolated from TREM2KOs revealed opposing expression levels, where the tissue demonstrated increased transcript numbers for many of the inflammatory molecules tested.

Hemispheric swelling, but not lesion volume or composition, was reduced following systemic inflammation and TREM2 deficiency at the time of TBI.

Experimental TBI and stroke studies have reported that T2WI provides a high correlation with tissue pathology (Kochanek 1995, Gerriets 2004, Walberer 2007). Kochanek et al. (1995) have specifically demonstrated that T2WI can also be used to accurately assess lesion volume non-invasively. Similar to other studies we found no changes in lesion volume between the experimental groups,

despite differences in inflammatory status at the time of a moderate-to-severe TBI. Models of experimental stroke have also reported the absence of changes in the amount of injured tissue in TREM2KOs and LPS challenged mice following injury (Denes 2011, Sieber 2013). We further characterized the composition of the lesion using a previously published method from our lab, however we found no differences in blood or edema volume within the injured tissue (Donovan 2012). Taken together this data indicates that TREM2 deficiency or systemic inflammation at the time of injury does not result in aggravation of lesion pathology at acute times.

However human TBI is often diffuse and affects regions distant from lesioned areas. In particular, brain swelling can impact large brain regions and is typically seen following moderate-to-severe injuries. Brain swelling is a result of increased edema formation, peaking 24-48 hrs, and/or blood deposition, which can continue to deposit over days, following TBI (Obenaus 2007, Simard 2010). We therefore assessed swelling as hemispheric volume. Unexpectedly, we found significantly less swelling in TREM2KOs and a non-significant reduction in hemispheric volume within LPS challenged animals from wildtype at 7 days post TBI. These hemispheric swelling changes occurred in the absence of lesion volume differences, indicating that lesion size was not contributing to differences in swelling. Additionally, our findings demonstrate that systemic inflammation at the time of injury does not exacerbate tissue damage and the lack of the putative anti-inflammatory molecule TREM2, improves swelling outcome at acute times

following experimental moderate-to-severe TBI. Only one study of CNS damage has been performed in TREM2KOs and they did not assess brain swelling (Sieber 2013). However, a model of stroke in which animals received IP LPS (0.2-0.4 mg/kg) 3 hrs prior to injury revealed increased edema formation at 24hrs (Denes 2011). This study also found that LPS doses similar to ours (4mg/kg) resulted in 100% mortality following stroke (Denes 2011). Discrepancies between this study and ours is likely due to differences in the evolution of pathology between stroke and TBI. These data indicate that the role of inflammation varies between diseases states and is likely dependent on ongoing pathology within the tissue.

Reductions in hemispheric swelling occur in the presence of increased microglial inflammation from naïve controls, independent of inflammatory status

The majority of TBI studies have focused on morphological and/or intensity changes in macrophage/microglial markers, such as Iba1, as indicators of cellular activation. Only a few studies have begun to examine the inflammatory gene expression of microglia following TBI. In purified microglia, we found that all TBI groups, despite differences in inflammatory status at the time of injury, exhibited increased expression of inflammatory molecules compared to naive animals. Similar to our study, Turtzo et al. (2014) also found increases in inflammatory molecules within microglia/macrophages isolated from the impact site 1-7 days post moderate-to-severe TBI. However in contrast to

our data, where we observed increased cytokine and interleukin expression following TBI, particularly in wildtype animals, this study reported a decrease in several interleukins 1-7 days post TBI compared to naïve (Turtzo 2014). Moreover there were several experimental differences that could potentially contribute to this discrepancy. Firstly, Turtzo et al. (2014) used female rats, while we used male mice. Secondly their study did not distinguish between microglia and infiltrating macrophages, while our study analyzed the inflammatory expression patterns only from purified microglia. Lastly, Turtzo et al. (2014) measured cytokine proteins within the tissue, while we measured the gene expression of inflammatory molecules. Taken together these data suggest that individual cell populations, in addition to the inflammatory tissue environment, need to be assessed separately as each cell type is likely expressing different molecules that contribute to TBI resolution and progression.

TREM2KOs and IP-LPS mice demonstrate decreased microglial inflammation compared to wildtype following TBI.

Chronic microglial inflammation following TBI has been correlated with persistent behavioral deficits in patients (Ramlackhansingh 2011). Positron emission tomography (PET) has revealed that patients with chronic (11mo-17 yrs) cognitive deficits also showed ongoing microglial activation in brain regions distant from the lesion following moderate-to-severe TBI (Ramlackhansingh 2011). Administration of anti-inflammatory molecules have been shown in

experimental TBI models to reduce the expression of molecules associated with both alternative and classical activation states (Cao 2012). Experimental TBI studies using acute administration of anti-inflammatory molecules have demonstrated some promise in animal models of TBI, however long-term administration of some anti-inflammatories, such as Ibuprofen, have resulted in worsened memory deficits (Browne 2006, Kumar and Loane 2012). Our data show that while TREM2KOs and IP-LPS have increased microglial activation when compared to naïve animals, this microglial inflammation is not as robust as that found in wildtype TBI animals. This suggests that while some microglial activation following TBI is beneficial, as increased inflammation occurred at a time of reduced swelling, too much may be detrimental or slow recovery. However it is important to note that we assessed numbers of activated genes and representation of pathways, but have not performed an extensive pathway analysis. Thus the amount of microglial activation, in addition to cellular pathways activated, likely plays an important role in TBI outcome. This notion is consistent with experiments demonstrating improved outcomes following acute anti-inflammatory treatments. However these anti-inflammatory treatments have failed to translate into clinical practice likely as a result of poor understanding of the mechanisms resulting in secondary damage and the roles of cellular pathways activated by various inflammatory cells (Kumar and Loane 2012). Future studies on the amount of activation and specific cellular pathways induced by microglia are needed to succeed in translation of therapies to the clinic.

Microglia demonstrate an opposing gene expression pattern compared to that found in the impacted tissue environment within TREM2KOs.

Microglia only make up approximately 15% of the total cell population within the CNS, thus brain tissue contains predominantly RNA from more abundant cells, such as neurons and astrocytes. Astrocytes and neurons can also contribute to the inflammatory environment through the release of various molecules, such as TNFα (Liu 1994, Rosenberg 1995, Dong and Benveniste 2001). Our data show that microglia and impacted cortical tissue from TREM2KOs demonstrate opposing gene expression patterns. These data indicate that 1) microglia can behave differently than other cells, which is not surprising as they are the CNS resident immune cell, and 2) changes in brain swelling can result from manipulation of microglia specifically, as TREM2 is only found on this cell population in the CNS. This provides evidence in support of targeting microglia for therapeutic use, however additional studies investigating the specific pathways activated or inhibited in TREM2KOs and their role in swelling outcome is needed.

Comparison of cortical tissue from TREM2KOs and wildtype at 7 days post injury, we found that knockouts demonstrated a more robust inflammatory response as more genes contained 2-fold or higher transcripts levels. In contrast, Sieber et al. (2013) et al demonstrated reduced expression of inflammatory molecules, such as TNFα, IL-1β and IL-6, in TREM2KOs undergoing experimental stroke compared to Sham at 7 days. However, the

experimental models (TBI versus stroke) and number of inflammatory molecules assessed between our study and that performed by Sieber et al. (2013) likely contributes to differences in our results. Thus different inflammatory pathways are potentially activated in various CNS diseases and need to be examined separately.

Conclusion:

Our starting hypothesis was that increased systemic inflammation or TREM2 deficiency at the time of TBI would result in exacerbated tissue pathology. However our data does not support these findings. Rather increased systemic inflammation, induced using IP LPS, at the time of TBI does not exacerbate gross tissue pathology (i.e. swelling or lesion size) within a week from injury. Additionally, the loss of TREM2, a putative microglial anti-inflammatory molecule, does not worsen tissue damage 7 days following experimental TBI. Rather reductions in hemispheric swelling within the TREM2KOs occurred in the presence of increased tissue inflammation from wildtype and elevated microglial activation compared to naïve controls. Thus not all inflammation is created equal. However, TREM2KO and IP-LPS microglial inflammation was not as robust as wildtype following TBI. Therefore the cellular pathways activated as well as the amount of cellular activation in the microglia contribute to beneficial TBI induced hemispheric swelling outcomes in our model. We also found that microglia and impacted tissue from TREM2KOs showed opposing gene

expression patterns, suggesting that other cell types are also contributing to the tissue inflammatory environment. Taken together these data show that both the type and amount of inflammation are important in determining TBI outcome. Further studies are required to better understand and identify cellular pathways activated within the microglia and their roles in the progression of pathology.

Figures and Legends

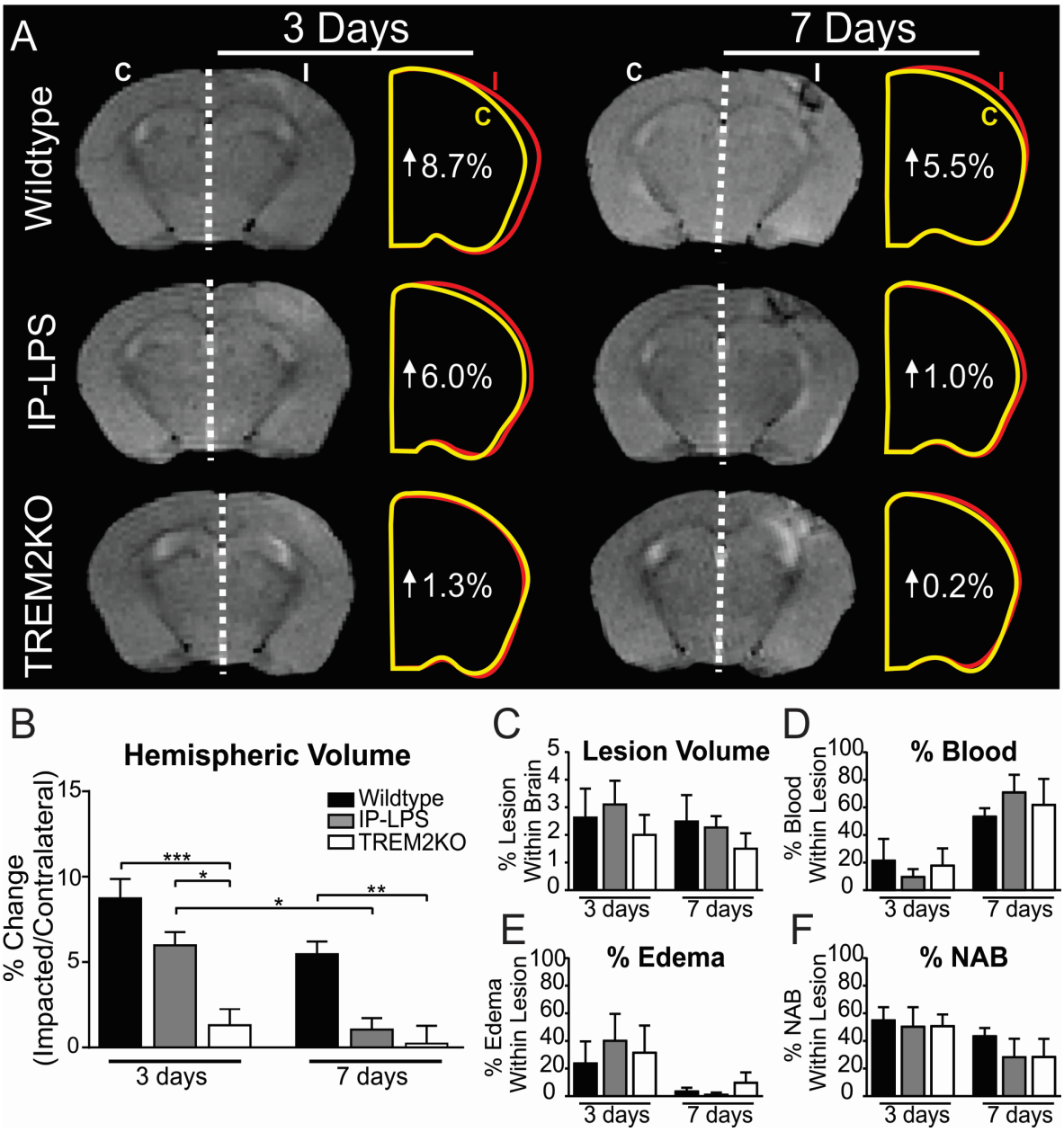

Figure 4.1: Systemic inflammation or TREM2 deficiency at the time of TBI decreased hemispheric swelling, but without affecting lesion volume or composition.

A. Shows representative T2 MRIs from wildtype (n=4), IP-LPS (n=3) and TREM2KO (n=4) animals at 3 and 7 days following TBI. Superimposed impacted (I; red) and contralateral (C; yellow) hemispheres illustrate changes in hemispheric volume. **B.** Depicts the percent change between the impacted and contralateral hemispheres of wildtype (black), IP-LPS (grey) and TREM2KO (white) groups 3 and 7 days post TBI. **C**. Shows the percent lesion of brain volume, for wildtype (black), IP-LPS (grey) and TREM2KOs (white) at 3 and 7 days post TBI. **D-F** Illustrates the percent of blood **(D)**, edema **(E)** and normal appearing brain (**F**; NAB) volume within the lesion of wildtype (black), IP-LPS (grey) and TREM2KO (white) animals 3 and 7 days following TBI. (****p<0.0001, ***p<0.001, **p<0.01, *p<0.05, One-Way and Repeated Measures One-Way ANOVA Tukey post-hoc).

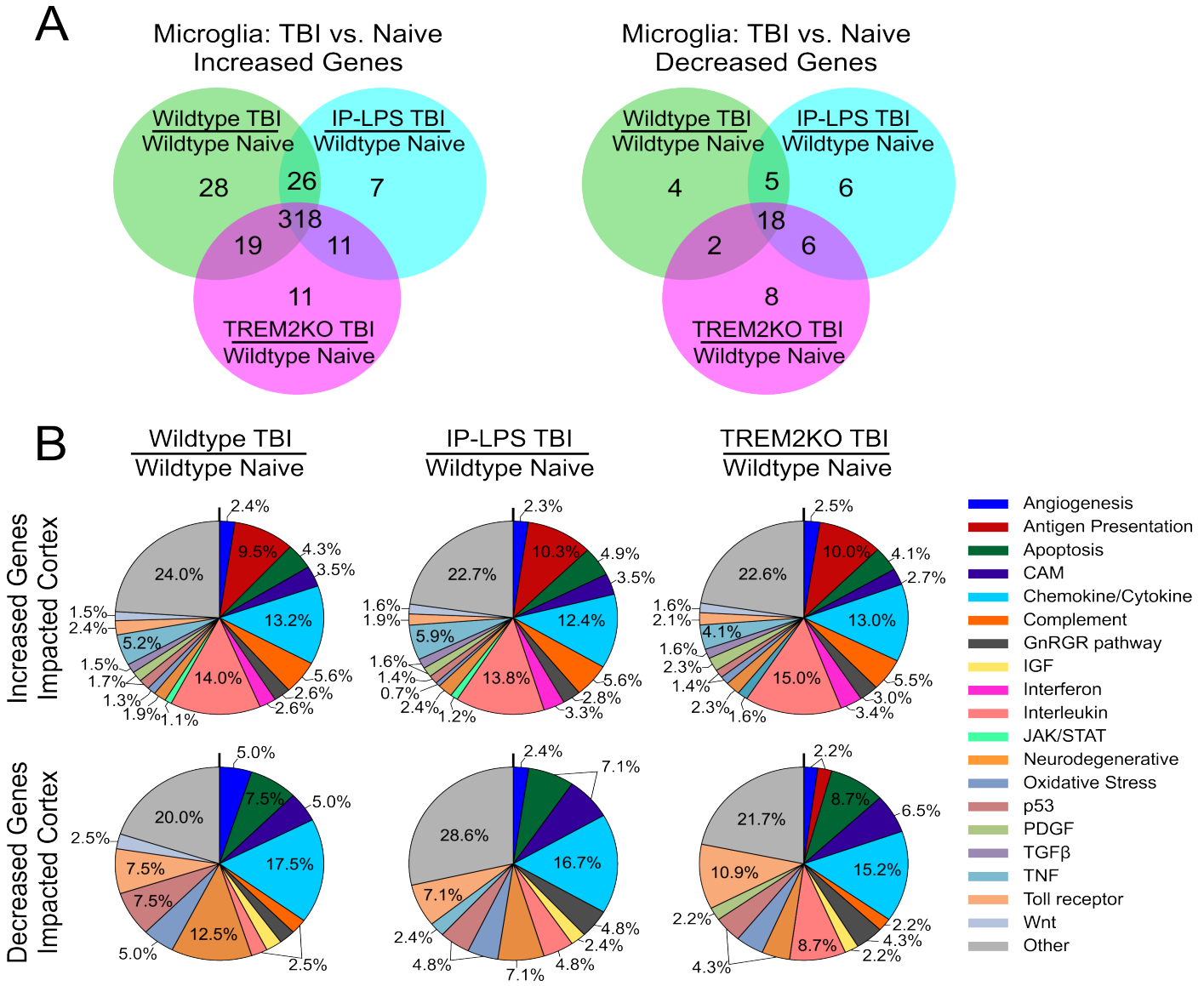
A
Microglia: TBI vs. Naive
Increased Genes
Wildtype TBI
Wildtype Naive
IP-LPS TBI
Wildtype Naive
TREM2KO TBI
Wildtype Naive
28
26
7
318
19
11
11
Microglia: TBI vs. Naive
Decreased Genes
Wildtype TBI
Wildtype Naive
IP-LPS TBI
Wildtype Naive
TREM2KO TBI
Wildtype Naive
4
5
6
18
2
6
8
B
Wildtype TBI
Wildtype Naive
IP-LPS TBI
Wildtype Naive
TREM2KO TBI
Wildtype Naive
Increased Genes
Impacted Cortex
Decreased Genes
Impacted Cortex
Angiogenesis
Antigen Presentation
Apoptosis
CAM
Chemokine/Cytokine
Complement
GnRGR pathway
IGF
Interferon
Interleukin
JAK/STAT
Neurodegenerative
Oxidative Stress
p53
PDGF
TGFβ
TNF
Toll receptor
Wnt
Other

Figure 4.2: TBI results in increased microglial activation in the impacted hemisphere regardless of inflammatory status by 7 days post TBI compared to naïve animals.

A. Depicts the number of microglial genes within wildtype (n=8), IP-LPS (n=12) and TREM2KOs (n=8) following TBI that demonstrated a 2-fold increase or decrease from naïve wildtype (n=7) animals. **B.** Shows the percent of pathway representation from 2-fold increased or decreased genes in wildtype, IP-LPS and TREM2KOs after TBI from naïve mice, using Panther. Pathways within the legend go in sequential order clockwise beginning at the notch (CAM= cell adhesion molecule, GnRHR= gonadotropin releasing hormone receptor; IGF= insulin-like growth factor; PDGF= platelet derived growth factor; TNF= Tumor Necrosis Factor).

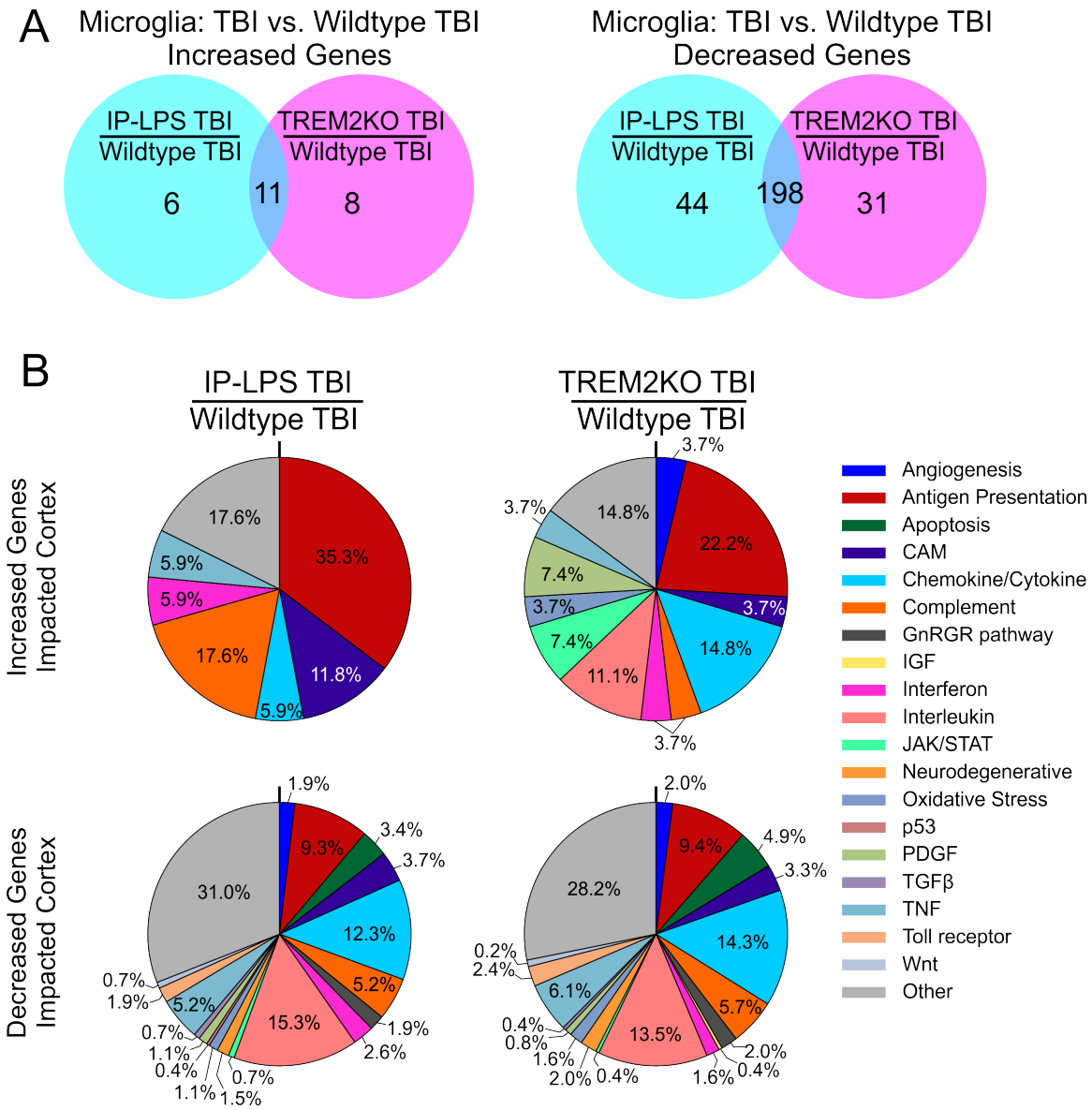
A
Microglia: TBI vs. Wildtype TBI
Increased Genes
IP-LPS TBI / Wildtype TBI
TREM2KO TBI / Wildtype TBI
6
11
8
Microglia: TBI vs. Wildtype TBI
Decreased Genes
IP-LPS TBI / Wildtype TBI
TREM2KO TBI / Wildtype TBI
44
198
31
B
IP-LPS TBI / Wildtype TBI
TREM2KO TBI / Wildtype TBI
Increased Genes Impacted Cortex
Decreased Genes Impacted Cortex
35.3%
11.8%
5.9%
17.6%
5.9%
5.9%
17.6%
22.2%
3.7%
14.8%
11.1%
3.7%
7.4%
3.7%
7.4%
3.7%
14.8%
3.7%
9.3%
3.4%
3.7%
12.3%
5.2%
1.9%
2.6%
0.7%
1.1%
0.4%
1.1%
1.5%
0.7%
5.2%
0.7%
1.9%
31.0%
1.9%
9.4%
4.9%
3.3%
14.3%
5.7%
2.0%
0.4%
1.6%
13.5%
2.0%
0.4%
1.6%
2.0%
0.8%
0.4%
6.1%
0.2%
2.4%
28.2%
Angiogenesis
Antigen Presentation
Apoptosis
CAM
Chemokine/Cytokine
Complement
GnRGR pathway
IGF
Interferon
Interleukin
JAK/STAT
Neurodegenerative
Oxidative Stress
p53
PDGF
TGFβ
TNF
Toll receptor
Wnt
Other

Figure 4.3: Microglia within the impacted hemisphere of IP-LPS and TREM2KOs demonstrated less inflammation compared to wildtypes 7 days following TBI.

A. Depicts the number of microglial genes within IP-LPS (n=12) and TREM2KOs (n=8) that demonstrated a 2-fold increase or decrease from wildtype (n=8) animals following TBI. **B.** Shows the percent of pathway representation from 2-fold increased or decreased genes in IP-LPS and TREM2KOs from wildtype following TBI, using Panther. Pathways within the legend go in sequential order clockwise beginning at the notch (CAM= cell adhesion molecule, GnRHR= gonadotropin releasing hormone receptor; IGF= insulin-like growth factor; PDGF= platelet derived growth factor; TNF= tumor Necrosis Factor).

A

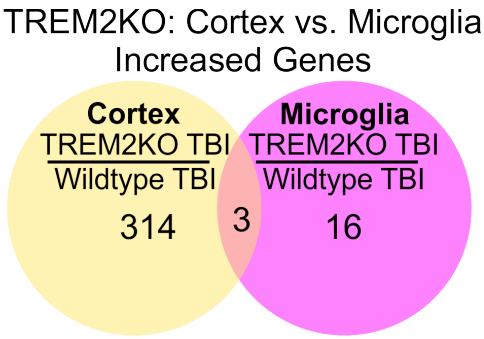
TREM2KO: Cortex vs. Microglia
Increased Genes
Cortex
TREM2KO TBI
Wildtype TBI
314
3
Microglia
TREM2KO TBI
Wildtype TBI
16

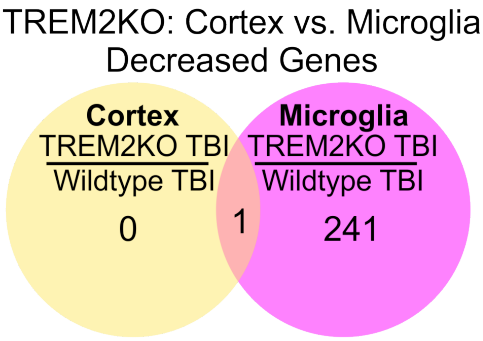
TREM2KO: Cortex vs. Microglia
Decreased Genes
Cortex
TREM2KO TBI
Wildtype TBI
0
1
Microglia
TREM2KO TBI
Wildtype TBI
241

B

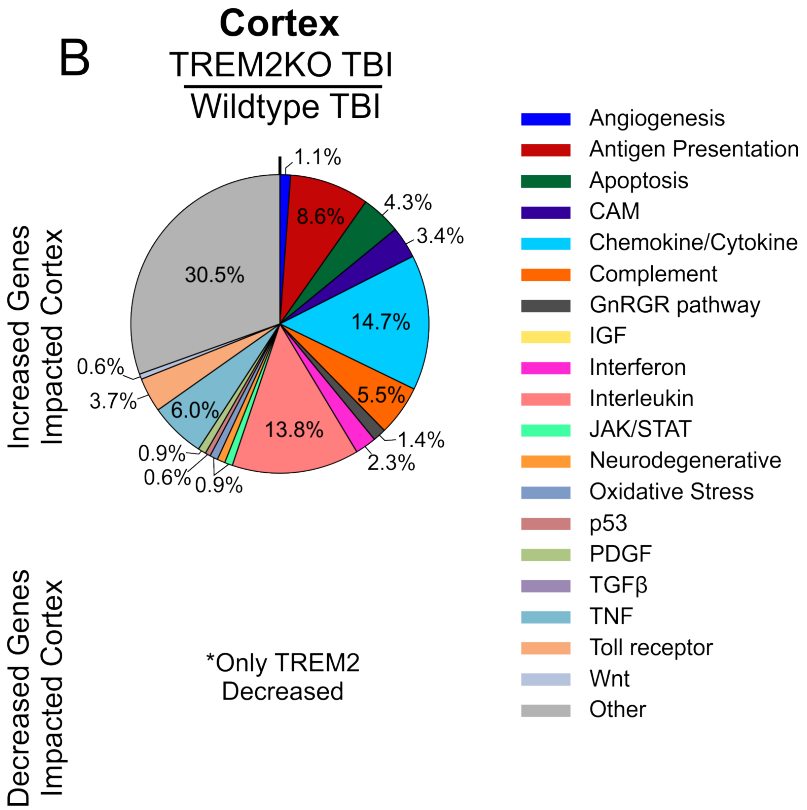
Cortex
TREM2KO TBI
Wildtype TBI
Increased Genes
Impacted Cortex
1.1%
8.6%
4.3%
3.4%
30.5%
14.7%
0.6%
3.7%
6.0%
5.5%
13.8%
1.4%
2.3%
0.9%
0.6%
0.9%
Decreased Genes
Impacted Cortex
*Only TREM2
Decreased
Angiogenesis
Antigen Presentation
Apoptosis
CAM
Chemokine/Cytokine
Complement
GnRGR pathway
IGF
Interferon
Interleukin
JAK/STAT
Neurodegenerative
Oxidative Stress
p53
PDGF
TGFβ
TNF
Toll receptor
Wnt
Other

Figure 4.4: The cortical tissue and isolated microglia demonstrated opposing inflammatory patterns within TREM2KOs.

A. Depicts the number of microglial genes within TREM2KO cortical tissue (n=2) and isolated microglia (n=8) that demonstrate a 2-fold increase or decrease from wildtype tissue (n=2) and microglia (n=8) following TBI. **B.** Shows the percent of pathway representation from 2-fold increased or decreased genes in the cortex of TREM2KO from wildtype following TBI, using Panther. Pathways within the legend go in sequential order clockwise beginning at the notch (CAM= cell adhesion molecule, GnRHR= gonadotropin releasing hormone receptor; IGF= insulin-like growth factor; PDGF= platelet derived growth factor; TNF= tumor Necrosis Factor).

TNF Signaling

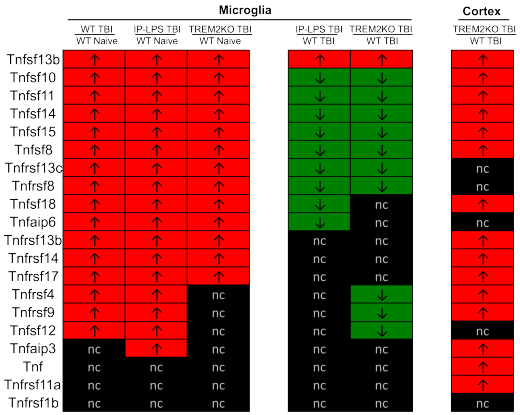

JAK/STAT Signaling

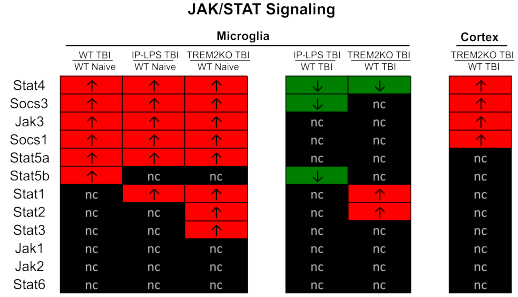

Interleukin Signaling

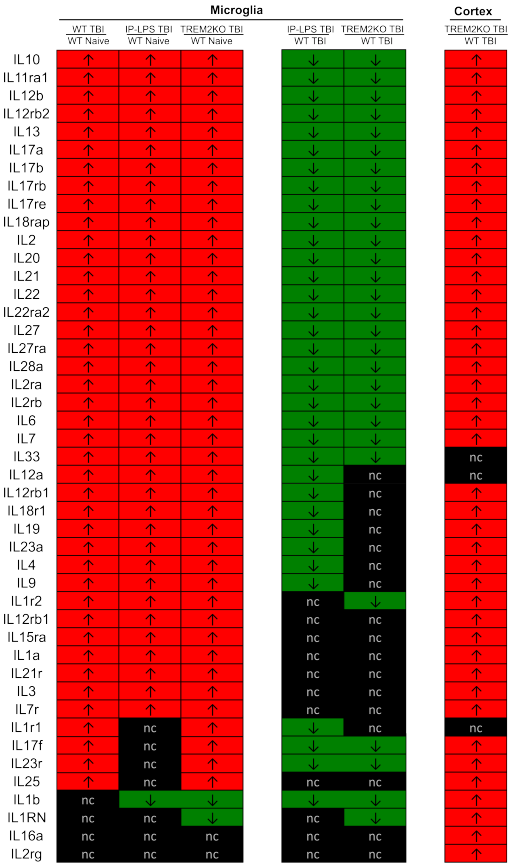

Chemokine Signaling

Figure 4.5: Microglial expression patterns of signaling molecules are influenced by inflammatory status at the time of TBI.

A-C Illustrates Nanostring analysis of gene transcript levels for TNF and Jak/Stat **(A)**, Interleukin **(B)** and Chemokine **(C)** signaling pathways within the cortical tissue and isolated microglia of TREM2KO and IP-LPS animals following TBI compared to either wildtype naïve or wildtype after TBI that increased (2-fold; red), decreased (2-fold; green) or did not change (-1.5 to +1.5 fold; black) from wildtype (wildtype) controls.

Chapter 5

Discussion

Traumatic brain injury (TBI) is an ongoing public health concern, particularly as awareness increases. mTBI or concussion can be difficult to diagnose as these mild injuries result in subtle transient alternations in cognition and no abnormalities on standard medical imaging. Difficulty in detecting mTBI leaves individuals susceptible to subsequent injuries that may exacerbate ongoing tissue damage. The secondary cascades that result in the progression and exacerbation of tissue damage following a single or repeated TBI are not well understood. Similar to other CNS diseases, such as stroke, TBI elicits an immediate inflammatory response mediated by the resident brain macrophages, microglia. Microglia can acquire classical (M1) or alternative (M2) activation states in response to injury or infection, which correlate with cytotoxic and cytoprotective processes, respectively. Thus these cells have been identified as potential aggravators of secondary damage, however, the role of microglia following TBI is poorly understood. This dissertation examines the evolution of grey and white matter pathology following repeated TBI and the role of microglial activation in injury progression and resolution.

Though patients can appear to recover from a brain injury, clinical and animal studies have demonstrated that the brain remains vulnerable to subsequent injuries that may result in worsened brain damage. Previous models of rmTBI have suggested short time windows (<5 days) in which the brain

remains vulnerable to subsequent injuries (Laurer 2001, Longhi 2005, Bennett 2012, Huang 2013). However these models induced mTBI to the same anatomical location, which would not occur clinically. Therefore we developed a novel model of repeated TBI in which injuries were given to distant locations on opposite hemispheres. Unexpectedly, using this new model we found that the temporal window of brain vulnerability was delayed from that seen previously, as injuries induced 7 days apart resulted in worsened outcome, but not those 3 days apart. This study also revealed that acute pathology was different between the injury intervals. Increased edema was seen when injuries were spaced 3 days apart and increased blood deposition occurred in animals with injuries spaced 7 days apart. For the first time, this study demonstrated that exacerbation of rmTBI is dependent on the location of and time interval between injuries.

Increased tissue damage following rmTBI 7 days apart was increased at the site of second injury, suggesting that distant brain regions are affected by a single mTBI. Neuroinflammatory studies following TBI have shown that microglia are activated and cytokines are present in regions distant from the lesion site (Ramlackhansingh 2011, Lagraoui 2012). Long-distance diffusion of inflammatory molecules, such as chemokines and cytokines, produced at the injury site may activate microglia in distant brain regions in such a way that they exacerbate damage following a second injury. Alternatively, signaling via neurons that may be damaged by the impact could also activate microglia at distant brain regions. Diffusion of inflammatory molecules and/or signaling away from the

injury site could explain the delayed time window of brain vulnerability seen in our model. Furthermore, inflammatory molecules may also contribute to hemorrhagic progression by acting on endothelial cells, which can themselves respond to cytokines (Quan 2008). Importantly, from our later studies on systemic inflammation at the time of injury we conclude that not all inflammation is the same. Thus it may be the diffusion or signaling of specific molecules to distant brain regions that increases vulnerability and not simply a general microglial activation state. Further studies investigating the mechanisms of increased vulnerability following rmTBI in which injuries are induced to distant locations are needed to better understand the mechanisms of brain vulnerability.

Grey matter pathology observed following rmTBI was transient, thus we wanted to determine whether white matter damage was ongoing at timepoints where the brain appeared to recover from injury. Using our rmTBI model, we assessed anterior white matter adjacent to, but not directly under, the second impact site in rmTBI animals. We found changes predominantly in axon integrity at sub-acute times, while myelin damage was seen chronically using DTI. Though EM analysis confirmed our DTI findings, it revealed that myelin around axons was thinner at both timepoints, while axons initially had a smaller caliber that increased in size over time. Progression of white matter damage is potentially a result of changing neurofilament and microtubule pathology. Studies performed by Jafari et al. (1998) have shown that changes in cytoskeletal compaction correlated with changes in axonal caliber in a model of

optic nerve stretch injury. Additionally at the second injury site, APC positive mature oligodendrocytes were increased in the CC at sub-acute times, suggesting an attempt to remyelinate, though the Olig2 positive progenitor population was reduced. Potentially, reductions in Olig2 are a result of accelerated differentiation into mature myelinating oligodendrocytes. Accelerated maturation onto damaged axons could potentially lead to the abnormalities in myelination and decompaction observed chronically. Similarly, in a study of moderate-to-severe TBI in the mouse demonstrated increased mature oligodendrocyte gene transcription following injury, however EM revealed abnormalities in myelin morphology (Sullivan 2013). Alternatively, replenishment of the Olig2 progenitor population may be slowed as we did not see any increases in proliferation (Ki67 staining) within the corpus callosum following injury. Sullivan et al. (2013) reported increases in oligodendrocyte progenitors within 1 week following injury. However our study investigated progenitors at sub-acute times and so earlier studies should be performed to assess oligodendrocyte proliferation. Future studies of oligodendrocyte maturation and remyelination following TBI as well as the cross-talk between oligodendrocytes and axons are needed to better understand the mechanisms of white matter damage following TBI.

Microglia are responsible for immune defense and maintenance of homeostasis. However following CNS injury or infection, microglia have demonstrated both protective and toxic roles based on their acquisition of

alternative and classical activation states, respectively. Therefore increased grey and white matter vulnerability following rmTBI led us to investigate the role of microglia in TBI damage and resolution. To assess the effects of microglial activation on TBI pathology we altered the inflammatory status at the time of injury using TREM2KOs and LPS challenge. We found that deficiency in TREM2, a microglial anti-inflammatory molecule, resulted in little swelling, while LPS challenged animals showed no exacerbation of swelling following a moderate-to severe TBI compared to wildtype. Microglia isolated from all TBI groups (wildtype, IP LPS, TREM2KO) revealed increased inflammation from naïve controls, however, TREM2KO and IP-LPS animals showed a less robust inflammatory response compared to wildtype. This data indicate that while some inflammation is beneficial, excessive inflammation may slow recovery or increase tissue damage. Similarly ongoing inflammation, which does not subside, has also been shown to correlate with increased tissue damage and ongoing neurological deficits (Ramlackhansingh 2011, Loane 2014). Administration of anti-inflammatory molecules, which can reduce both anti- and pro-inflammatory molecules, has shown acute improvements following TBI, supporting the notion of limited inflammation being beneficial to injury outcome (Cao 2012, Kumar and Loane 2012).

However it is important to note that the specific pathways activated in microglia that may contribute to beneficial and/or detrimental outcomes following TBI are still unknown. Thus, while acute anti-inflammatory treatments have

shown promise, they have failed to translate to the clinic, likely as a result of also reducing inflammatory pathways beneficial to tissue recovery after TBI. Our data show that in TREM2KOs, microglia and the tissue have opposing inflammatory patterns. As the majority of the RNA in the tissue is likely from astrocytes and neurons, this data indicate that microglia behave differently from other cell types and their role in TBI outcome needs to be studied independently from other cell populations. A better understanding of the role of microglial activation and induction of specific inflammatory pathways will facilitate the development of therapeutics for TBI.

Overall this work sets a foundation for future studies to investigate the role of inflammation and specifically microglia following single and repeated TBI. Our inflammation study is the first to assess microglial activation as other studies have only examined inflammation from the whole tissue. While we have only studied the impacted cortex, examining the contralateral tissue will potentially give insight into inflammation ongoing in uninjured tissue that may render it vulnerable to subsequent TBIs. Additionally, future investigations should focus on specific cellular pathways activated and downstream signaling of inflammatory molecules in microglia as this is not known. As there is no current treatment for damage caused by TBI, ongoing research investigating the role of microglia following TBI will uncover cellular mechanisms involved in secondary tissue damage that can be specifically targeted therapeutically for clinical use.

References

Abduljaleel, Z., F. A. Al-Allaf, W. Khan, M. Athar, N. Shahzad, M. M. Taher, M. Elrobh, M. S. Alanazi and W. El-Huneidi (2014). "Evidence of trem2 variant associated with triple risk of Alzheimer's disease." PLoS One 9(3): e92648.

Alahmadi, H., S. Vachhrajani and M. D. Cusimano (2010). "The natural history of brain contusion: an analysis of radiological and clinical progression." J Neurosurg 112(5): 1139-1145.

Balestreri, M., M. Czosnyka, P. Hutchinson, L. A. Steiner, M. Hiler, P. Smielewski and J. D. Pickard (2006). "Impact of intracranial pressure and cerebral perfusion pressure on severe disability and mortality after head injury." Neurocrit Care 4(1): 8-13.

Barkhoudarian, G., D. A. Hovda and C. C. Giza (2011). "The molecular pathophysiology of concussive brain injury." Clin Sports Med 30(1): 33-48, vii-iii.

Barzo, P., A. Marmarou, P. Fatouros, K. Hayasaki and F. Corwin (1997). "Contribution of vasogenic and cellular edema to traumatic brain swelling measured by diffusion-weighted imaging." J Neurosurg 87(6): 900-907.

Belanger, H. G., E. Spiegel and R. D. Vanderploeg (2010). "Neuropsychological performance following a history of multiple self-reported concussions: a meta-analysis." J Int Neuropsychol Soc 16(2): 262-267.

Belayev, L., A. Obenaus, W. Zhao, I. Saul, R. Busto, C. Wu, A. Vigdorchik, B. Lin and M. D. Ginsberg (2007). "Experimental intracerebral hematoma in the rat: characterization by sequential magnetic resonance imaging, behavior, and histopathology. Effect of albumin therapy." Brain Res 1157: 146-155.

Bennett, R. E., C. L. Mac Donald and D. L. Brody (2012). "Diffusion tensor imaging detects axonal injury in a mouse model of repetitive closed-skull traumatic brain injury." Neurosci Lett 513(2): 160-165.

Benson, R. R., S. A. Meda, S. Vasudevan, Z. Kou, K. A. Govindarajan, R. A. Hanks, S. R. Millis, M. Makki, Z. Latif, W. Coplin, J. Meythaler and E. M. Haacke (2007). "Global white matter analysis of diffusion tensor images is predictive of injury severity in traumatic brain injury." J Neurotrauma 24(3): 446-459.

Bianchi, A., B. Bhanu, V. Donovan and A. Obenaus (2013). "Visual and Contextual Modeling for the Detection of Repeated Mild Traumatic Brain Injury." IEEE Trans Med Imaging.

Biesmans, S., T. F. Meert, J. A. Bouwknecht, P. D. Acton, N. Davoodi, P. De Haes, J. Kuijlaars, X. Langlois, L. J. Matthews, L. Ver Donck, N. Hellings and R. Nuydens (2013). "Systemic immune activation leads to neuroinflammation and sickness behavior in mice." Mediators Inflamm 2013: 271359.

Block, M. L. and J. S. Hong (2005). "Microglia and inflammation-mediated neurodegeneration: multiple triggers with a common mechanism." Prog Neurobiol 76(2): 77-98.

Blumbergs, P. C., G. Scott, J. Manavis, H. Wainwright, D. A. Simpson and A. J. McLean (1994). "Staining of amyloid precursor protein to study axonal damage in mild head injury." Lancet 344(8929): 1055-1056.

Boje, K. M. and P. K. Arora (1992). "Microglial-produced nitric oxide and reactive nitrogen oxides mediate neuronal cell death." Brain Res 587(2): 250-256.

Browne, K. D., A. Iwata, M. E. Putt and D. H. Smith (2006). "Chronic ibuprofen administration worsens cognitive outcome following traumatic brain injury in rats." Exp Neurol 201(2): 301-307.

Buki, A. and J. T. Povlishock (2006). "All roads lead to disconnection? Traumatic axonal injury revisited." Acta Neurochirurgica 148(2): 181-+.

Cantu, R. C. and A. D. Gean (2010). "Second-impact syndrome and a small subdural hematoma: an uncommon catastrophic result of repetitive head injury with a characteristic imaging appearance." J Neurotrauma 27(9): 1557-1564.

Cao, T., T. C. Thomas, J. M. Ziebell, J. R. Pauly and J. Lifshitz (2012). "Morphological and genetic activation of microglia after diffuse traumatic brain injury in the rat." Neuroscience 225: 65-75.

Chang, E. F., M. Meeker and M. C. Holland (2006). "Acute traumatic intraparenchymal hemorrhage: risk factors for progression in the early post-injury period." Neurosurgery 58(4): 647-656; discussion 647-656.

Chen, X. H., V. E. Johnson, K. Uryu, J. Q. Trojanowski and D. H. Smith (2009). "A lack of amyloid beta plaques despite persistent accumulation of amyloid beta in axons of long-term survivors of traumatic brain injury." Brain Pathol 19(2): 214-223.

Colgan, N. C., M. M. Cronin, O. L. Gobbo, S. M. O'Mara, W. T. O'Connor and M. D. Gilchrist (2010). "Quantitative MRI analysis of brain volume changes due to controlled cortical impact." J Neurotrauma 27(7): 1265-1274.

Coronado, V. G., L. Xu, S. V. Basavaraju, L. C. McGuire, M. M. Wald, M. D. Faul, B. R. Guzman, J. D. Hemphill, C. Centers for Disease and Prevention (2011). "Surveillance for traumatic brain injury-related deaths--United States, 1997-2007." MMWR Surveill Summ 60(5): 1-32.

Corrigan, J. D., A. W. Selassie and J. A. Orman (2010). "The epidemiology of traumatic brain injury." J Head Trauma Rehabil 25(2): 72-80.

Crawford, D. K., M. Mangiardi, X. Xia, H. E. Lopez-Valdes and S. K. Tiwari-Woodruff (2009). "Functional recovery of callosal axons following demyelination: a critical window." Neuroscience 164(4): 1407-1421.

Creed, J. A., A. M. DiLeonardi, D. P. Fox, A. R. Tessler and R. Raghupathi (2011). "Concussive brain trauma in the mouse results in acute cognitive deficits and sustained impairment of axonal function." J Neurotrauma 28(4): 547-563.

Czigner, A., A. Mihaly, O. Farkas, A. Buki, B. Krisztin-Peva, E. Dobo and P. Barzo (2007). "Kinetics of the cellular immune response following closed head injury." Acta Neurochir (Wien) 149(3): 281-289.

Dantzer, R. (2001). "Cytokine-induced sickness behavior: where do we stand?" Brain Behav Immun 15(1): 7-24.

Davalos, D., J. Grutzendler, G. Yang, J. V. Kim, Y. Zuo, S. Jung, D. R. Littman, M. L. Dustin and W. B. Gan (2005). "ATP mediates rapid microglial response to local brain injury in vivo." Nat Neurosci 8(6): 752-758.

Davis, D. S. (2011). CNS Immunity is Developmentally Regulated. PhD, UC Riverside.

DeFord, S. M., M. S. Wilson, A. C. Rice, T. Clausen, L. K. Rice, A. Barabnova, R. Bullock and R. J. Hamm (2002). "Repeated mild brain injuries result in cognitive impairment in B6C3F1 mice." J Neurotrauma 19(4): 427-438.

Del Zoppo, G. J., H. Frankowski, Y. H. Gu, T. Osada, M. Kanazawa, R. Milner, X. Wang, N. Hosomi, T. Mabuchi and J. A. Koziol (2012). "Microglial cell activation is a source of metalloproteinase generation during hemorrhagic transformation." J Cereb Blood Flow Metab.

Denes, A., S. Ferenczi and K. J. Kovacs (2011). "Systemic inflammatory challenges compromise survival after experimental stroke via augmenting brain inflammation, blood- brain barrier damage and brain oedema independently of infarct size." J Neuroinflammation 8: 164.

Ding, J. Y., C. W. Kreipke, P. Schafer, S. Schafer, S. L. Speirs and J. A. Rafols (2009). "Synapse loss regulated by matrix metalloproteinases in traumatic brain injury is associated with hypoxia inducible factor-1alpha expression." Brain Res 1268: 125-134.

Dong, Y. and E. N. Benveniste (2001). "Immune function of astrocytes." Glia 36(2): 180-190.

Donovan, V., A. Bianchi, R. Hartman, B. Bhanu, M. J. Carson and A. Obenaus (2012). "Computational analysis reveals increased blood deposition following repeated mild traumatic brain injury." Neuroimage Clin 1(1): 18-28.

Donovan, V., C. Kim, A. K. Anugerah, J. S. Coats, U. Oyoyo, A. C. Pardo and A. Obenaus (2014). "Repeated mild traumatic brain injury results in long-term white-matter disruption." J Cereb Blood Flow Metab 34(4): 715-723.

Edlow, B. L. and O. Wu (2012). "Advanced neuroimaging in traumatic brain injury." Semin Neurol 32(4): 374-400.

Emblem, K. E., D. Scheie, P. Due-Tonnessen, B. Nedregaard, T. Nome, J. K. Hald, K. Beiske, T. R. Meling and A. Bjornerud (2008). "Histogram analysis of MR imaging-derived cerebral blood volume maps: combined glioma grading and identification of low-grade oligodendroglial subtypes." AJNR Am J Neuroradiol 29(9): 1664-1670.

Faul, M., L. Xu, M. M. Wald and V. G. Coronado (2010). "Traumatic Brain Injury in the United States: Emergency Department Visits, Hospitalizations and Deaths." Atlanta, GA: Centers for Disease Control and Prevention National Center for Injury Prevention and Control.

Faul, M. D., L. Xu, M. M. Wald and V. G. Coronado (2010). "Traumatic Brain Injury in the United States: Emergency Department Visits, Hospitalizations and Deaths." Atlanta, GA: Centers for Disease Control and Prevention, National Center for Injury Prevention and Control.

Flygt, J., A. Djupsjo, F. Lenne and N. Marklund (2013). "Myelin loss and oligodendrocyte pathology in white matter tracts following traumatic brain injury in the rat." Eur J Neurosci 38(1): 2153-2165.

Fukuda, S., C. A. Fini, T. Mabuchi, J. A. Koziol, L. L. Eggleston, Jr. and G. J. del Zoppo (2004). "Focal cerebral ischemia induces active proteases that degrade microvascular matrix." Stroke 35(4): 998-1004.

Gaasch, J. A., P. R. Lockman, W. J. Geldenhuys, D. D. Allen and C. J. Van der Schyf (2007). "Brain iron toxicity: differential responses of astrocytes, neurons, and endothelial cells." Neurochem Res 32(7): 1196-1208.

Gerriets, T., E. Stolz, M. Walberer, C. Muller, A. Kluge, A. Bachmann, M. Fisher, M. Kaps and G. Bachmann (2004). "Noninvasive quantification of brain edema and the space-occupying effect in rat stroke models using magnetic resonance imaging." Stroke 35(2): 566-571.

Gerzanich, V., S. K. Woo, R. Vennekens, O. Tsymbalyuk, S. Ivanova, A. Ivanov, Z. Geng, Z. Chen, B. Nilius, V. Flockerzi, M. Freichel and J. M. Simard (2009). "De novo expression of Trpm4 initiates secondary hemorrhage in spinal cord injury." Nat Med 15(2): 185-191.

Gidday, J. M., Y. G. Gasche, J. C. Copin, A. R. Shah, R. S. Perez, S. D. Shapiro, P. H. Chan and T. S. Park (2005). "Leukocyte-derived matrix metalloproteinase-9 mediates blood-brain barrier breakdown and is proinflammatory after transient focal cerebral ischemia." Am J Physiol Heart Circ Physiol 289(2): H558-568.

Gong, C., J. T. Hoff and R. F. Keep (2000). "Acute inflammatory reaction following experimental intracerebral hemorrhage in rat." Brain Res 871(1): 57-65.

Graham, D. I., J. H. Adams, J. A. Nicoll, W. L. Maxwell and T. A. Gennarelli (1995). "The nature, distribution and causes of traumatic brain injury." Brain Pathol 5(4): 397-406.

Guerreiro, R., A. Wojtas, J. Bras, M. Carrasquillo, E. Rogaeva, E. Majounie, C. Cruchaga, C. Sassi, J. S. Kauwe, S. Younkin, L. Hazrati, J. Collinge, J. Pocock, T. Lashley, J. Williams, J. C. Lambert, P. Amouyel, A. Goate, R. Rademakers, K. Morgan, J. Powell, P. St George-Hyslop, A. Singleton, J. Hardy and G. Alzheimer Genetic Analysis (2013). "TREM2 variants in Alzheimer's disease." N Engl J Med 368(2): 117-127.

Gupta, R. K., V. Tomar, R. Awasthi, A. Yadav, N. Husain, V. Bharadwaj, B. K. Ojha, S. Behari, K. N. Prasad and R. K. Rathore (2012). "T2*-weighted MR angiography substantially increases the detection of hemorrhage in the wall of brain abscess: implications in clinical interpretation." Neuroradiology 54(6): 565-572.

Hamann, G. F., Y. Okada, R. Fitridge and G. J. del Zoppo (1995). "Microvascular basal lamina antigens disappear during cerebral ischemia and reperfusion." Stroke 26(11): 2120-2126.

Hang, C. H., J. X. Shi, J. Tian, J. S. Li, W. Wu and H. X. Yin (2004). "Effect of systemic LPS injection on cortical NF-kappaB activity and inflammatory response following traumatic brain injury in rats." Brain Res 1026(1): 23-32.

Hayashi, T., Y. Kaneko, S. Yu, E. Bae, C. E. Stahl, T. Kawase, H. van Loveren, P. R. Sanberg and C. V. Borlongan (2009). "Quantitative analyses of matrix metalloproteinase activity after traumatic brain injury in adult rats." Brain Res 1280: 172-177.

Hines, D. J., R. M. Hines, S. J. Mulligan and B. A. Macvicar (2009). "Microglia processes block the spread of damage in the brain and require functional chloride channels." Glia 57(15): 1610-1618.

Hoge, C. W., D. McGurk, J. L. Thomas, A. L. Cox, C. C. Engel and C. A. Castro (2008). "Mild traumatic brain injury in U.S. Soldiers returning from Iraq." N Engl J Med 358(5): 453-463.

Homsi, S., F. Federico, N. Croci, B. Palmier, M. Plotkine, C. Marchand-Leroux and M. Jafarian-Tehrani (2009). "Minocycline effects on cerebral edema: relations with inflammatory and oxidative stress markers following traumatic brain injury in mice." Brain Res 1291: 122-132.

Hsieh, C. L., C. C. Kim, B. E. Ryba, E. C. Niemi, J. K. Bando, R. M. Locksley, J. Liu, M. C. Nakamura and W. E. Seaman (2013). "Traumatic brain injury induces macrophage subsets in the brain." Eur J Immunol 43(8): 2010-2022.

Hsieh, C. L., M. Koike, S. C. Spusta, E. C. Niemi, M. Yenari, M. C. Nakamura and W. E. Seaman (2009). "A role for TREM2 ligands in the phagocytosis of apoptotic neuronal cells by microglia." J Neurochem 109(4): 1144-1156.

Hsieh, C. L., E. C. Niemi, S. H. Wang, C. C. Lee, D. Bingham, J. Zhang, M. Cozen, I. F. Charo, E. J. Huang, J. Liu and M. C. Nakamura (2014). "CCR2 deficiency impairs macrophage infiltration and improves cognitive function after traumatic brain injury." J Neurotrauma.

Huang, L., J. S. Coats, A. Mohd-Yusof, Y. Yin, S. Assaad, M. J. Muellner, J. E. Kamper, R. E. Hartman, M. Dulcich, V. M. Donovan, U. Oyoyo and A. Obenaus (2013). "Tissue vulnerability is increased following repetitive mild traumatic brain injury in the rat." Brain Res 1499: 109-120.

Immonen, R. J., I. Kharatishvili, H. Grohn, A. Pitkanen and O. H. Grohn (2009). "Quantitative MRI predicts long-term structural and functional outcome after experimental traumatic brain injury." Neuroimage 45(1): 1-9.

Inglese, M., S. Makani, G. Johnson, B. A. Cohen, J. A. Silver, O. Gonen and R. I. Grossman (2005). "Diffuse axonal injury in mild traumatic brain injury: a diffusion tensor imaging study." J Neurosurg 103(2): 298-303.

Irimia, A., M. C. Chambers, J. R. Alger, M. Filippou, M. W. Prastawa, B. Wang, D. A. Hovda, G. Gerig, A. W. Toga, R. Kikinis, P. M. Vespa and J. D. Van Horn (2011). "Comparison of acute and chronic traumatic brain injury using semi-automatic multimodal segmentation of MR volumes." J Neurotrauma 28(11): 2287-2306.

Jafari, S. S., W. L. Maxwell, M. Neilson and D. I. Graham (1997). "Axonal cytoskeletal changes after non-disruptive axonal injury." J Neurocytol 26(4): 207-221.

Jotwani, V. and K. G. Harmon (2010). "Postconcussion syndrome in athletes." Curr Sports Med Rep 9(1): 21-26.

Kane, M. J., M. Angoa-Perez, D. I. Briggs, D. C. Viano, C. W. Kreipke and D. M. Kuhn (2012). "A mouse model of human repetitive mild traumatic brain injury." J Neurosci Methods 203(1): 41-49.

Kenne, E., A. Erlandsson, L. Lindbom, L. Hillered and F. Clausen (2012). "Neutrophil depletion reduces edema formation and tissue loss following traumatic brain injury in mice." J Neuroinflammation 9: 17.

Kharatishvili, I., A. Sierra, R. J. Immonen, O. H. Grohn and A. Pitkanen (2009). "Quantitative T2 mapping as a potential marker for the initial assessment of the severity of damage after traumatic brain injury in rat." Exp Neurol 217(1): 154-164.

Kinnunen, K. M., R. Greenwood, J. H. Powell, R. Leech, P. C. Hawkins, V. Bonnelle, M. C. Patel, S. J. Counsell and D. J. Sharp (2011). "White matter damage and cognitive impairment after traumatic brain injury." Brain 134(Pt 2): 449-463.

Klawiter, E. C., R. E. Schmidt, K. Trinkaus, H. F. Liang, M. D. Budde, R. T. Naismith, S. K. Song, A. H. Cross and T. L. Benzinger (2011). "Radial diffusivity predicts demyelination in ex vivo multiple sclerosis spinal cords." Neuroimage 55(4): 1454-1460.

Kluver, H. and E. Barrera (1953). "A method for the combined staining of cells and fibers in the nervous system." J Neuropathol Exp Neurol 12(4): 400-403.

Ko, S. B., H. A. Choi, G. Parikh, J. M. Schmidt, K. Lee, N. Badjatia, J. Claassen, E. S. Connolly and S. A. Mayer (2012). "Real time estimation of brain water content in comatose patients." Ann Neurol 72(3): 344-350.

Kochanek, P. M., D. W. Marion, W. Zhang, J. K. Schiding, M. White, A. M. Palmer, R. S. Clark, M. E. O'Malley, S. D. Styren, C. Ho and et al. (1995). "Severe controlled cortical impact in rats: assessment of cerebral edema, blood flow, and contusion volume." J Neurotrauma 12(6): 1015-1025.

Konrad, C., A. J. Geburek, F. Rist, H. Blumenroth, B. Fischer, I. Husstedt, V. Arolt, H. Schiffbauer and H. Lohmann (2011). "Long-term cognitive and emotional consequences of mild traumatic brain injury." Psychol Med 41(6): 1197-1211.

Kopelman, R., Y. K. Lee, M. Philbert, B. A. Moffat, G. R. Reddy, P. McConville, D. Hall, T. L. Chenevert, T. L. Bhojani, S. M. Buck, A. Rehemtulla and B. D. Ross (2005). "Multifunctional nanoparticle platforms for in vivo MRI enhancement and photodynamic therapy of a rat brain cancer." Journal of Magnetism and Magnetic Materials 293: 404-410.

Kotter, M. R., W. W. Li, C. Zhao and R. J. Franklin (2006). "Myelin impairs CNS remyelination by inhibiting oligodendrocyte precursor cell differentiation." J Neurosci 26(1): 328-332.

Kraus, M. F., T. Susmaras, B. P. Caughlin, C. J. Walker, J. A. Sweeney and D. M. Little (2007). "White matter integrity and cognition in chronic traumatic brain injury: a diffusion tensor imaging study." Brain 130(Pt 10): 2508-2519.

Kumar, A. and D. J. Loane (2012). "Neuroinflammation after traumatic brain injury: opportunities for therapeutic intervention." Brain Behav Immun 26(8): 1191-1201.

Kumar, R., M. Husain, R. K. Gupta, K. M. Hasan, M. Haris, A. K. Agarwal, C. M. Pandey and P. A. Narayana (2009). "Serial changes in the white matter diffusion tensor imaging metrics in moderate traumatic brain injury and correlation with neuro-cognitive function." J Neurotrauma 26(4): 481-495.

Kurland, D., C. Hong, B. Aarabi, V. Gerzanich and J. M. Simard (2012). "Hemorrhagic progression of a contusion after traumatic brain injury: a review." J Neurotrauma 29(1): 19-31.

Lagraoui, M., J. R. Latoche, N. G. Cartwright, G. Sukumar, C. L. Dalgard and B. C. Schaefer (2012). "Controlled cortical impact and craniotomy induce strikingly similar profiles of inflammatory gene expression, but with distinct kinetics." Front Neurol 3: 155.

Laurer, H. L., F. M. Bareyre, V. M. Lee, J. Q. Trojanowski, L. Longhi, R. Hoover, K. E. Saatman, R. Raghupathi, S. Hoshino, M. S. Grady and T. K. McIntosh (2001). "Mild head injury increasing the brain's vulnerability to a second concussive impact." J Neurosurg 95(5): 859-870.

Lee, B. and A. Newberg (2005). "Neuroimaging in traumatic brain imaging." NeuroRx 2(2): 372-383.

Lee, H., M. Wintermark, A. D. Gean, J. Ghajar, G. T. Manley and P. Mukherjee (2008). "Focal lesions in acute mild traumatic brain injury and neurocognitive outcome: CT versus 3T MRI." J Neurotrauma 25(9): 1049-1056.

Li, J., X. Y. Li, D. F. Feng and L. Gu (2011). "Quantitative evaluation of microscopic injury with diffusion tensor imaging in a rat model of diffuse axonal injury." Eur J Neurosci 33(5): 933-945.

Li, S., Y. Sun, D. Shan, B. Feng, J. Xing, Y. Duan, J. Dai, H. Lei and Y. Zhou (2013). "Temporal profiles of axonal injury following impact acceleration traumatic brain injury in rats--a comparative study with diffusion tensor imaging and morphological analysis." Int J Legal Med 127(1): 159-167.

Lipton, M. L., E. Gellella, C. Lo, T. Gold, B. A. Ardekani, K. Shifteh, J. A. Bello and C. A. Branch (2008). "Multifocal white matter ultrastructural abnormalities in mild traumatic brain injury with cognitive disability: a voxel-wise analysis of diffusion tensor imaging." J Neurotrauma 25(11): 1335-1342.

Liu, T., R. K. Clark, P. C. McDonnell, P. R. Young, R. F. White, F. C. Barone and G. Z. Feuerstein (1994). "Tumor necrosis factor-alpha expression in ischemic neurons." Stroke 25(7): 1481-1488.

Loane, D. J., A. Kumar, B. A. Stoica, R. Cabatbat and A. I. Faden (2014). "Progressive neurodegeneration after experimental brain trauma: association with chronic microglial activation." J Neuropathol Exp Neurol 73(1): 14-29.

Longhi, L., R. Gesuete, C. Perego, F. Ortolano, N. Sacchi, P. Villa, N. Stocchetti and M. G. De Simoni (2011). "Long-lasting protection in brain trauma by endotoxin preconditioning." J Cereb Blood Flow Metab 31(9): 1919-1929.

Longhi, L., K. E. Saatman, S. Fujimoto, R. Raghupathi, D. F. Meaney, J. Davis, B. S. A. McMillan, V. Conte, H. L. Laurer, S. Stein, N. Stocchetti and T. K. McIntosh (2005). "Temporal window of vulnerability to repetitive experimental concussive brain injury." Neurosurgery 56(2): 364-374; discussion 364-374.

Mac Donald, C. L., K. Dikranian, P. Bayly, D. Holtzman and D. Brody (2007). "Diffusion tensor imaging reliably detects experimental traumatic axonal injury and indicates approximate time of injury." J Neurosci 27(44): 11869-11876.

Mac Donald, C. L., K. Dikranian, S. K. Song, P. V. Bayly, D. M. Holtzman and D. L. Brody (2007). "Detection of traumatic axonal injury with diffusion tensor imaging in a mouse model of traumatic brain injury." Exp Neurol 205(1): 116-131.

Malojcic, B., Z. Mubrin, B. Coric, M. Susnic and G. J. Spilich (2008). "Consequences of mild traumatic brain injury on information processing assessed with attention and short-term memory tasks." J Neurotrauma 25(1): 30-37.

Marmarou, A., G. Portella, P. Barzo, S. Signoretti, P. Fatouros, A. Beaumont, T. Jiang and R. Bullock (2000). "Distinguishing between cellular and vasogenic edema in head injured patients with focal lesions using magnetic resonance imaging." Acta Neurochir Suppl 76: 349-351.

Marquez de la Plata, C. D., F. G. Yang, J. Y. Wang, K. Krishnan, K. Bakhadirov, C. Paliotta, S. Aslan, M. D. Devous, C. Moore, C. Harper, R. McColl, C. Munro Cullum and R. Diaz-Arrastia (2011). "Diffusion tensor imaging biomarkers for traumatic axonal injury: analysis of three analytic methods." J Int Neuropsychol Soc 17(1): 24-35.

Matsushita, K., W. Meng, X. Y. Wang, M. Asahi, K. Asahi, M. A. Moskowitz and E. H. Lo (2000). "Evidence for apoptosis after intracerebral hemorrhage in rat striatum." Journal of Cerebral Blood Flow and Metabolism 20(2): 396-404.

Maxwell, W. L. (1996). "Histopathological changes at central nodes of Ranvier after stretch-injury." Microscopy Research and Technique 34(6): 522-535.

Mi, H., A. Muruganujan, J. T. Casagrande and P. D. Thomas (2013). "Large-scale gene function analysis with the PANTHER classification system." Nat Protoc 8(8): 1551-1566.

Mnatsakanyan, L., F. N. Ross-Cisneros, V. Carelli, M. Y. Wang and A. A. Sadun (2011). "Axonal degeneration in peripheral nerves in a case of Leber hereditary optic neuropathy." J Neuroophthalmol 31(1): 6-11.

Mosser, D. M. and J. P. Edwards (2008). "Exploring the full spectrum of macrophage activation." Nat Rev Immunol 8(12): 958-969.

Mouzon, B. C., C. Bachmeier, A. Ferro, J. O. Ojo, G. Crynen, C. M. Acker, P. Davies, M. Mullan, W. Stewart and F. Crawford (2014). "Chronic neuropathological and neurobehavioral changes in a repetitive mild traumatic brain injury model." Ann Neurol 75(2): 241-254.

Muehlschlegel, S., R. Carandang, C. Ouillette, W. Hall, F. Anderson and R. Goldberg (2013). "Frequency and impact of intensive care unit complications on moderate-severe traumatic brain injury: early results of the Outcome Prognostication in Traumatic Brain Injury (OPTIMISM) Study." Neurocrit Care 18(3): 318-331.

Namiki, J., M. Yamazaki, T. Funabiki and S. Hori (2011). "Inaccuracy and misjudged factors of Glasgow Coma Scale scores when assessed by inexperienced physicians." Clin Neurol Neurosurg 113(5): 393-398.

Narayan, R. K., A. I. Maas, F. Servadei, B. E. Skolnick, M. N. Tillinger and L. F. Marshall (2008). "Progression of traumatic intracerebral hemorrhage: a prospective observational study." J Neurotrauma 25(6): 629-639.

Nevo, U., E. Hauben, E. Yoles, E. Agranov, S. Akselrod, M. Schwartz and M. Neeman (2001). "Diffusion anisotropy MRI for quantitative assessment of recovery in injured rat spinal cord." Magn Reson Med 45(1): 1-9.

Nimmerjahn, A., F. Kirchhoff and F. Helmchen (2005). "Resting microglial cells are highly dynamic surveillants of brain parenchyma in vivo." Science 308(5726): 1314-1318.

Niogi, S. N. and P. Mukherjee (2010). "Diffusion tensor imaging of mild traumatic brain injury." J Head Trauma Rehabil 25(4): 241-255.

Obenaus, A., N. Dilmac, B. Tone, H. R. Tian, R. Hartman, M. Digicaylioglu, E. Y. Snyder and S. Ashwal (2011). "Long-term magnetic resonance imaging of stem cells in neonatal ischemic injury." Ann Neurol 69(2): 282-291.

Obenaus, A., L. Huang, A. Smith, C. J. Favre, G. Nelson and E. Kendall (2008). "Magnetic resonance imaging and spectroscopy of the rat hippocampus 1 month after exposure to 56Fe-particle radiation." Radiat Res 169(2): 149-161.

Obenaus, A., M. Robbins, G. Blanco, N. R. Galloway, E. Snissarenko, E. Gillard, S. Lee and M. Curras-Collazo (2007). "Multi-modal magnetic resonance imaging

alterations in two rat models of mild neurotrauma." J Neurotrauma 24(7): 1147-1160.

Oehmichen, M., T. Walter, C. Meissner and H. J. Friedrich (2003). "Time course of cortical hemorrhages after closed traumatic brain injury: statistical analysis of posttraumatic histomorphological alterations." J Neurotrauma 20(1): 87-103.

Pais, T. F., C. Figueiredo, R. Peixoto, M. H. Braz and S. Chatterjee (2008). "Necrotic neurons enhance microglial neurotoxicity through induction of glutaminase by a MyD88-dependent pathway." Journal of Neuroinflammation 5.

Paloneva, J., T. Autti, P. Hakola and M. J. Haltia (1993). Polycystic Lipomembranous Osteodysplasia with Sclerosing Leukoencephalopathy (PLOSL). GeneReviews(R). R. A. Pagon, M. P. Adam, H. H. Ardinger et al. Seattle (WA).

Payne, S. C., C. A. Bartlett, A. R. Harvey, S. A. Dunlop and M. Fitzgerald (2011). "Chronic swelling and abnormal myelination during secondary degeneration after partial injury to a central nervous system tract." J Neurotrauma 28(6): 1077-1088.

Pettus, E. H. and J. T. Povlishock (1996). "Characterization of a distinct set of intra-axonal ultrastructural changes associated with traumatically induced alteration in axolemmal permeability." Brain Research 722(1-2): 1-11.

Piccio, L., C. Buonsanti, M. Mariani, M. Cella, S. Gilfillan, A. H. Cross, M. Colonna and P. Panina-Bordignon (2007). "Blockade of TREM-2 exacerbates experimental autoimmune encephalomyelitis." Eur J Immunol 37(5): 1290-1301.

Pinteaux-Jones, F., I. G. Sevastou, V. A. Fry, S. Heales, D. Baker and J. M. Pocock (2008). "Myelin-induced microglial neurotoxicity can be controlled by microglial metabotropic glutamate receptors." J Neurochem 106(1): 442-454.

Povlishock, J. T. and D. I. Katz (2005). "Update of neuropathology and neurological recovery after traumatic brain injury." J Head Trauma Rehabil 20(1): 76-94.

Quan, N. (2008). "Immune-to-brain signaling: how important are the blood-brain barrier-independent pathways?" Mol Neurobiol 37(2-3): 142-152.

Ramlackhansingh, A. F., D. J. Brooks, R. J. Greenwood, S. K. Bose, F. E. Turkheimer, K. M. Kinnunen, S. Gentleman, R. A. Heckemann, K. Gunanayagam, G. Gelosa and D. J. Sharp (2011). "Inflammation after trauma: microglial activation and traumatic brain injury." Ann Neurol 70(3): 374-383.

Rodriguez-Paez, A. C., J. P. Brunschwig and H. M. Bramlett (2005). "Light and electron microscopic assessment of progressive atrophy following moderate traumatic brain injury in the rat." Acta Neuropathol 109(6): 603-616.

Rosenberg, G. A., E. Y. Estrada, J. E. Dencoff and W. G. Stetler-Stevenson (1995). "Tumor necrosis factor-alpha-induced gelatinase B causes delayed opening of the blood-brain barrier: an expanded therapeutic window." Brain Res 703(1-2): 151-155.

Rosenzweig, H. L., N. S. Lessov, D. C. Henshall, M. Minami, R. P. Simon and M. P. Stenzel-Poore (2004). "Endotoxin preconditioning prevents cellular inflammatory response during ischemic neuroprotection in mice." Stroke 35(11): 2576-2581.

Rosidi, N. L., J. Zhou, S. Pattanaik, P. Wang, W. Jin, M. Brophy, W. L. Olbricht, N. Nishimura and C. B. Schaffer (2011). "Cortical microhemorrhages cause local inflammation but do not trigger widespread dendrite degeneration." PLoS One 6(10): e26612.

Roth, T. L., D. Nayak, T. Atanasijevic, A. P. Koretsky, L. L. Latour and D. B. McGavern (2014). "Transcranial amelioration of inflammation and cell death after brain injury." Nature 505(7482): 223-228.

Rubovitch, V., M. Ten-Bosch, O. Zohar, C. R. Harrison, C. Tempel-Brami, E. Stein, B. J. Hoffer, C. D. Balaban, S. Schreiber, W. T. Chiu and C. G. Pick (2011). "A mouse model of blast-induced mild traumatic brain injury." Exp Neurol 232(2): 280-289.

Schindelin, J., I. Arganda-Carreras, E. Frise, V. Kaynig, M. Longair, T. Pietzsch, S. Preibisch, C. Rueden, S. Saalfeld, B. Schmid, J. Y. Tinevez, D. J. White, V. Hartenstein, K. Eliceiri, P. Tomancak and A. Cardona (2012). "Fiji: an open-source platform for biological-image analysis." Nat Methods 9(7): 676-682.

Schmued, L. C. and K. J. Hopkins (2000). "Fluoro-Jade: novel fluorochromes for detecting toxicant-induced neuronal degeneration." Toxicol Pathol 28(1): 91-99.

Schnaar, R. L. and P. H. Lopez (2009). "Myelin-associated glycoprotein and its axonal receptors." J Neurosci Res 87(15): 3267-3276.

Shanmuganathan, K., R. P. Gullapalli, S. E. Mirvis, S. Roys and P. Murthy (2004). "Whole-brain apparent diffusion coefficient in traumatic brain injury: correlation with Glasgow Coma Scale score." AJNR Am J Neuroradiol 25(4): 539-544.

Shinozaki, Y., M. Nomura, K. Iwatsuki, Y. Moriyama, C. Gachet and S. Koizumi (2014). "Microglia trigger astrocyte-mediated neuroprotection via purinergic gliotransmission." Sci Rep 4: 4329.

Shitaka, Y., H. T. Tran, R. E. Bennett, L. Sanchez, M. A. Levy, K. Dikranian and D. L. Brody (2011). "Repetitive closed-skull traumatic brain injury in mice causes persistent multifocal axonal injury and microglial reactivity." J Neuropathol Exp Neurol 70(7): 551-567.

Shultz, S. R., F. Bao, V. Omana, C. Chiu, A. Brown and D. P. Cain (2012). "Repeated mild lateral fluid percussion brain injury in the rat causes cumulative long-term behavioral impairments, neuroinflammation, and cortical loss in an animal model of repeated concussion." J Neurotrauma 29(2): 281-294.

Shultz, S. R., D. F. MacFabe, K. A. Foley, R. Taylor and D. P. Cain (2011). "A single mild fluid percussion injury induces short-term behavioral and neuropathological changes in the Long-Evans rat: support for an animal model of concussion." Behav Brain Res 224(2): 326-335.

Sieber, M. W., N. Jaenisch, M. Brehm, M. Guenther, B. Linnartz-Gerlach, H. Neumann, O. W. Witte and C. Frahm (2013). "Attenuated inflammatory response in triggering receptor expressed on myeloid cells 2 (TREM2) knock-out mice following stroke." PLoS One 8(1): e52982.

Sifri, Z. C., A. T. Homnick, A. Vaynman, R. Lavery, W. Liao, A. Mohr, C. J. Hauser, A. Manniker and D. Livingston (2006). "A prospective evaluation of the value of repeat cranial computed tomography in patients with minimal head injury and an intracranial bleed." J Trauma 61(4): 862-867.

Sifri, Z. C., D. H. Livingston, R. F. Lavery, A. T. Homnick, A. C. Mosenthal, A. M. Mohr and C. J. Hauser (2004). "Value of repeat cranial computed axial tomography scanning in patients with minimal head injury." Am J Surg 187(3): 338-342.

Simard, J. M., K. T. Kahle and V. Gerzanich (2010). "Molecular mechanisms of microvascular failure in central nervous system injury--synergistic roles of NKCC1 and SUR1/TRPM4." J Neurosurg 113(3): 622-629.

Simard, J. M., M. Kilbourne, O. Tsymbalyuk, C. Tosun, J. Caridi, S. Ivanova, K. Keledjian, G. Bochicchio and V. Gerzanich (2009). "Key role of sulfonylurea receptor 1 in progressive secondary hemorrhage after brain contusion." J Neurotrauma 26(12): 2257-2267.

Smith, D. H., V. E. Johnson and W. Stewart (2013). "Chronic neuropathologies of single and repetitive TBI: substrates of dementia?" Nat Rev Neurol 9(4): 211-221.

Song, S. K., S. W. Sun, M. J. Ramsbottom, C. Chang, J. Russell and A. H. Cross (2002). "Dysmyelination revealed through MRI as increased radial (but unchanged axial) diffusion of water." Neuroimage 17(3): 1429-1436.

Spain, A., S. Daumas, J. Lifshitz, J. Rhodes, P. J. Andrews, K. Horsburgh and J. H. Fowler (2010). "Mild fluid percussion injury in mice produces evolving selective axonal pathology and cognitive deficits relevant to human brain injury." J Neurotrauma 27(8): 1429-1438.

Su, Y., W. Fan, Z. Ma, X. Wen, W. Wang, Q. Wu and H. Huang (2014). "Taurine improves functional and histological outcomes and reduces inflammation in traumatic brain injury." Neuroscience 266: 56-65.

Sullivan, G. M., A. J. Mierzwa, N. Kijpaisalratana, H. Tang, Y. Wang, S. K. Song, R. Selwyn and R. C. Armstrong (2013). "Oligodendrocyte lineage and subventricular zone response to traumatic axonal injury in the corpus callosum." J Neuropathol Exp Neurol 72(12): 1106-1125.

Sun, S. W., H. F. Liang, T. Q. Le, R. C. Armstrong, A. H. Cross and S. K. Song (2006). "Differential sensitivity of in vivo and ex vivo diffusion tensor imaging to evolving optic nerve injury in mice with retinal ischemia." Neuroimage 32(3): 1195-1204.

Tagliaferri, F., C. Compagnone, M. Korsic, F. Servadei and J. Kraus (2006). "A systematic review of brain injury epidemiology in Europe." Acta Neurochir (Wien) 148(3): 255-268; discussion 268.

Takahashi, K., M. Prinz, M. Stagi, O. Chechneva and H. Neumann (2007). "TREM2-transduced myeloid precursors mediate nervous tissue debris clearance and facilitate recovery in an animal model of multiple sclerosis." PLoS Med 4(4): e124.

Tang-Schomer, M. D., V. E. Johnson, P. W. Baas, W. Stewart and D. H. Smith (2012). "Partial interruption of axonal transport due to microtubule breakage accounts for the formation of periodic varicosities after traumatic axonal injury." Exp Neurol 233(1): 364-372.

Tavazzi, B., R. Vagnozzi, S. Signoretti, A. M. Amorini, A. Belli, M. Cimatti, R. Delfini, V. Di Pietro, A. Finocchiaro and G. Lazzarino (2007). "Temporal window of metabolic brain vulnerability to concussions: oxidative and nitrosative stresses--part II." Neurosurgery 61(2): 390-395; discussion 395-396.

Thulborn, K. R., A. G. Sorensen, N. W. Kowall, A. McKee, A. Lai, R. C. McKinstry, J. Moore, B. R. Rosen and T. J. Brady (1990). "The role of ferritin and hemosiderin in the MR appearance of cerebral hemorrhage: a histopathologic biochemical study in rats." AJR Am J Roentgenol 154(5): 1053-1059.

Turrin, N. P., D. Gayle, S. E. Ilyin, M. C. Flynn, W. Langhans, G. J. Schwartz and C. R. Plata-Salaman (2001). "Pro-inflammatory and anti-inflammatory cytokine mRNA induction in the periphery and brain following intraperitoneal administration of bacterial lipopolysaccharide." Brain Res Bull 54(4): 443-453.

Turtzo, L. C., J. Lescher, L. Janes, D. D. Dean, M. D. Budde and J. A. Frank (2014). "Macrophagic and microglial responses after focal traumatic brain injury in the female rat." J Neuroinflammation 11(1): 82.

Unterberg, A. W., J. Stover, B. Kress and K. L. Kiening (2004). "Edema and brain trauma." Neuroscience 129(4): 1021-1029.

VA/DoD (2009). "Management of Concussion/ mild Traumatic Brain Injury." VA/DoD Evidence Based Practice: Clinical Practice Guideline.

Vagnozzi, R., S. Signoretti, B. Tavazzi, R. Floris, A. Ludovici, S. Marziali, G. Tarascio, A. M. Amorini, V. Di Pietro, R. Delfini and G. Lazzarino (2008). "Temporal window of metabolic brain vulnerability to concussion: a pilot 1H-magnetic resonance spectroscopic study in concussed athletes--part III." Neurosurgery 62(6): 1286-1295; discussion 1295-1286.

Vagnozzi, R., B. Tavazzi, S. Signoretti, A. M. Amorini, A. Belli, M. Cimatti, R. Delfini, V. Di Pietro, A. Finocchiaro and G. Lazzarino (2007). "Temporal window of metabolic brain vulnerability to concussions: mitochondrial-related impairment--part I." Neurosurgery 61(2): 379-388; discussion 388-379.

Veltkamp, R., D. A. Siebing, S. Heiland, P. Schoenffeldt-Varas, C. Veltkamp, M. Schwaninger and S. Schwab (2005). "Hyperbaric oxygen induces rapid protection against focal cerebral ischemia." Brain Res 1037(1-2): 134-138.

von Holst, H., X. Li and S. Kleiven (2012). "Increased strain levels and water content in brain tissue after decompressive craniotomy." Acta Neurochir (Wien) 154(9): 1583-1593.

Walberer, M., F. Blaes, E. Stolz, C. Muller, M. Schoenburg, M. Tschernatsch, G. Bachmann and T. Gerriets (2007). "Midline-shift corresponds to the amount of brain edema early after hemispheric stroke--an MRI study in rats." J Neurosurg Anesthesiol 19(2): 105-110.

Wang, J., R. J. Hamm and J. T. Povlishock (2011). "Traumatic axonal injury in the optic nerve: evidence for axonal swelling, disconnection, dieback, and reorganization." J Neurotrauma 28(7): 1185-1198.

Wang, X., J. Jung, M. Asahi, W. Chwang, L. Russo, M. A. Moskowitz, C. E. Dixon, M. E. Fini and E. H. Lo (2000). "Effects of matrix metalloproteinase-9 gene knock-out on morphological and motor outcomes after traumatic brain injury." J Neurosci 20(18): 7037-7042.

Wang, X., T. Mori, T. Sumii and E. H. Lo (2002). "Hemoglobin-induced cytotoxicity in rat cerebral cortical neurons: caspase activation and oxidative stress." Stroke 33(7): 1882-1888.

Wang, Y., Q. Wang, J. P. Haldar, F. C. Yeh, M. Xie, P. Sun, T. W. Tu, K. Trinkaus, R. S. Klein, A. H. Cross and S. K. Song (2011). "Quantification of increased cellularity during inflammatory demyelination." Brain 134(Pt 12): 3590-3601.

Wood, R. L. (2004). "Understanding the 'miserable minority': a diasthesis-stress paradigm for post-concussional syndrome." Brain Inj 18(11): 1135-1153.

Xi, G., Y. Hua, R. R. Bhasin, S. R. Ennis, R. F. Keep and J. T. Hoff (2001). "Mechanisms of edema formation after intracerebral hemorrhage: effects of extravasated red blood cells on blood flow and blood-brain barrier integrity." Stroke 32(12): 2932-2938.

Xue, M. and M. R. Del Bigio (2000). "Intracerebral injection of autologous whole blood in rats: time course of inflammation and cell death." Neurosci Lett 283(3): 230-232.

Zivadinov, R., M. Stosic, J. L. Cox, D. P. Ramasamy and M. G. Dwyer (2008). "The place of conventional MRI and newly emerging MRI techniques in monitoring different aspects of treatment outcome." J Neurol 255 Suppl 1: 61-74.